Electronic Supporting Information for

Probing a variation of the inverse-trans-influence in americium and lanthanide tribromide tris(tricyclohexylphosphine oxide) complexes

Cory J. Windorff, Cristian Celis-Barros, Joseph M. Sperling, Noah C. McKinnon, Thomas E. Albrecht–Schmitt*

Department of Chemistry and Biochemistry, Florida State University, 95 Chieftan Way, RM. 118 DLC, Tallahassee, Florida 32306, USA. E-mail: talbrechtschmitt@fsu.edu;

Table of Contents

PHOTOGRAPHS OF AMERICIUM SYNTHESIS

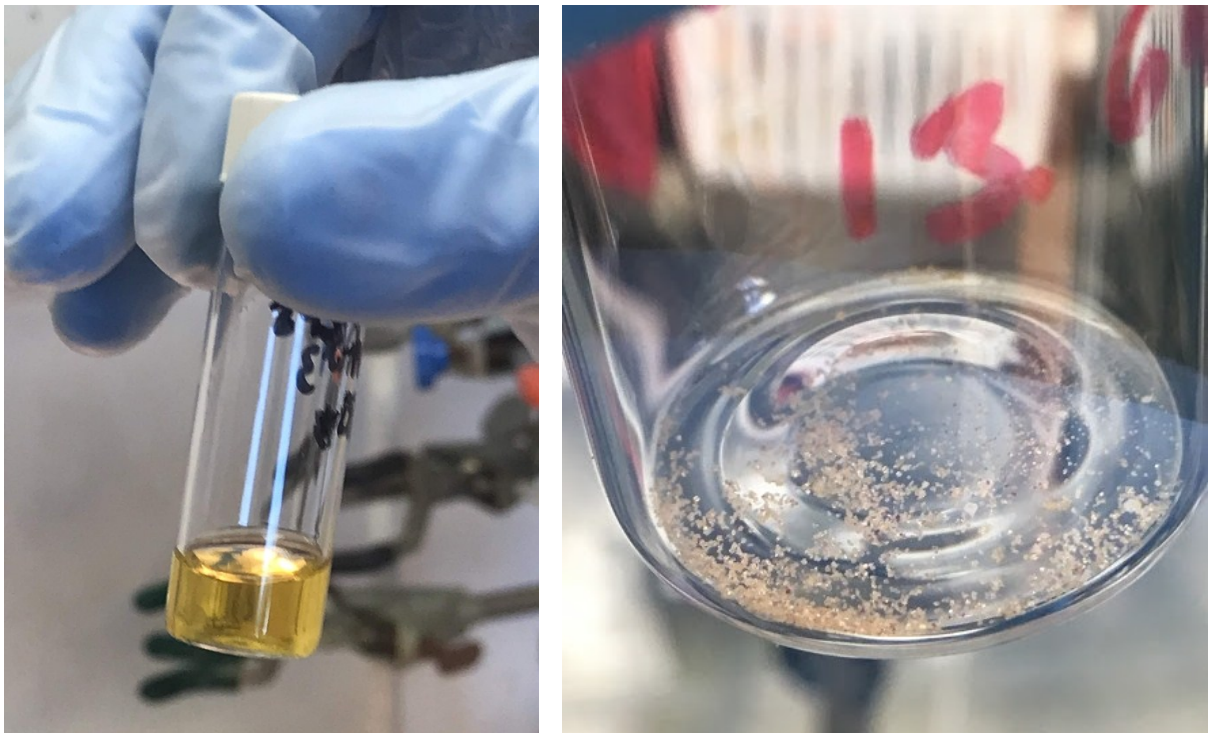

Figure S1. Photograph of **$AmBr_3(OPcy_3)_3$** in ^{i}PrOH (left) and 9.0 mg of crystalline material (Right).

Figure S2. Photograph of **$AmBr_3(OPcy_3)_3$** NMR sample in $CDCl_3$ (left), and additional photograph of isolated crystals (right).

UV/VIS/NIR SPECTROSCOPY

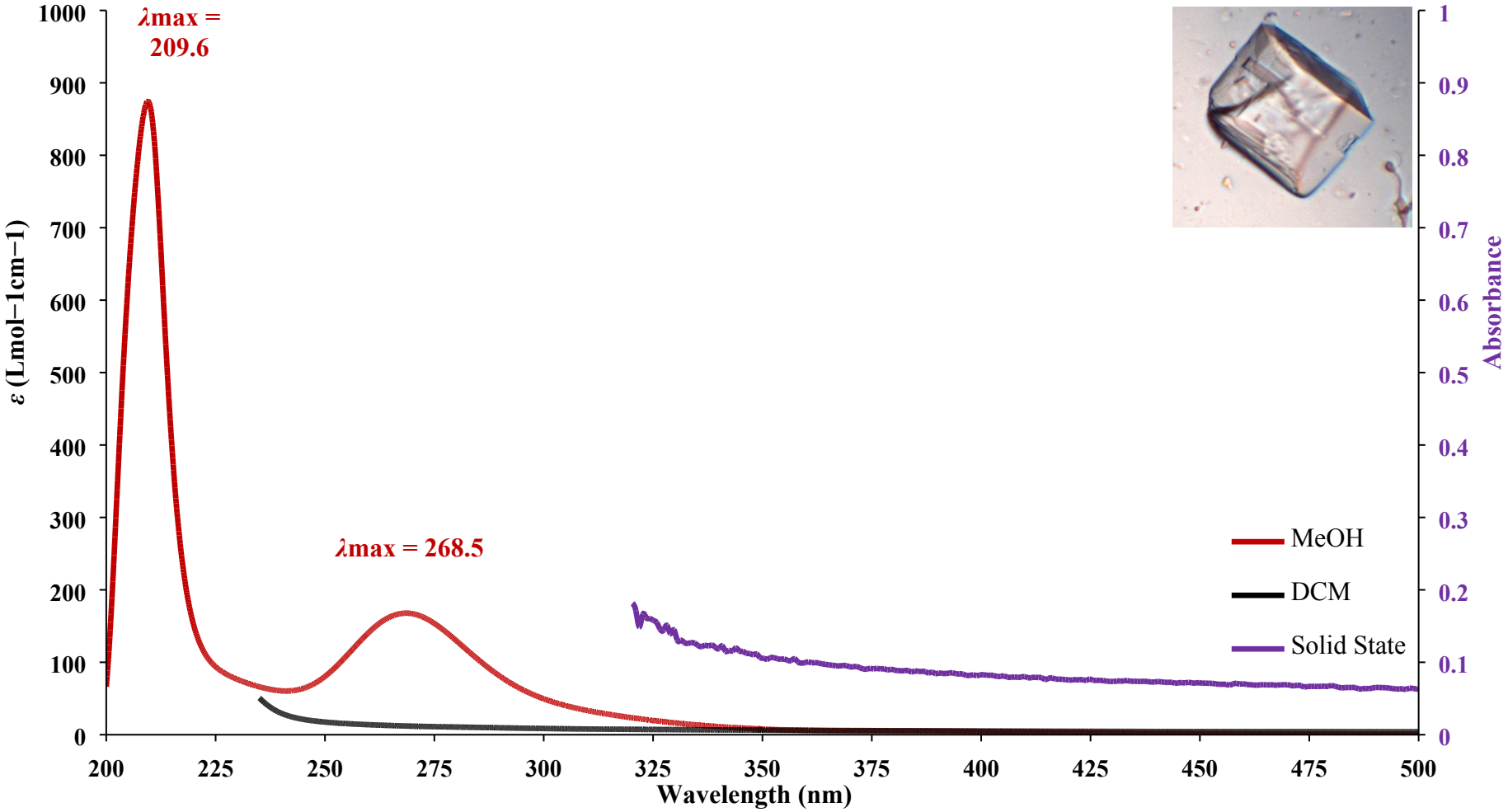

Figure S3. Room temperature UV/vis/NIR spectra of $LaBr_3(OPcy_3)_3$ in MeOH (red trace), DCM (black trace) and in the solid state (purple trace, right axis) and a photograph of a typical crystal. Identifiable peaks labeled with their λ_{max} and ε values are labeled in their corresponding colors. No identifiable transitions occur past 500 nm and the spectra have been truncated for clarity.

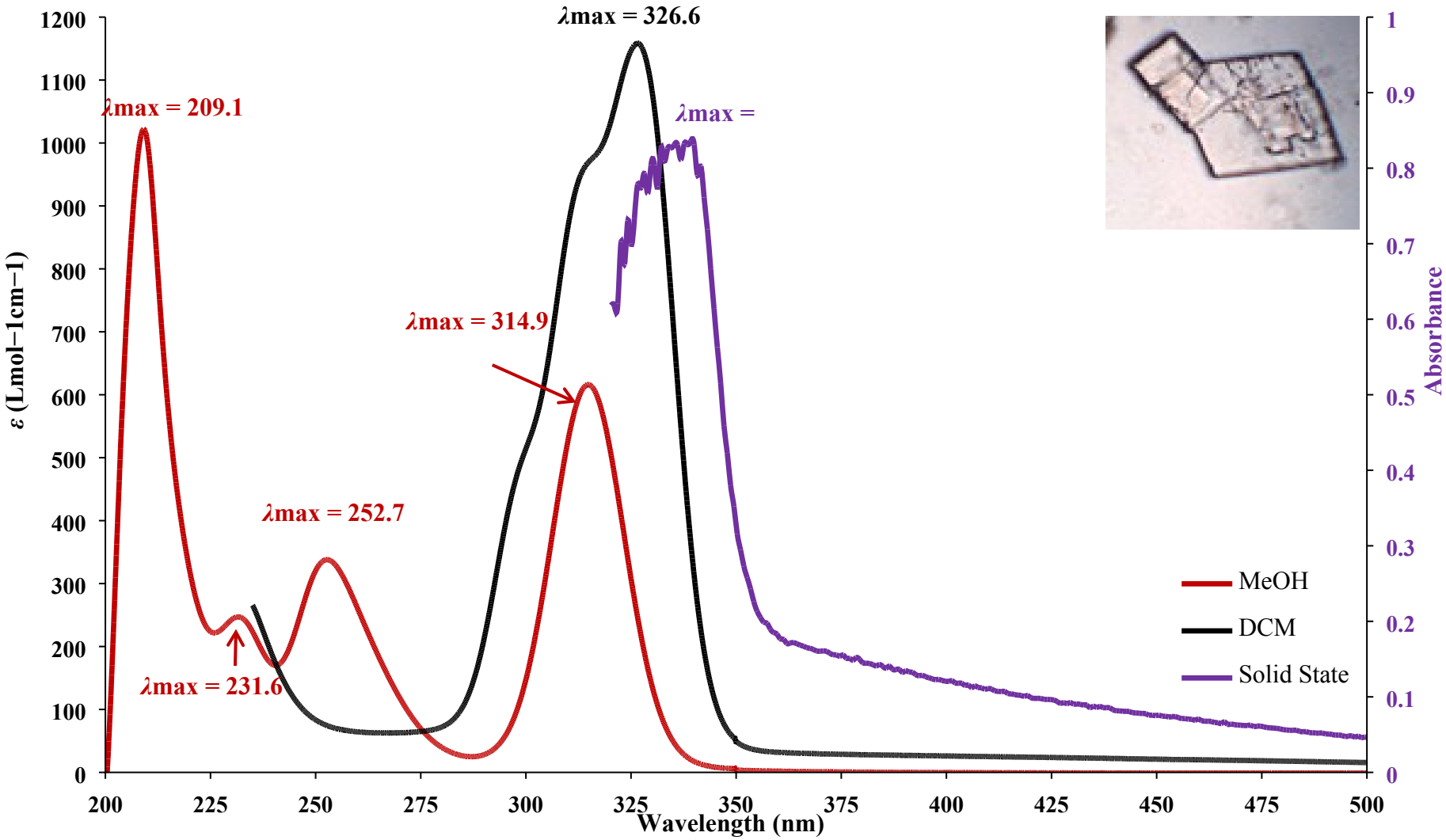

Figure S4. Room temperature UV/vis/NIR spectra of $CeBr_3(OPcy_3)_3$ in MeOH (red trace), DCM (black trace) and in the solid state (purple trace, right axis) and a photograph of a typical crystal. Identifiable peaks labeled with their λ_{max} and ε values are labeled in their corresponding colors. No identifiable transitions occur past 500 nm and the spectra have been truncated for clarity.

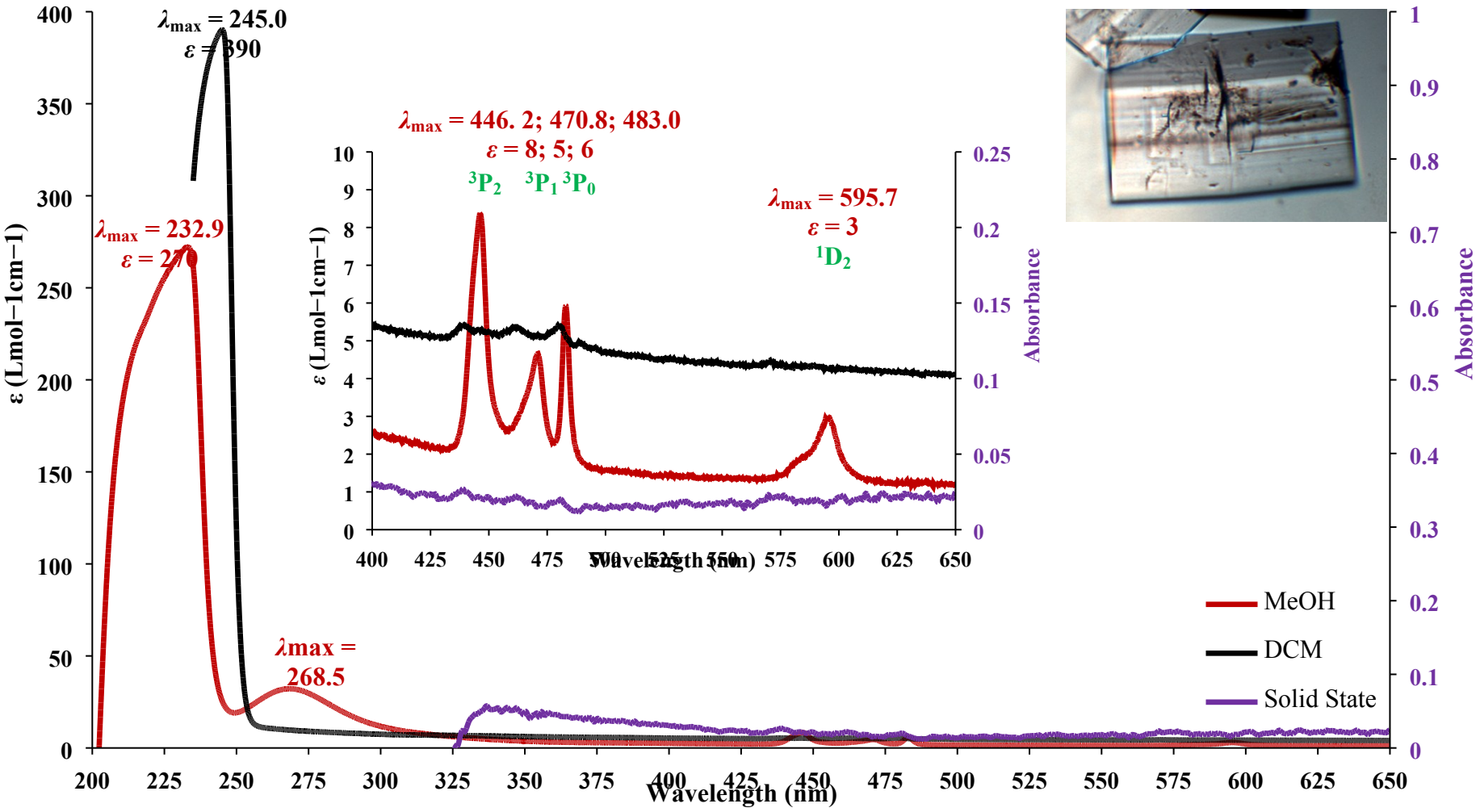

Figure S5. Room temperature UV/vis/NIR spectra of $PrBr_3(OPcy_3)_3$ in MeOH (black trace), DCM (red trace) and in the solid state (purple trace, right axis) inset of 400-650 nm region and a photograph of a typical crystal. Identifiable peaks labeled with their λ_{max} and ε values are labeled in their corresponding colors with excitation symmetry labels. No identifiable transitions occur past 650 nm and the spectra have been truncated for clarity.

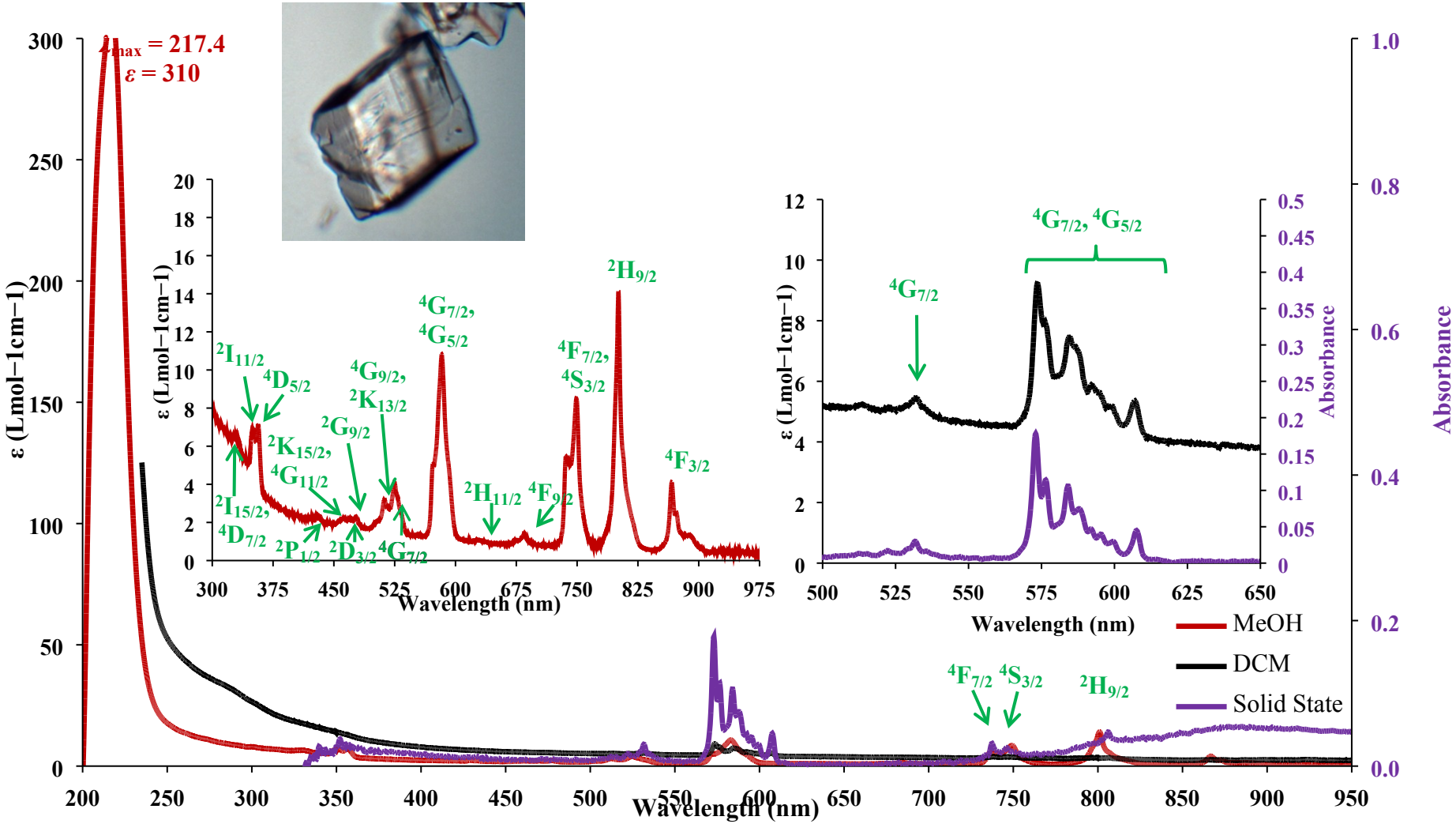

Figure S6. Room temperature UV/vis/NIR spectra of $NdBr_3(OPcy_3)_3$ in MeOH (red trace), DCM (black trace) and in the solid state (purple trace, right axis) inset of 300-950 nm region of MeOH spectrum (left), inset of 500-650 region for DCM and solid state spectra (right) and a photograph of a typical crystal. Due to the high number of excitations only excitation symmetry labels have been included. No identifiable transitions occur past 950 nm and the spectra have been truncated for clarity.

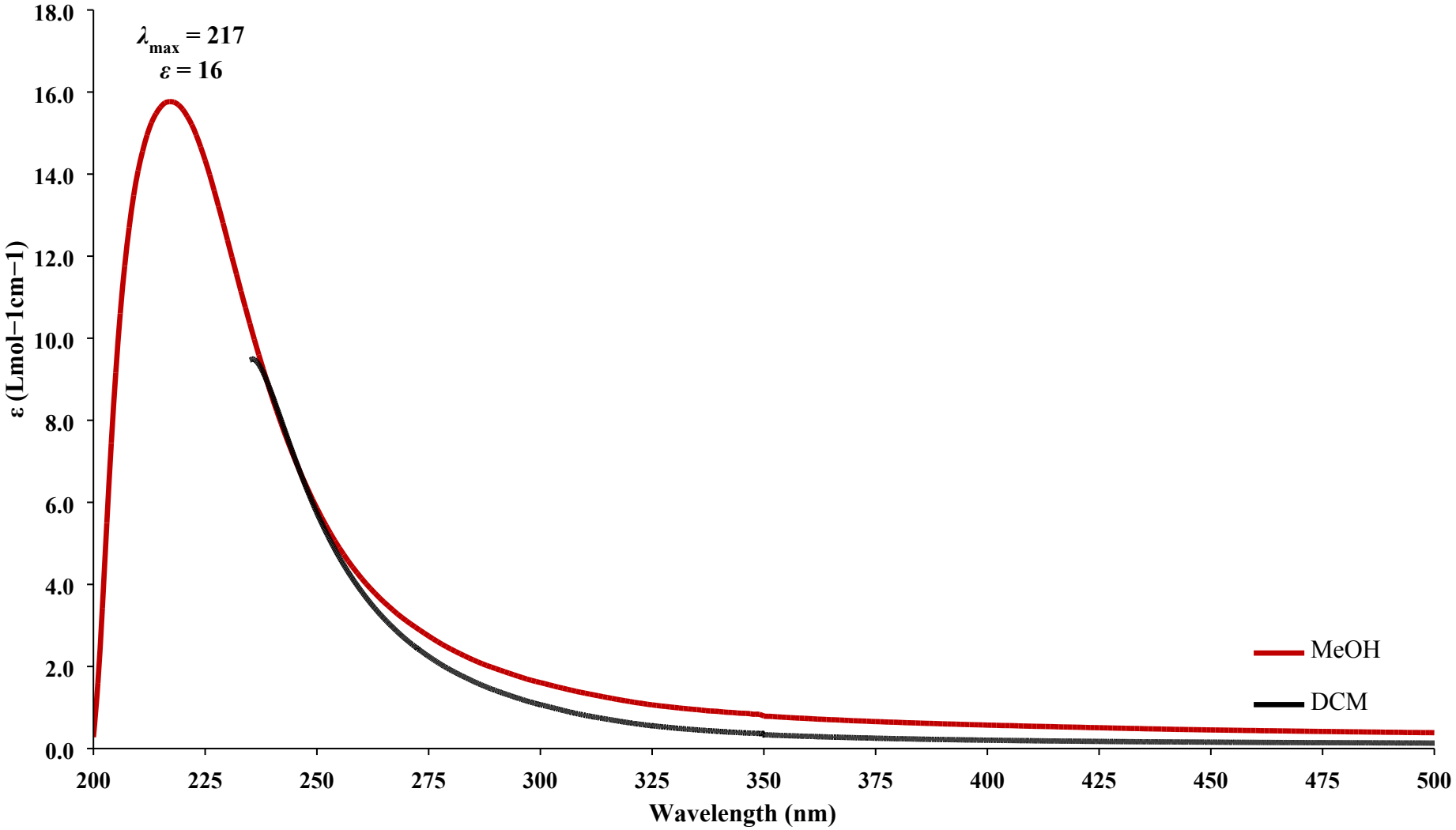

Figure S7. Room temperature UV/vis/NIR spectra of $OPcy_3$ in MeOH (red trace), and DCM (black trace), identifiable excitation labeled with its λ_{max} and ε values. No identifiable transitions occur past 500 nm and the spectra have been truncated for clarity.

MULTI NUCLEAR NMR SPECTROSCOPY

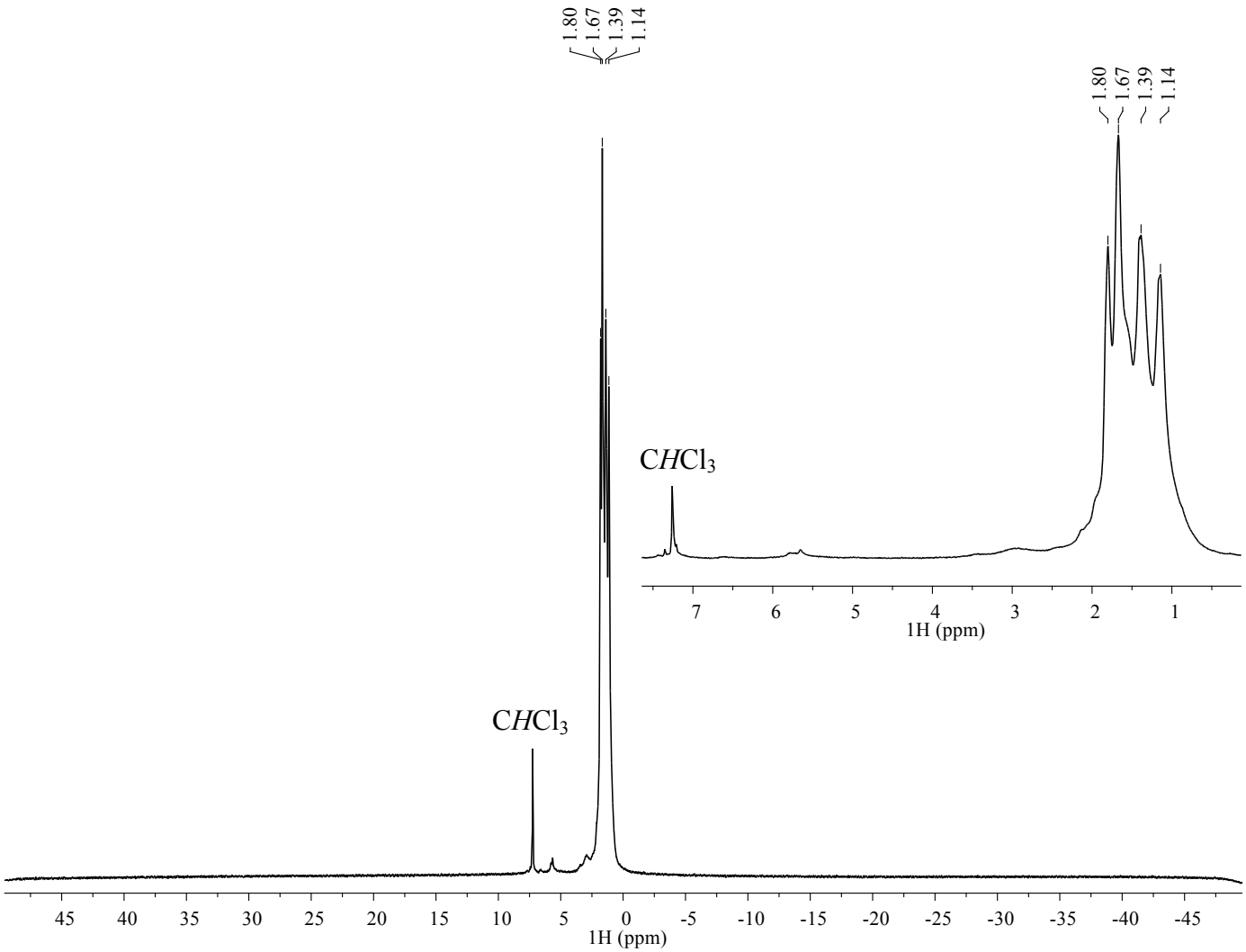

Figure S8. ^{1}H NMR spectrum of **$AmBr_3(OPcy_3)_3$** in $CDCl_3$ at 295 K with expansion of 8 – 0 ppm region, Because the chemical identity of the peaks is unclear the peaks are not integrated.

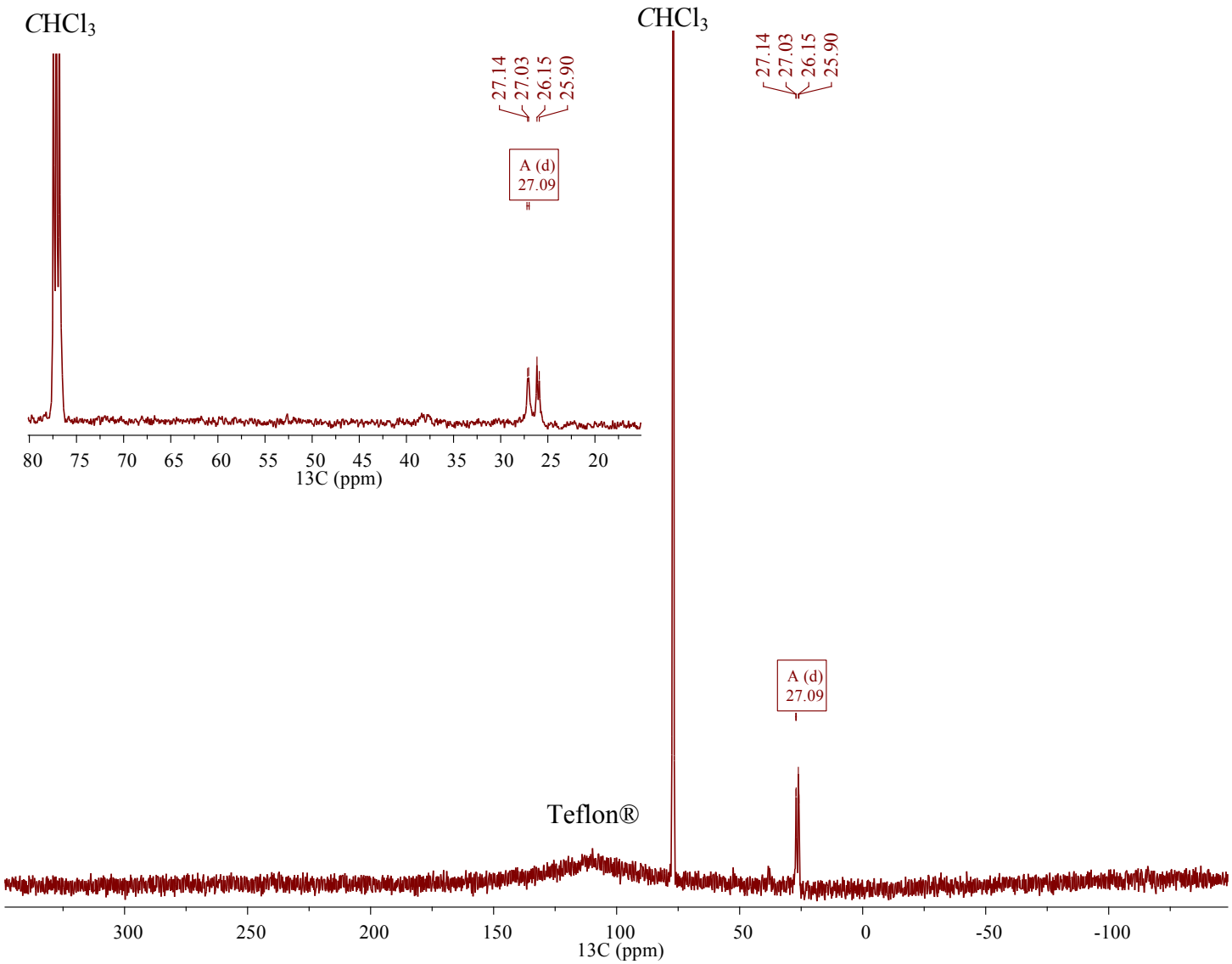

Figure S9. $^{13}C\{^{1}H\}$ NMR spectrum of **$AmBr_3(OPcy_3)_3$** in $CDCl_3$ at 295 K with expansion of 80 – 15 ppm region processed with a 5 Hz line broadening.

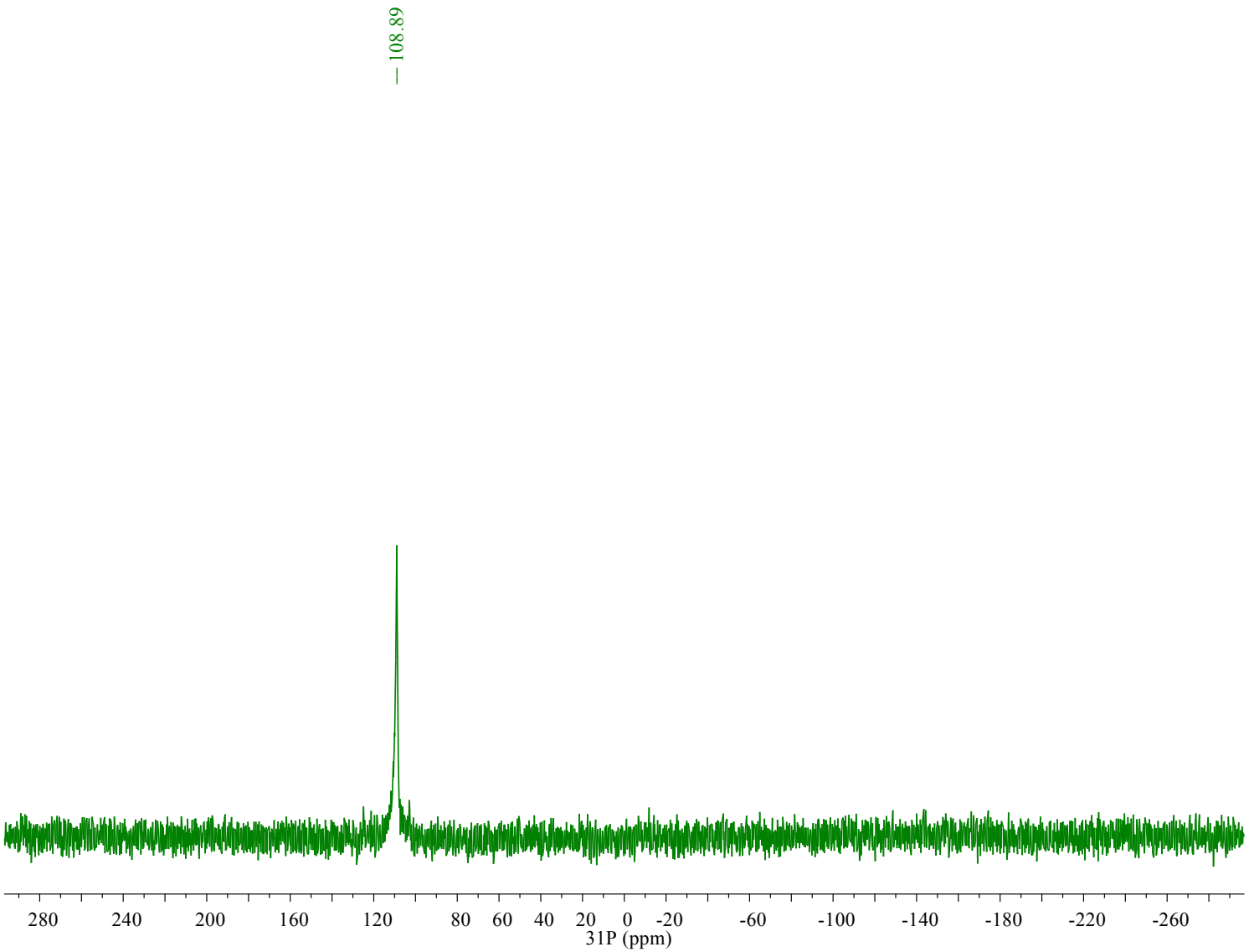

Figure S10. $^{31}P\{^{1}H\}$ NMR spectrum of **$AmBr_3(OPcy_3)_3$** in $CDCl_3$ at 295 K processed with a 10 Hz line broadening.

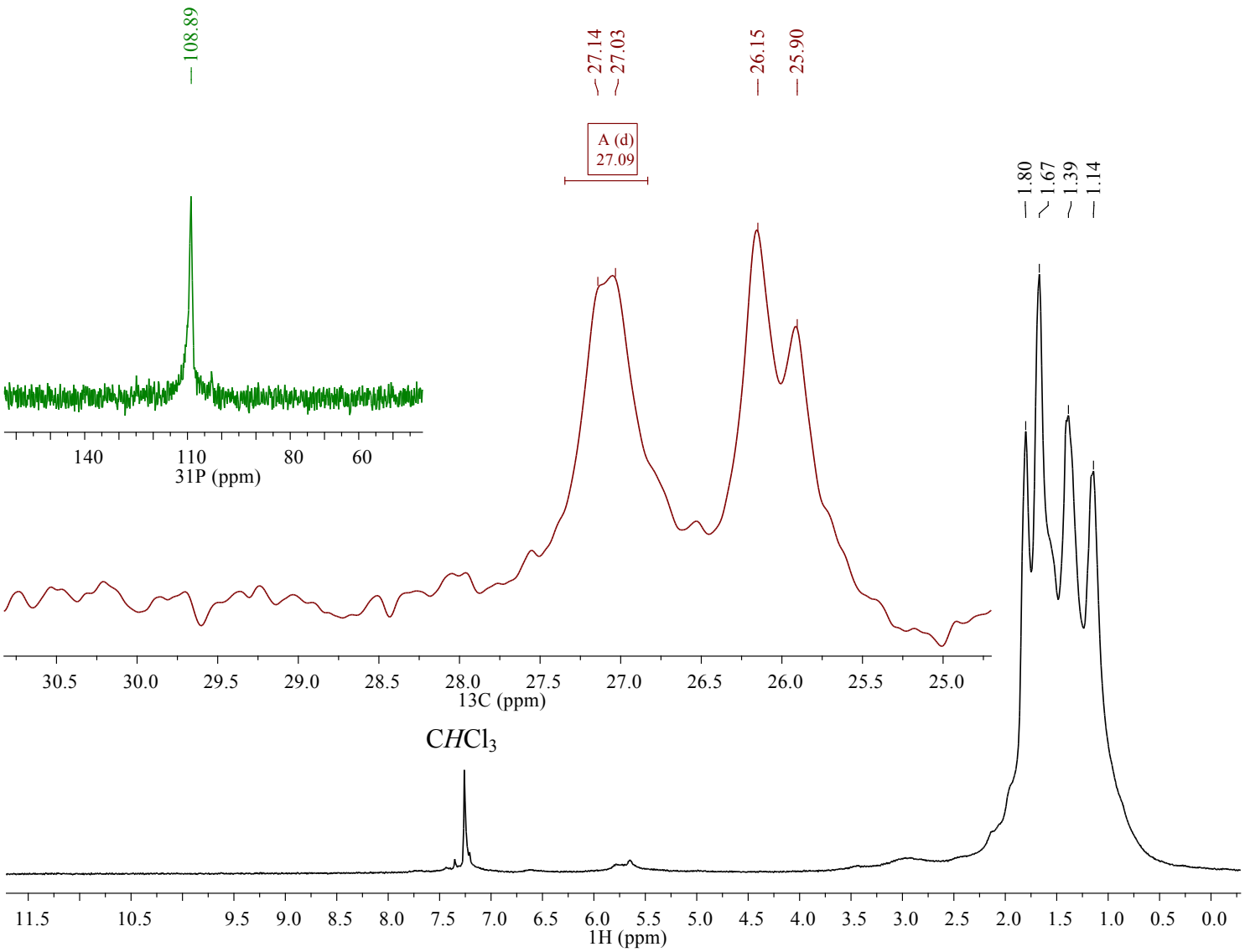

Figure S11. Multinuclear NMR spectra of **$AmBr_3(OPcy_3)_3$** at 295 K in $CDCl_3$, ^1H (black), $^{13}C\{^1H\}$ (red) and $^{31}P\{^1H\}$ (green).

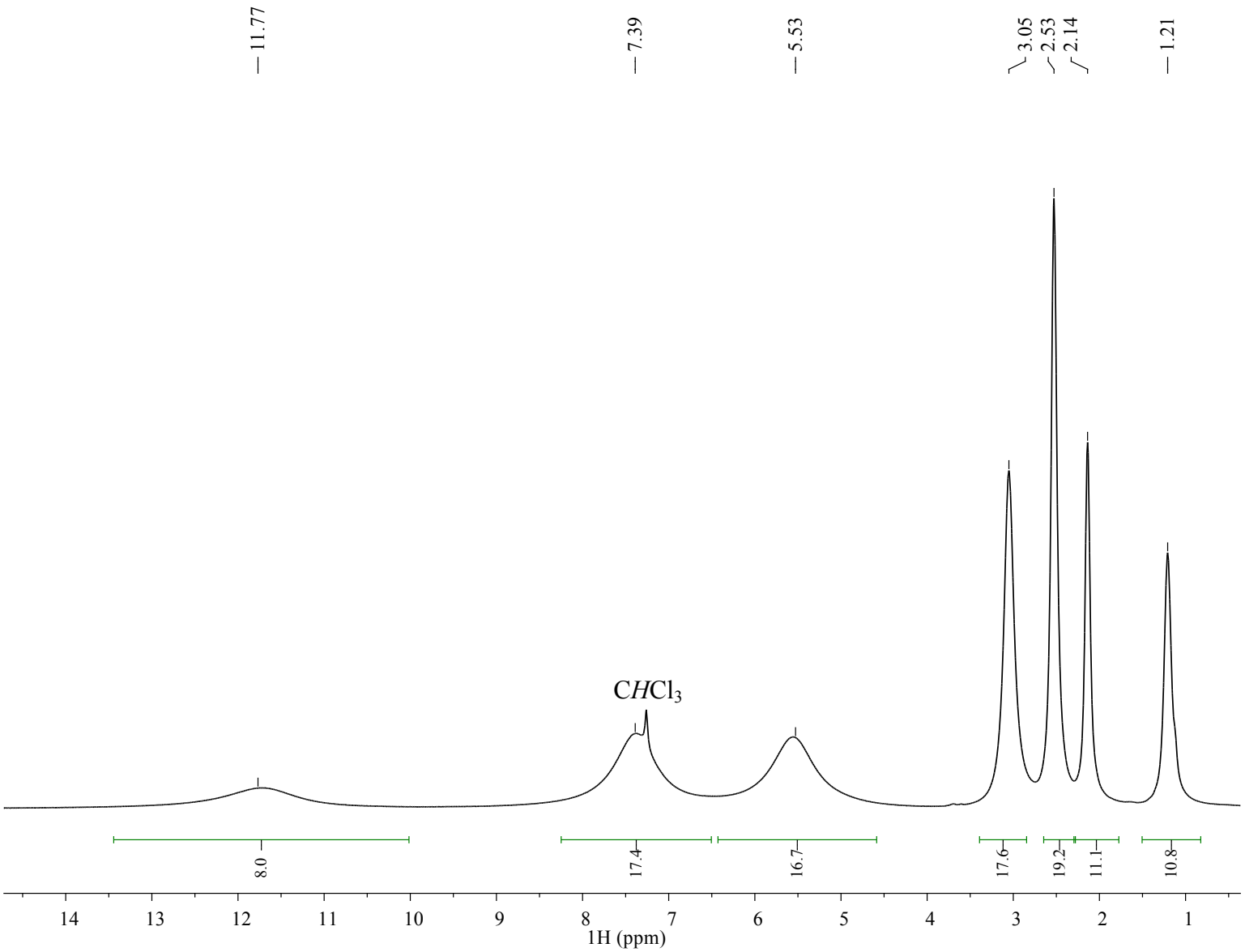

Figure S12. ^{1}H NMR spectrum of **$NdBr_3(OPcy_3)_3$** at 298 K in $CDCl_3$.

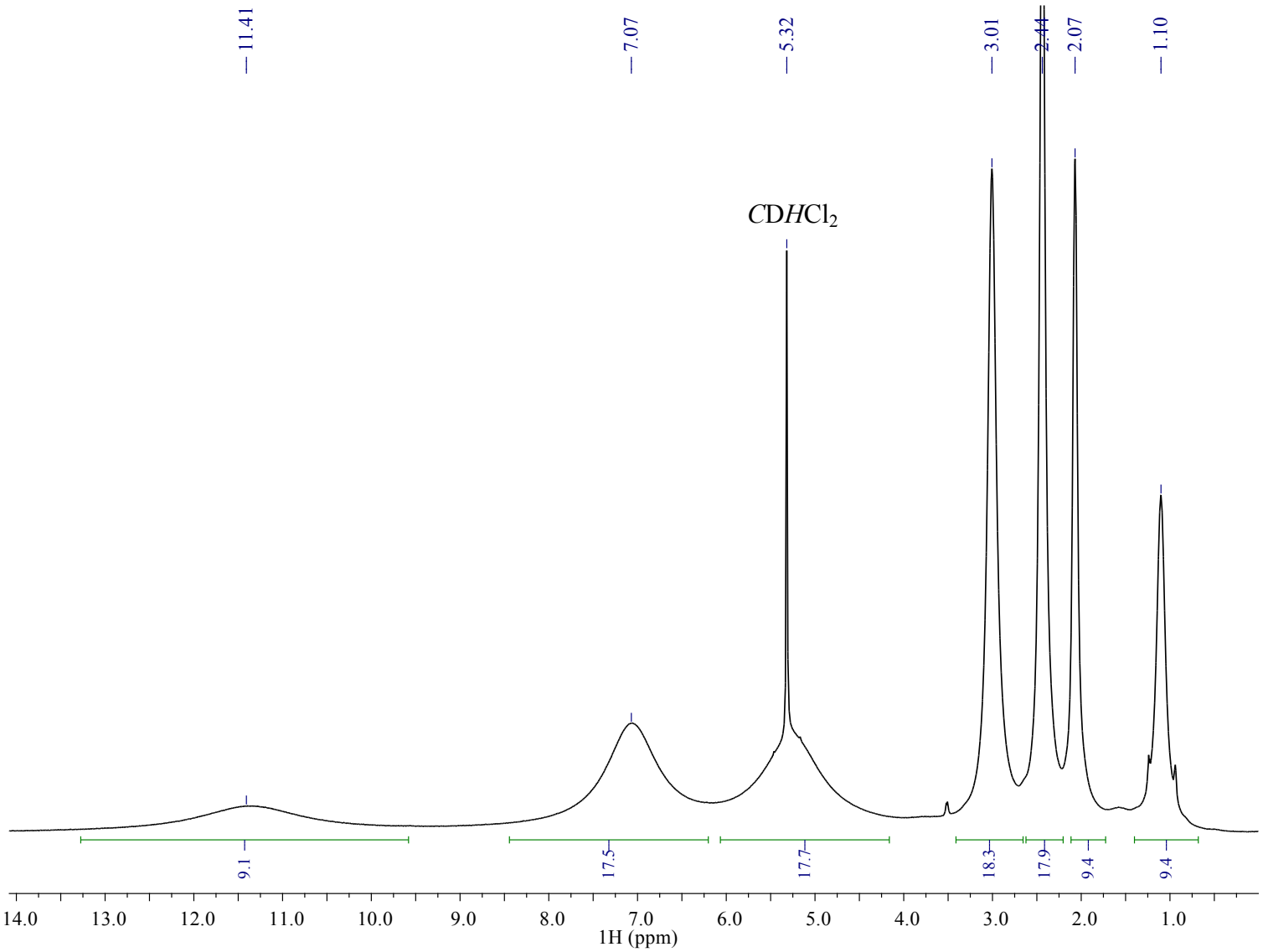

Figure S13. ^{1}H NMR spectrum of **$NdBr_3(OPcy_3)_3$** at 298 K in CD_2Cl_2.

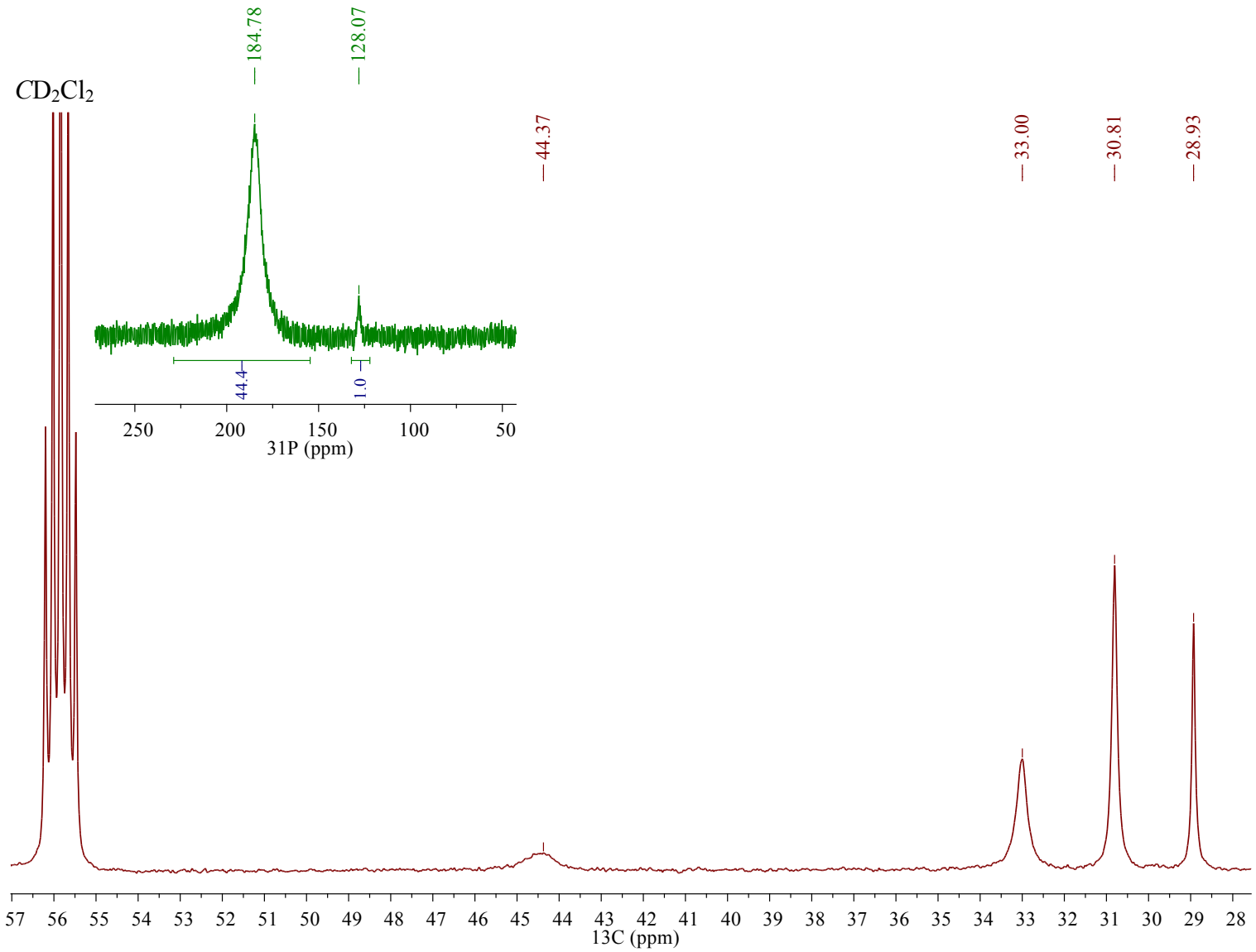

Figure S14. Multinuclear NMR spectra of **$NdBr_3(OPcy_3)_3$** at 298 K in CD_2Cl_2, $^{13}C\{^1H\}$ (red) and $^{31}P\{^1H\}$ (green).

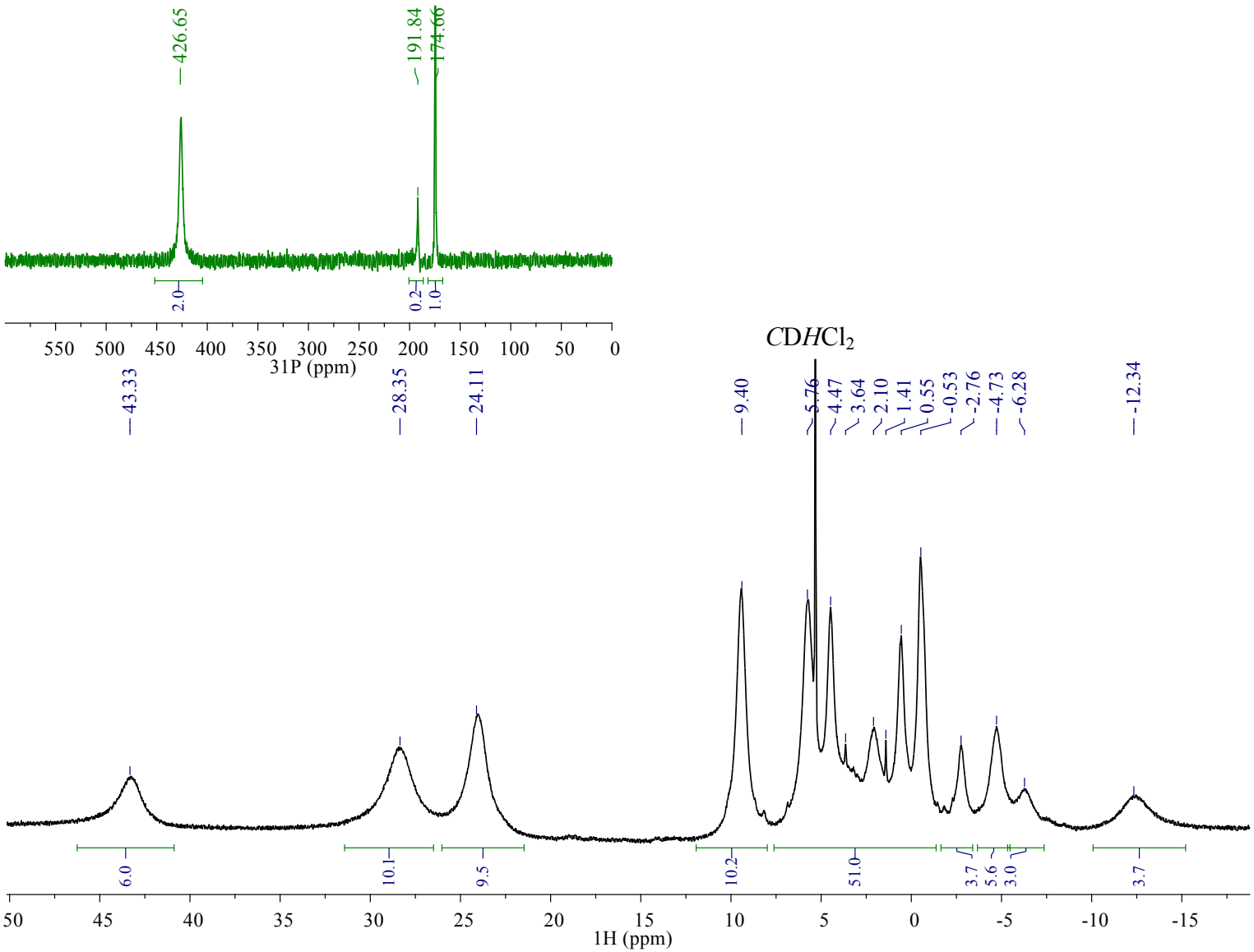

Figure S15. Multinuclear NMR spectra of **$NdBr_3(OPcy_3)_3$** at 187 K in CD_2Cl_2 ^1H (black), and $^{31}P\{^1H\}$ (green).

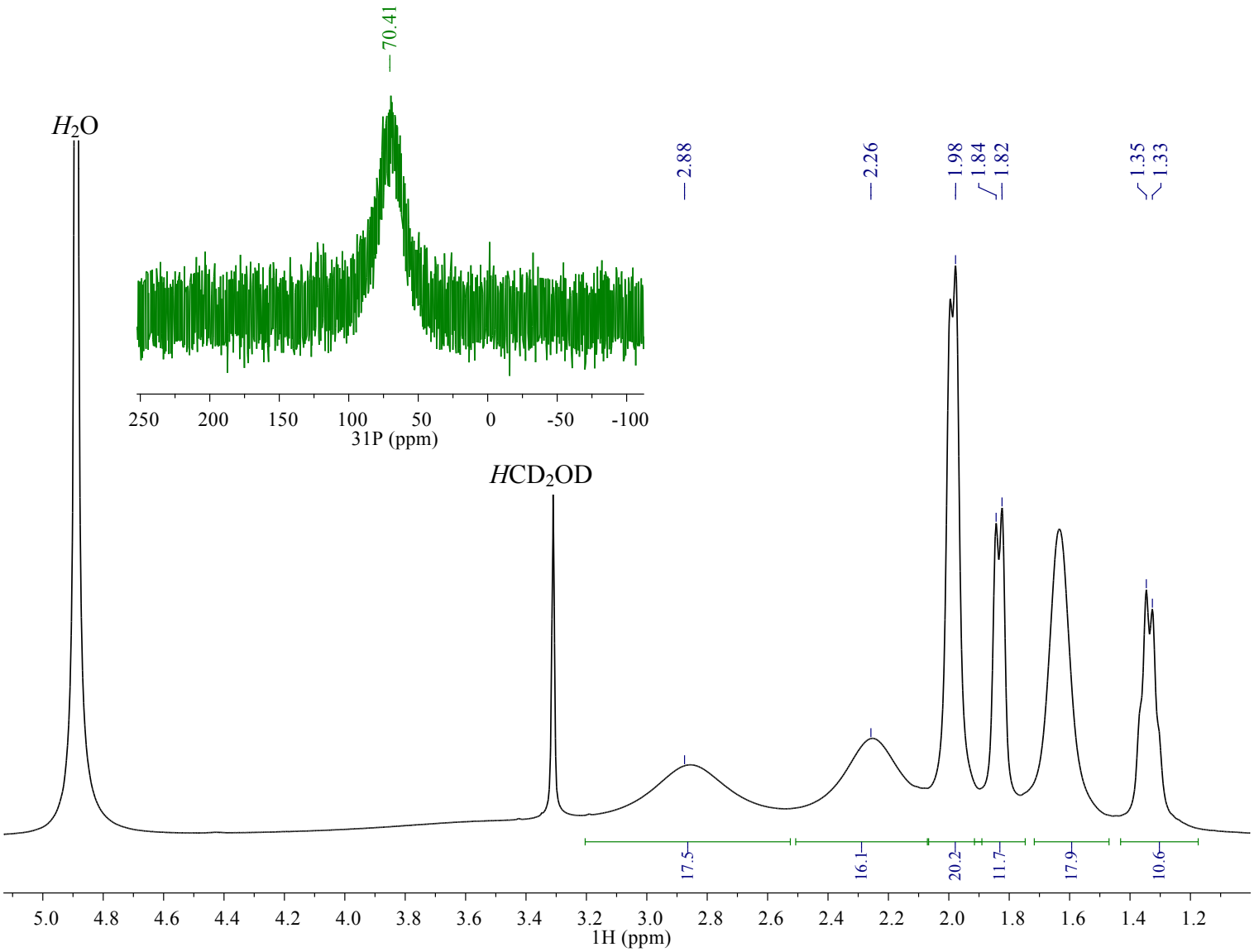

Figure S16. Multinuclear NMR spectra of **$NdBr_3(OPcy_3)_3$** at 298 K in MeOD-d_4 ^{1}H (black), and ^{31}P{^{1}H} (green).

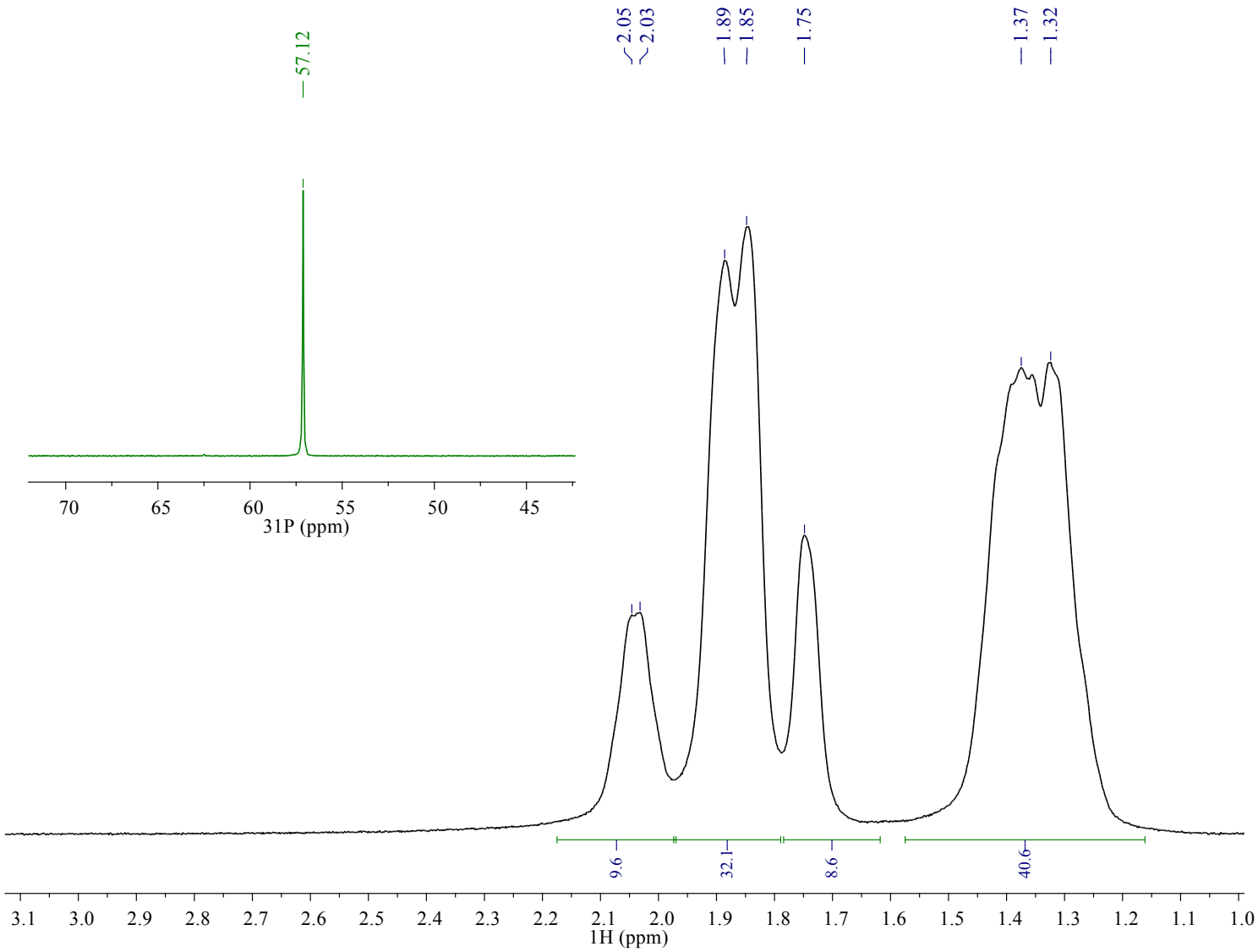

Figure S17. Multinuclear NMR spectra of **$NdBr_3(OPcy_3)_3$** at 187 K in MeOD-d_4 ^{1}H (black), and ^{31}P{^{1}H} (green).

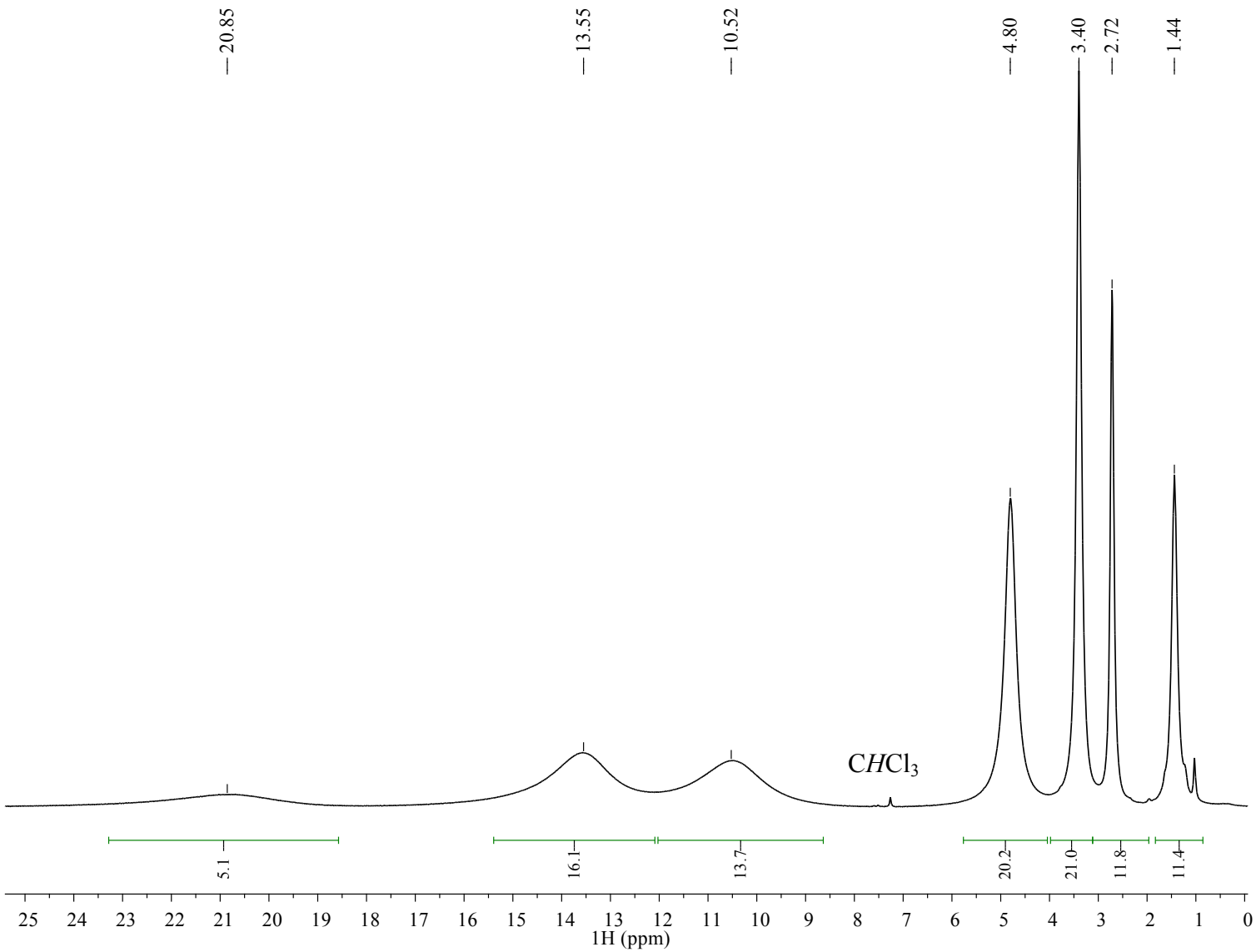

Figure S18. ^{1}H NMR spectrum of **$PrBr_3(OPcy_3)_3$** at 298 K in $CDCl_3$.

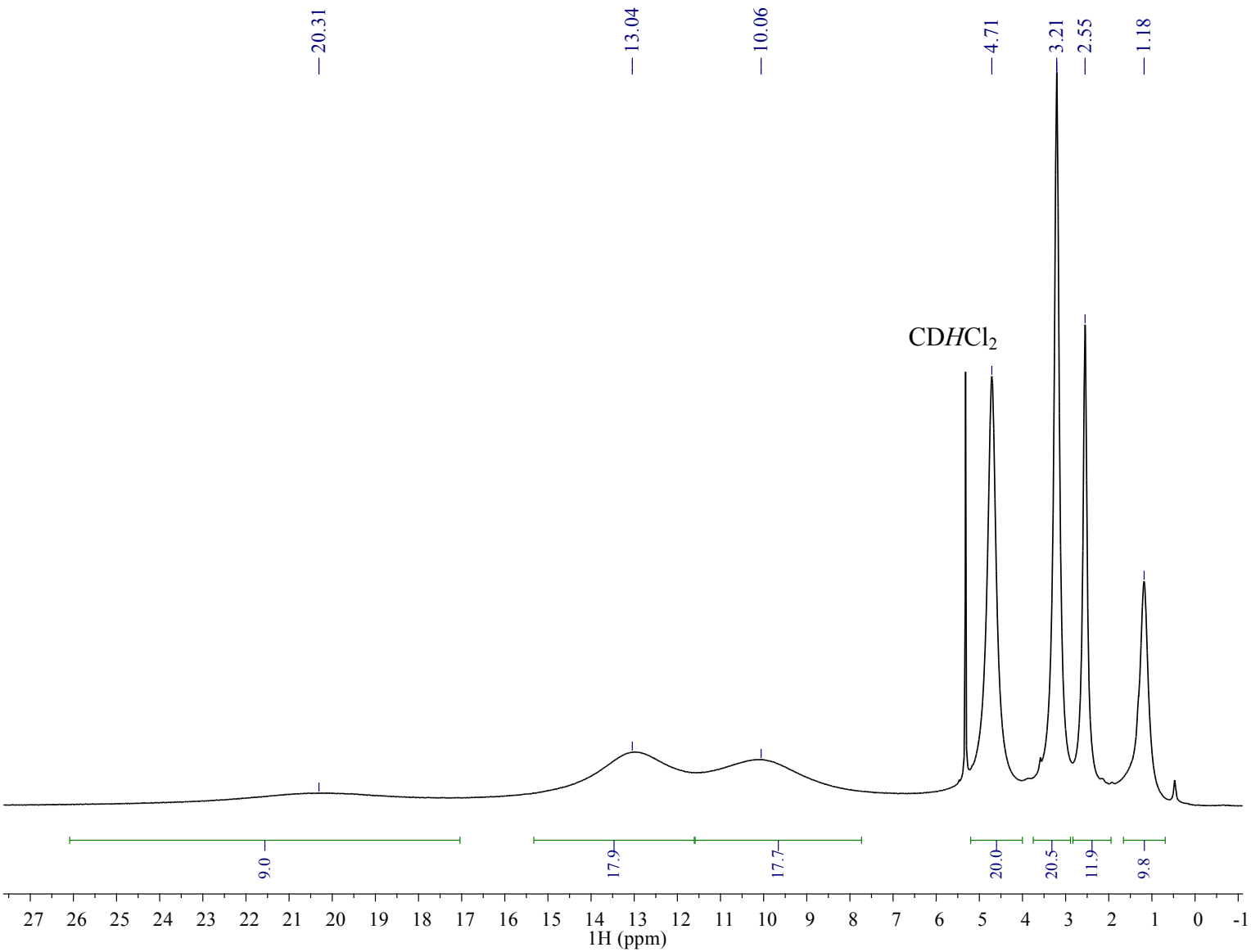

Figure S19. ^{1}H NMR spectrum of **$PrBr_3(OPcy_3)_3$** at 298 K in CD_2Cl_2.

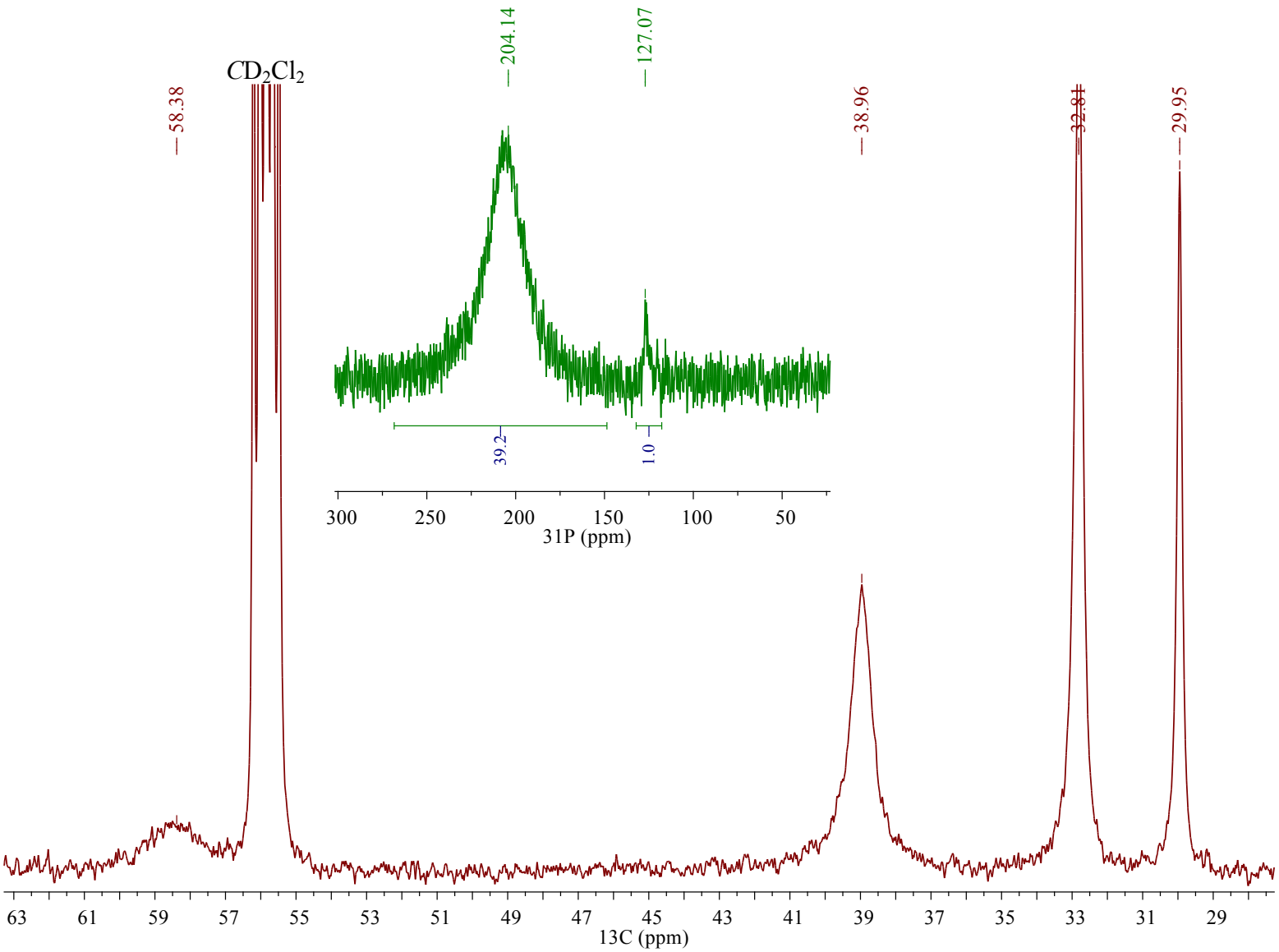

Figure S20. Multinuclear NMR spectra of **$PrBr_3(OPcy_3)_3$** at 298 K in CD_2Cl_2, $^{13}C\{^1H\}$ (red) and $^{31}P\{^1H\}$ (green).

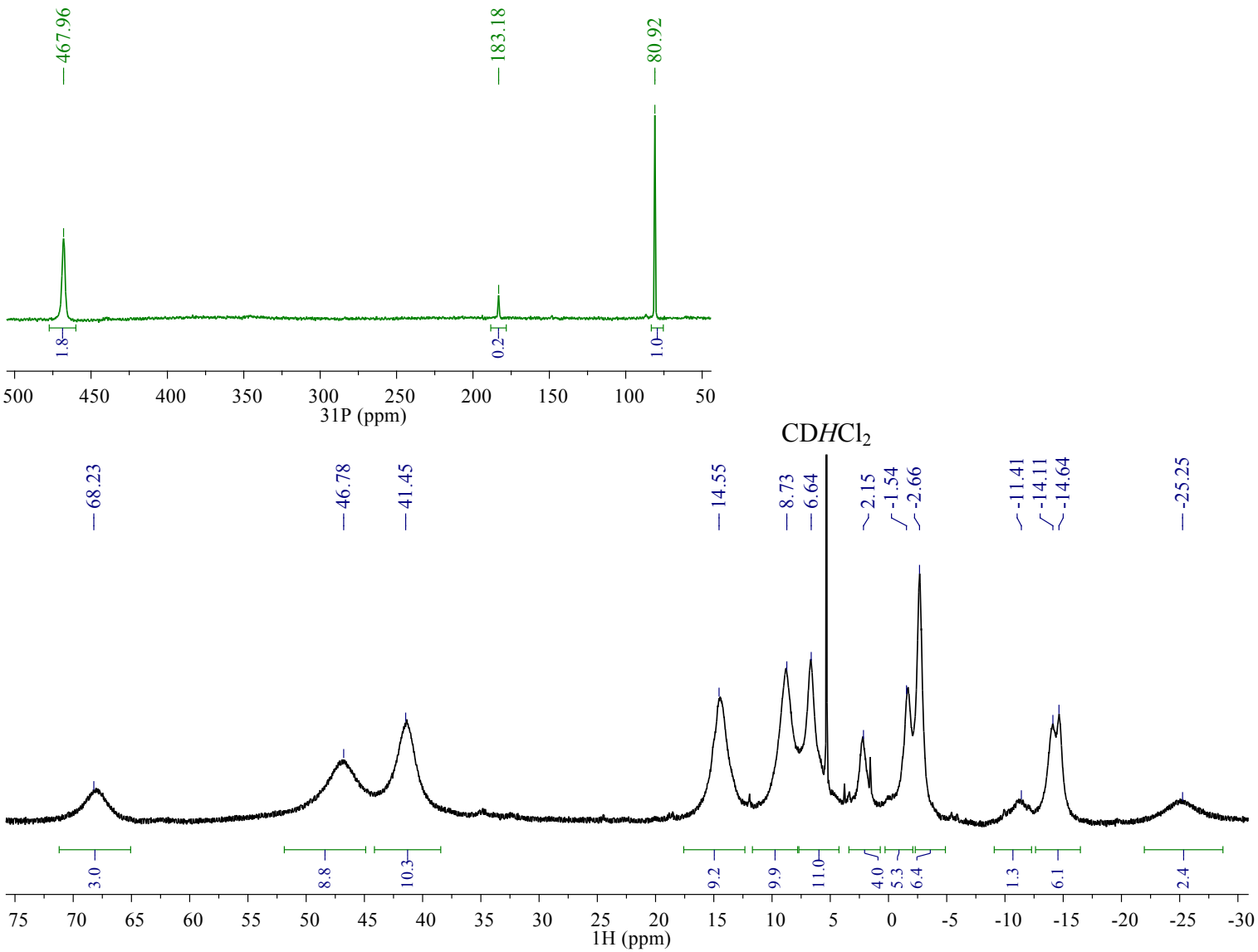

Figure S21. Multinuclear NMR spectra of **$PrBr_3(OPcy_3)_3$** at 187 K in CD_2Cl_2, ^1H (black), and $^{31}P\{^1H\}$ (green).

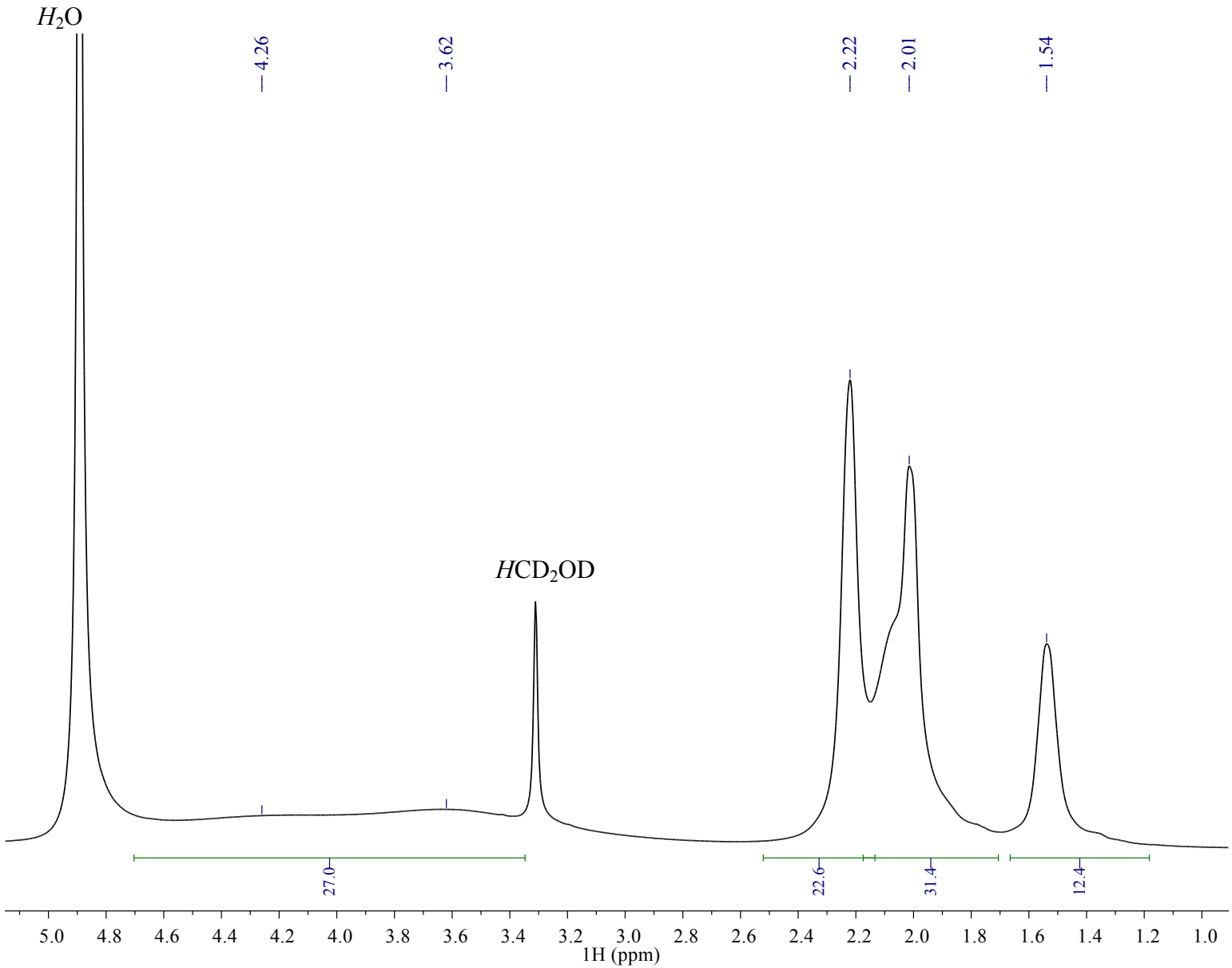

Figure S22. ^{1}H NMR spectrum of **$PrBr_3(OPcy_3)_3$** at 298 K in MeOD-d_4.

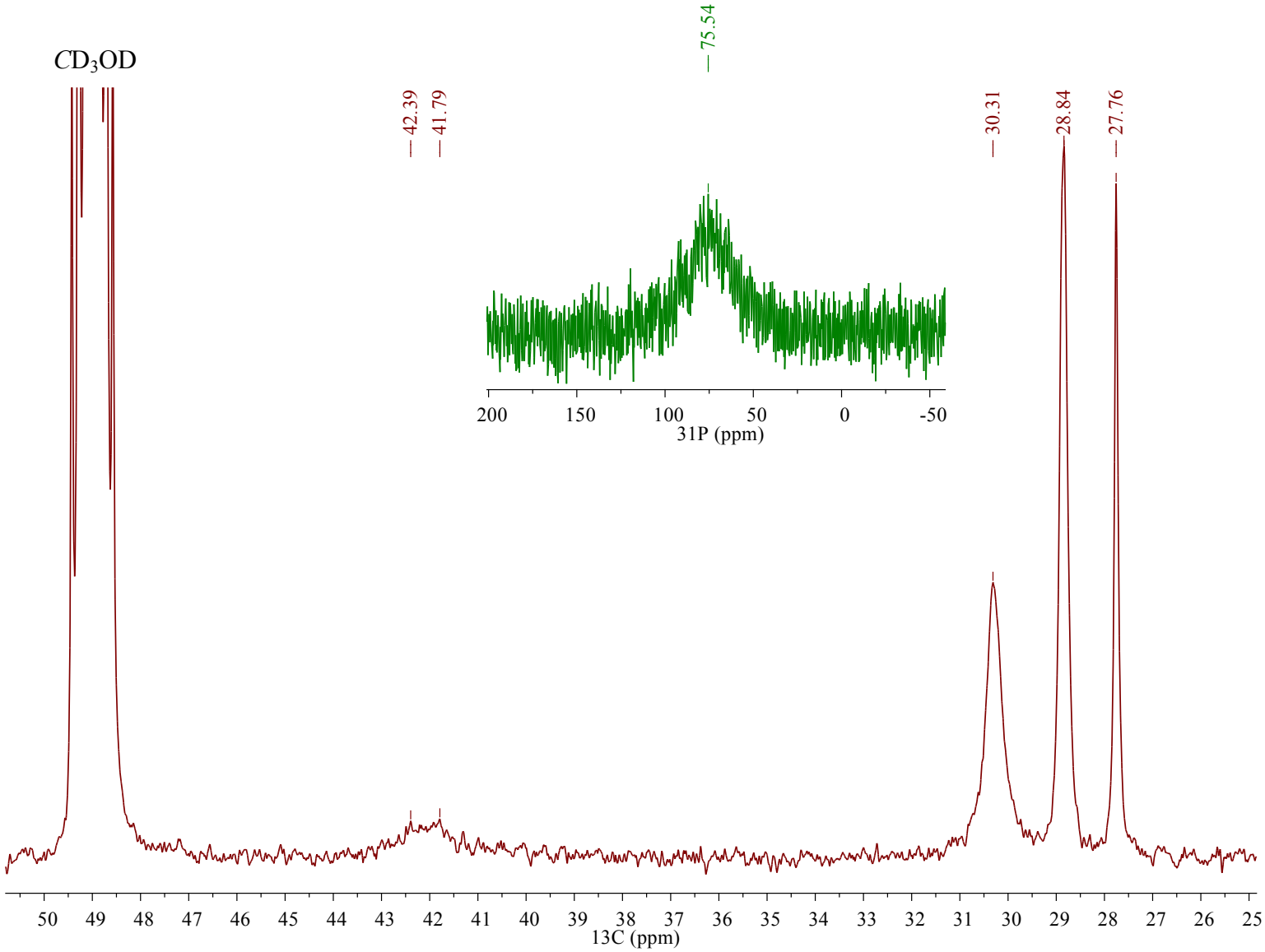

Figure S23. Multinuclear NMR spectra of **$PrBr_3(OPcy_3)_3$** at 298 K in MeOD-d_4, $^{13}C\{^1H\}$ (red) and $^{31}P\{^1H\}$ (green).

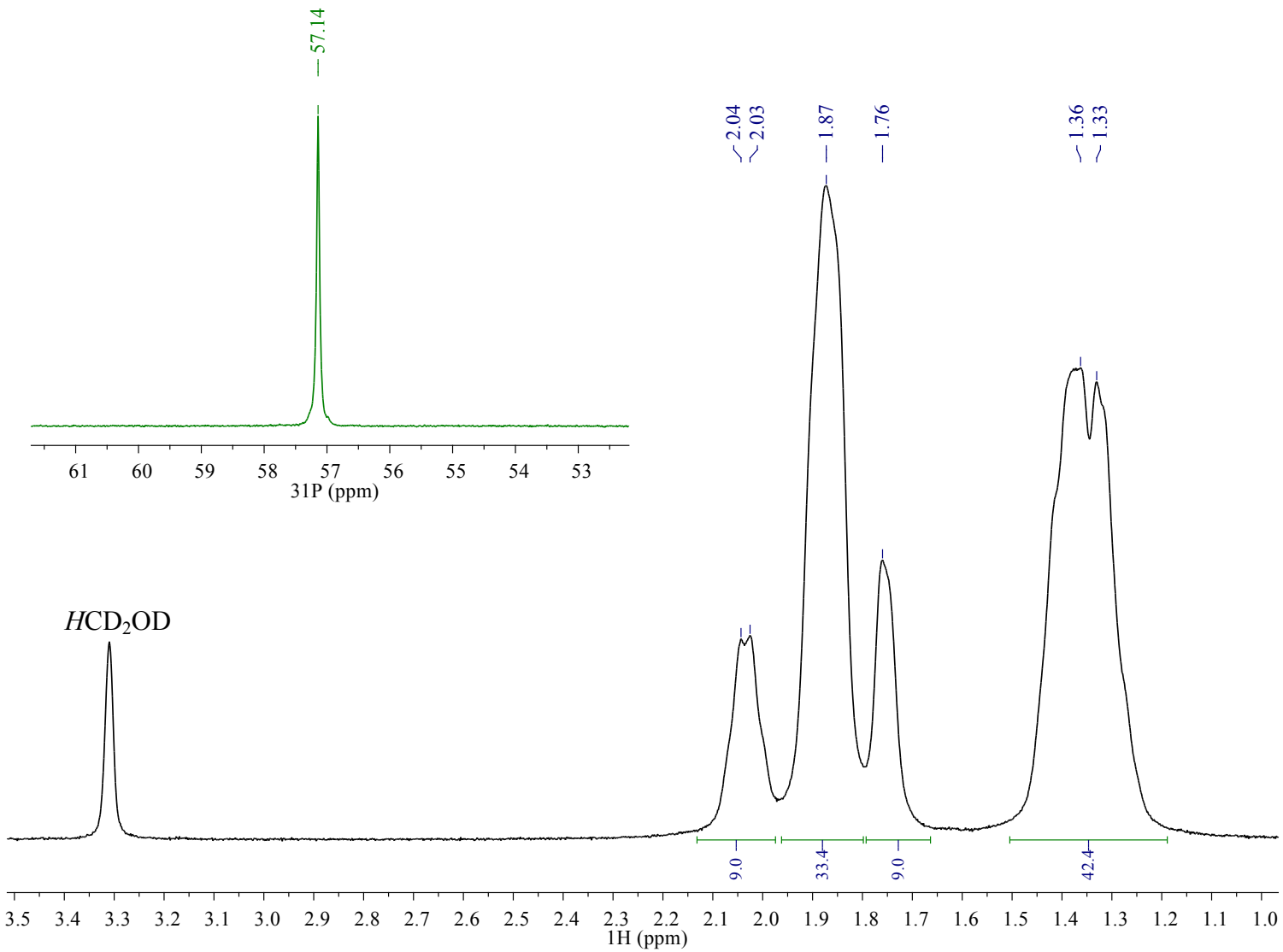

Figure S24. Multinuclear NMR spectra of **$PrBr_3(OPcy_3)_3$** at 187 K in MeOD-d_4, ^{1}H (black), and ^{31}P{^{1}H} (green).

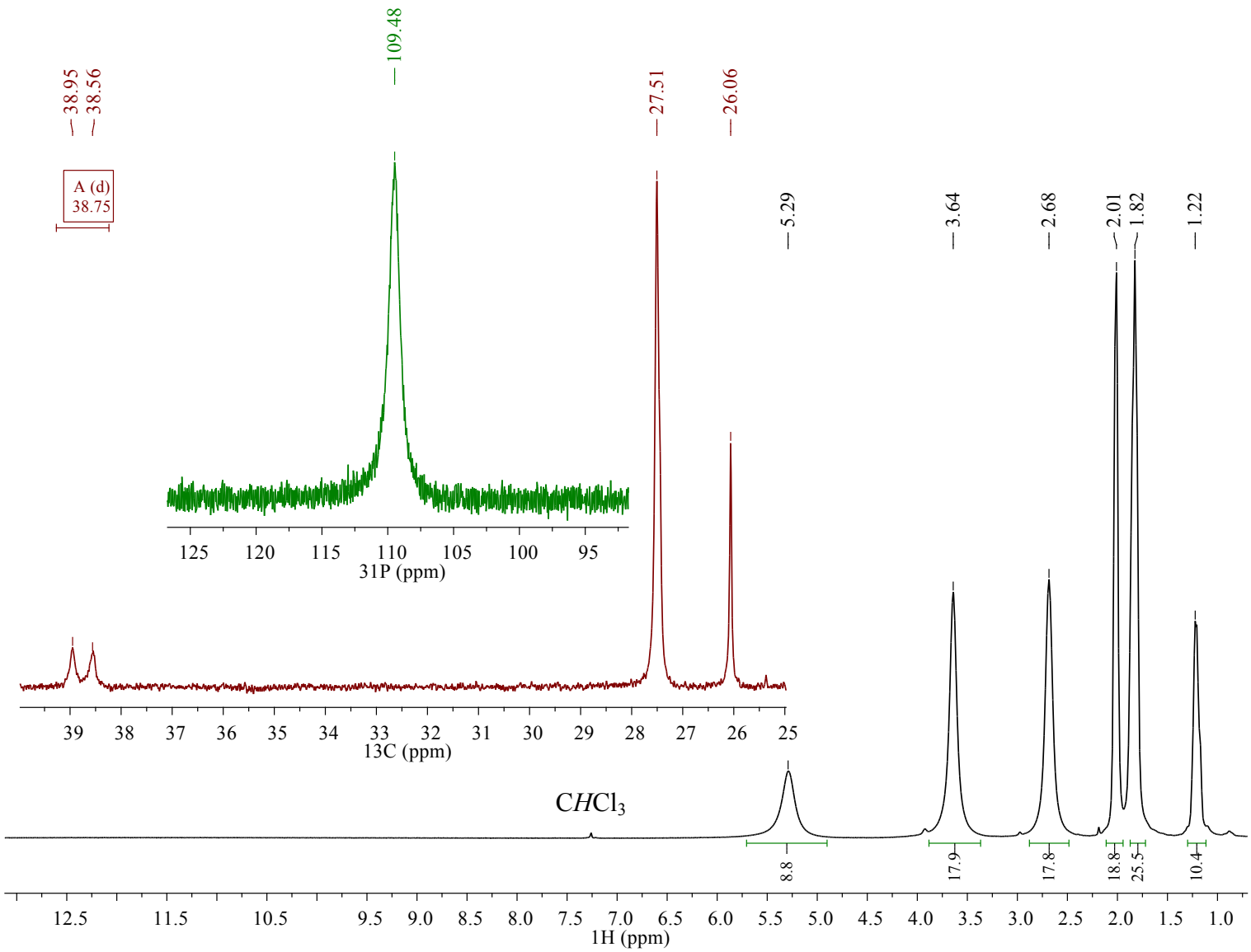

Figure S25. Multinuclear NMR spectra of **$CeBr_3(OPcy_3)_3$** at 294 K in $CDCl_3$, ^{1}H (black), $^{13}C\{^{1}H\}$ (red) and $^{31}P\{^{1}H\}$ (green).

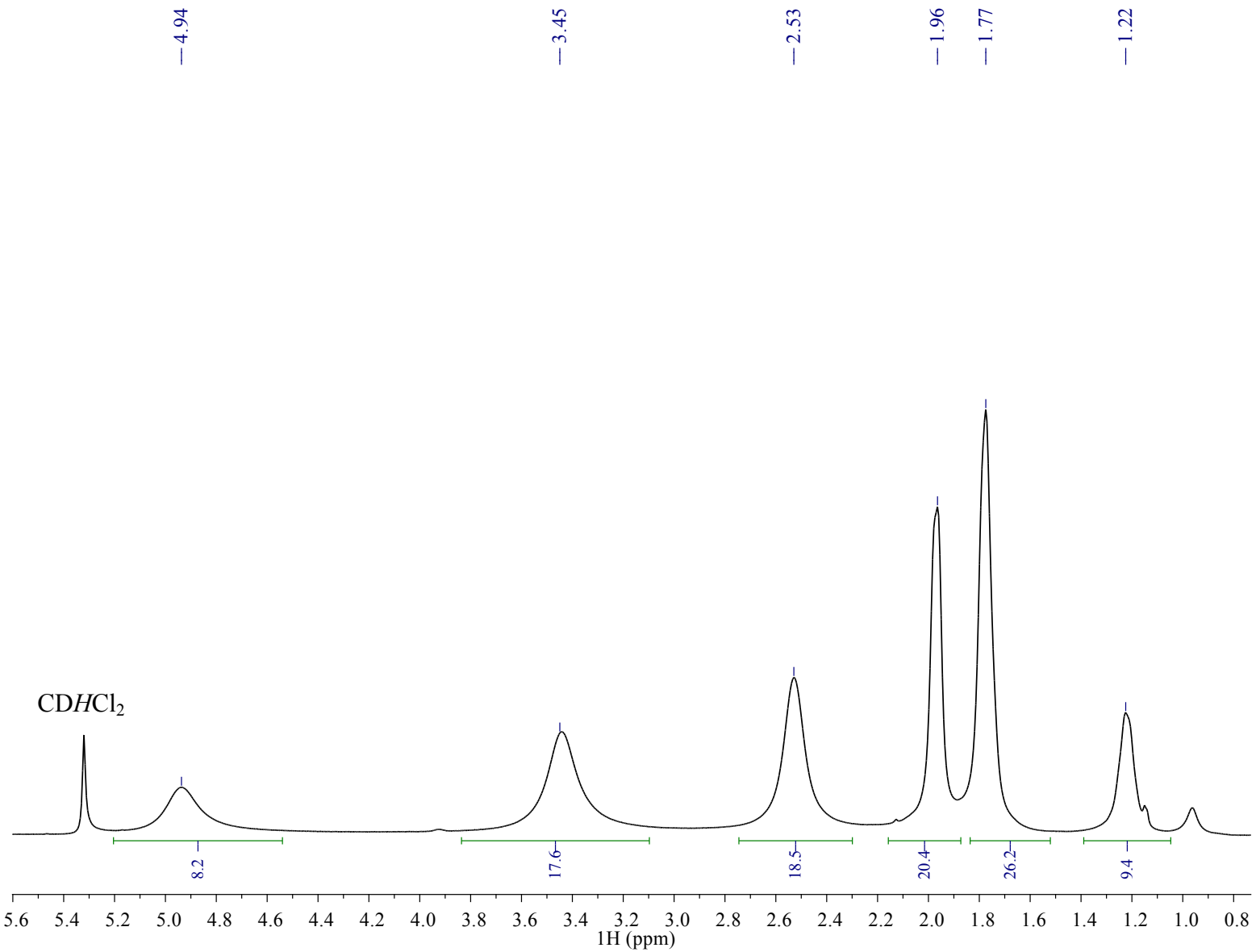

Figure S26. ^{1}H NMR spectrum of **$CeBr_3(OPcy_3)_3$** at 298 K in CD_2Cl_2.

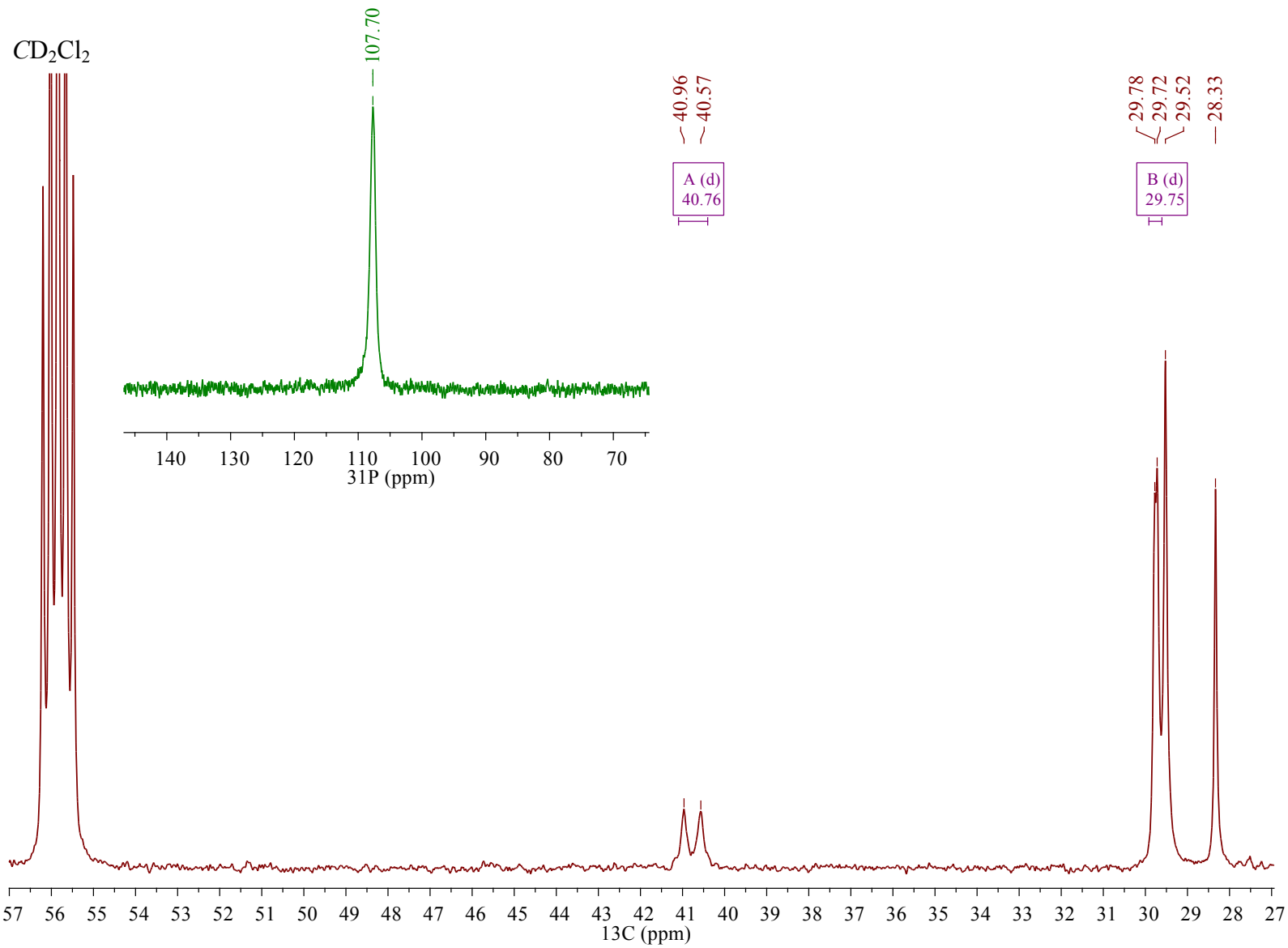

Figure S27. Multinuclear NMR spectra of **$CeBr_3(OPcy_3)_3$** at 298 K in CD_2Cl_2, $^{13}C\{^1H\}$ (red) and $^{31}P\{^1H\}$ (green).

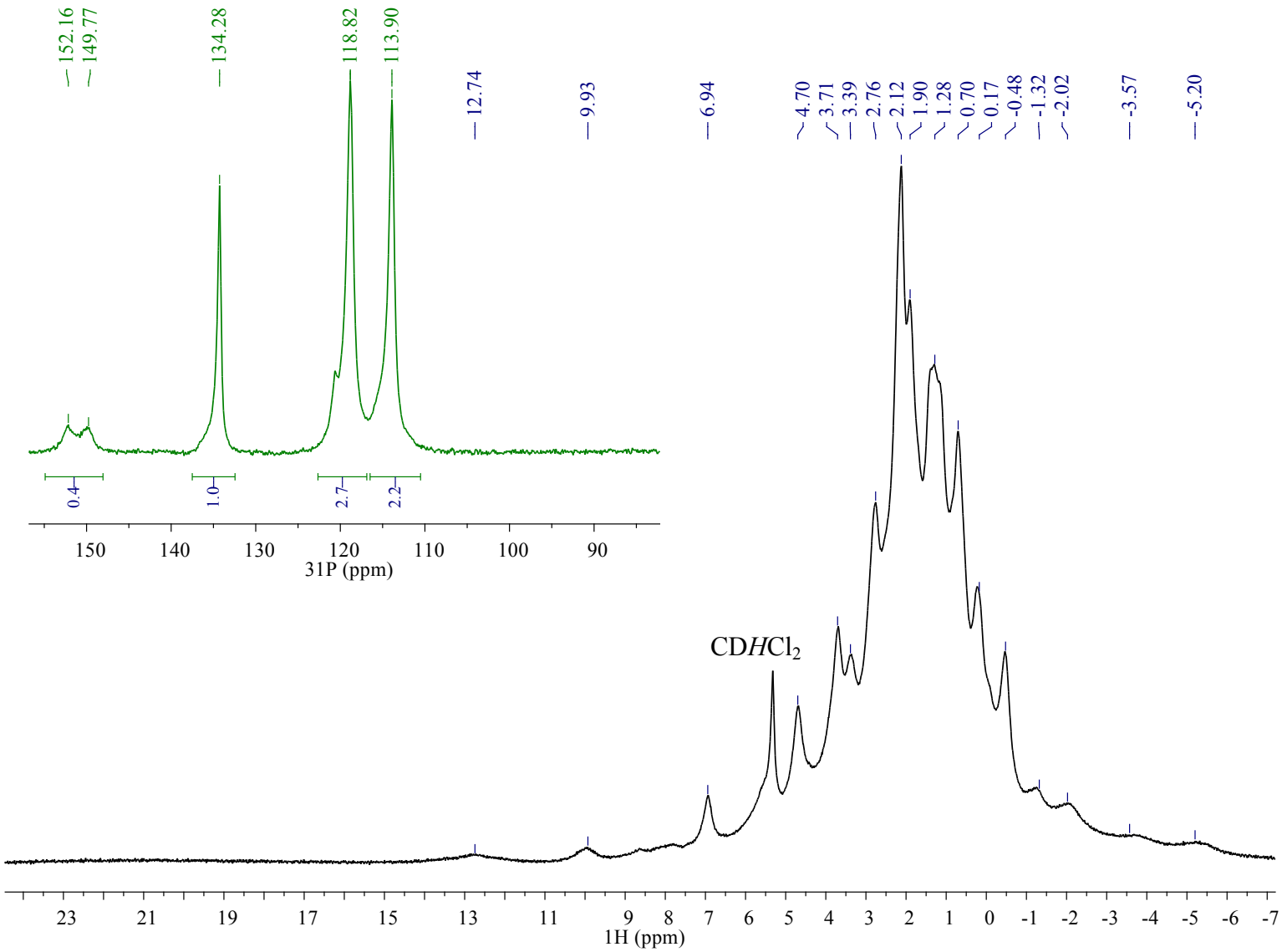

Figure S28. Multinuclear NMR spectra of **$CeBr_3(OPcy_3)_3$** at 187 K in CD_2Cl_2, ^1H (black), and $^{31}P\{^1H\}$ (green).

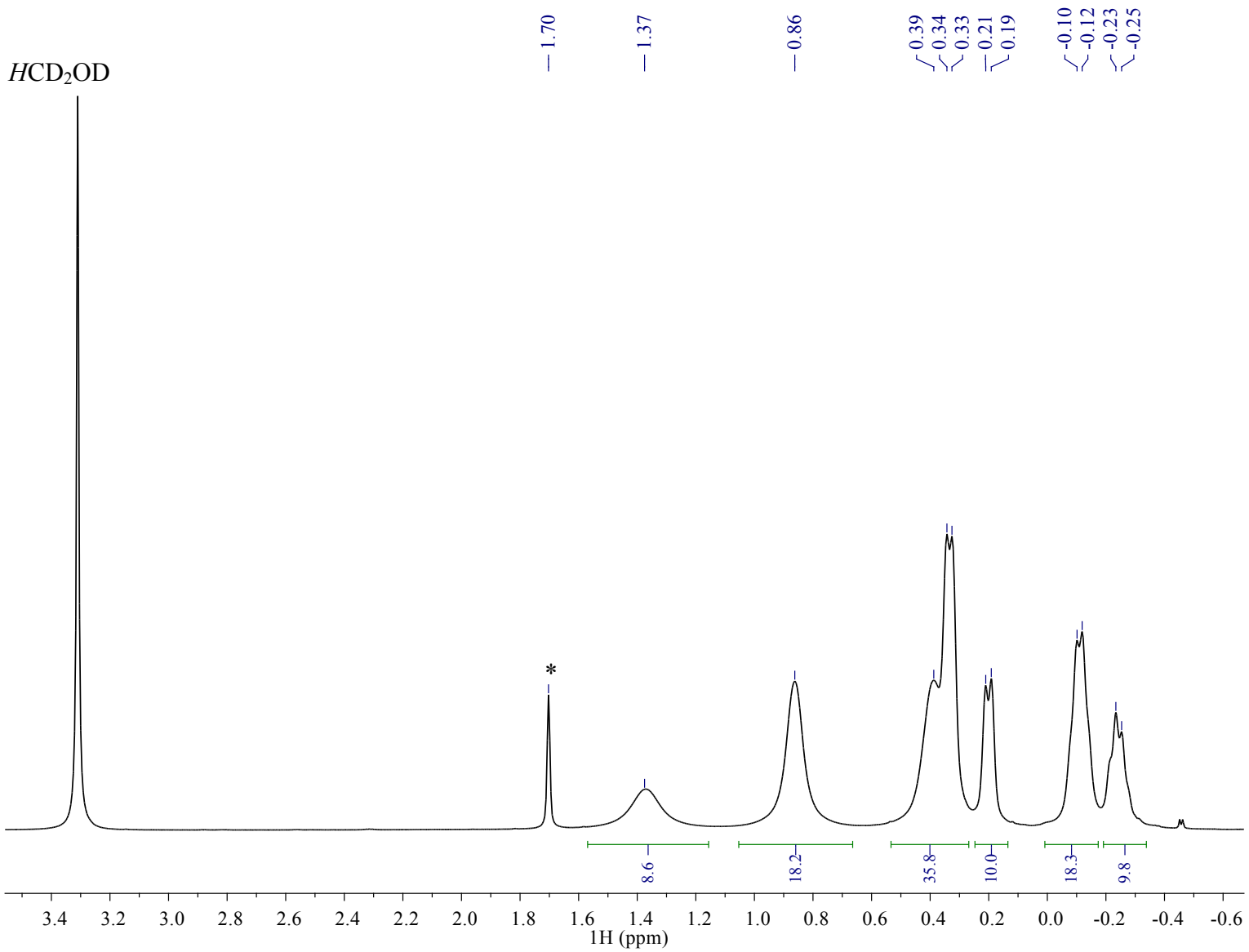

Figure S29. ^{1}H NMR spectrum of **$CeBr_3(OPcy_3)_3$** at 298 K in MeOD-d_4, *unidentified impurity.

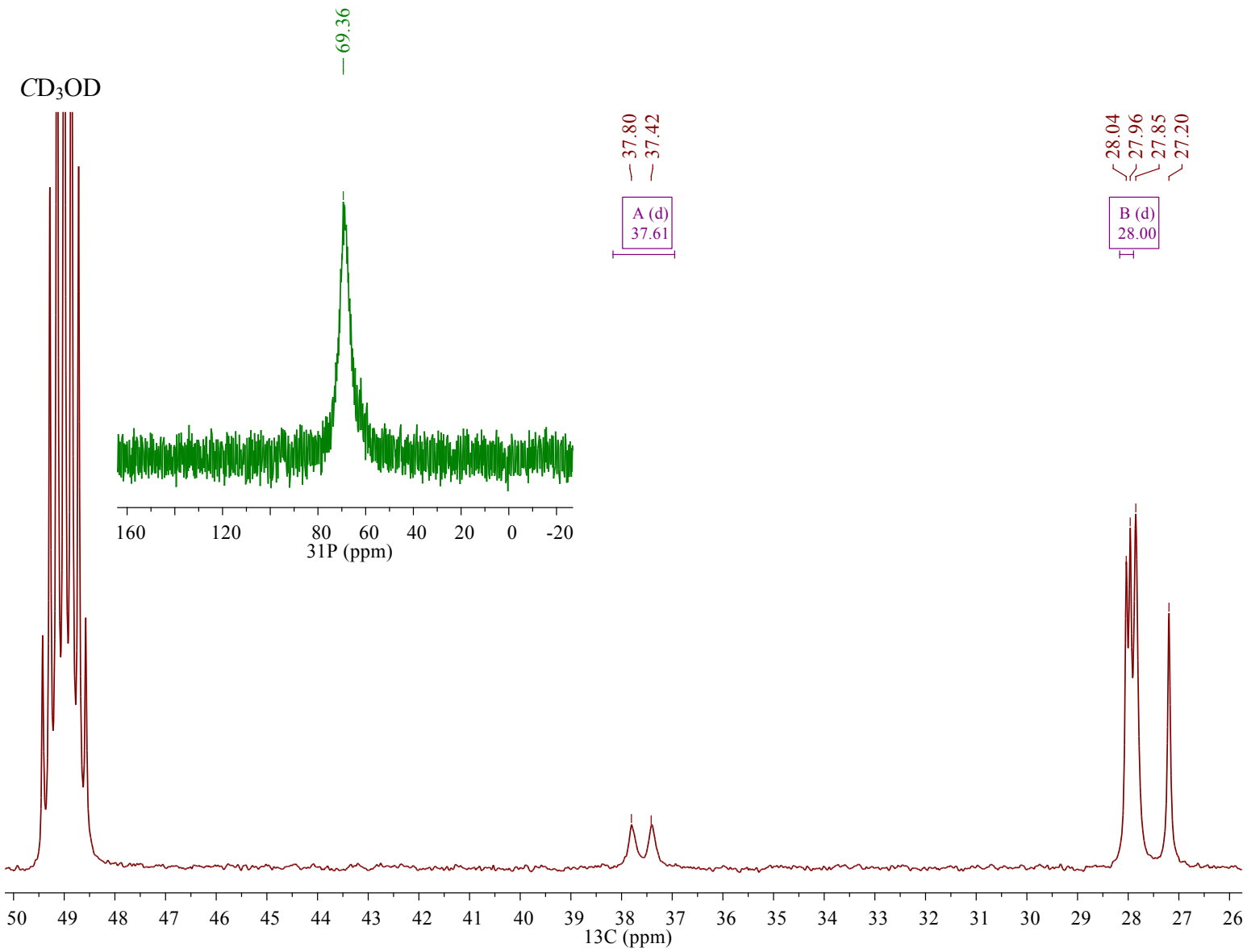

Figure S30. Multinuclear NMR spectra of **$CeBr_3(OPcy_3)_3$** at 298 K in MeOD-d_4, $^{13}C\{^1H\}$ (red) and $^{31}P\{^1H\}$ (green).

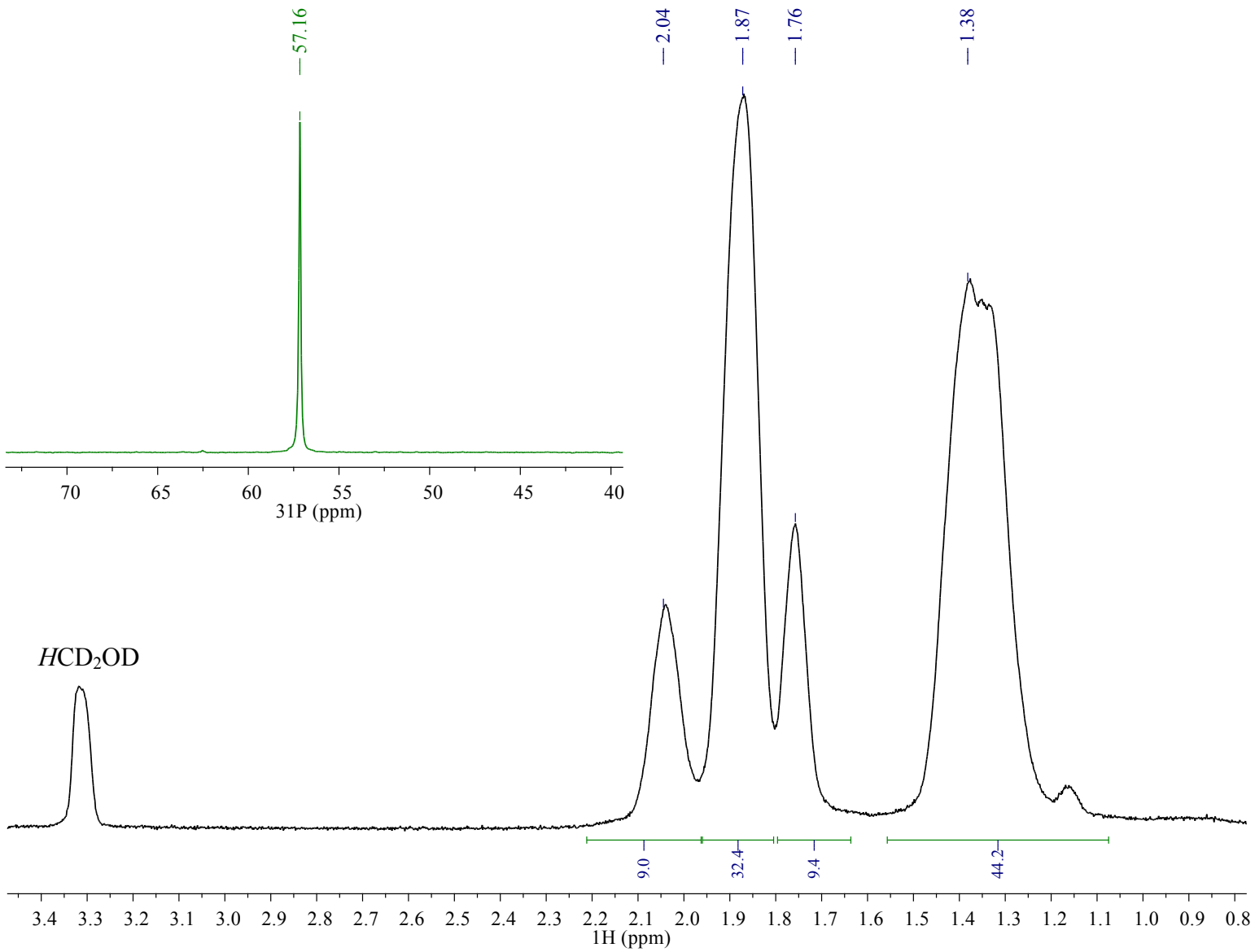

Figure S31. Multinuclear NMR spectra of **$CeBr_3(OPcy_3)_3$** at 187 K in MeOD-d_4, ^{1}H (black), and ^{31}P{^{1}H} (green).

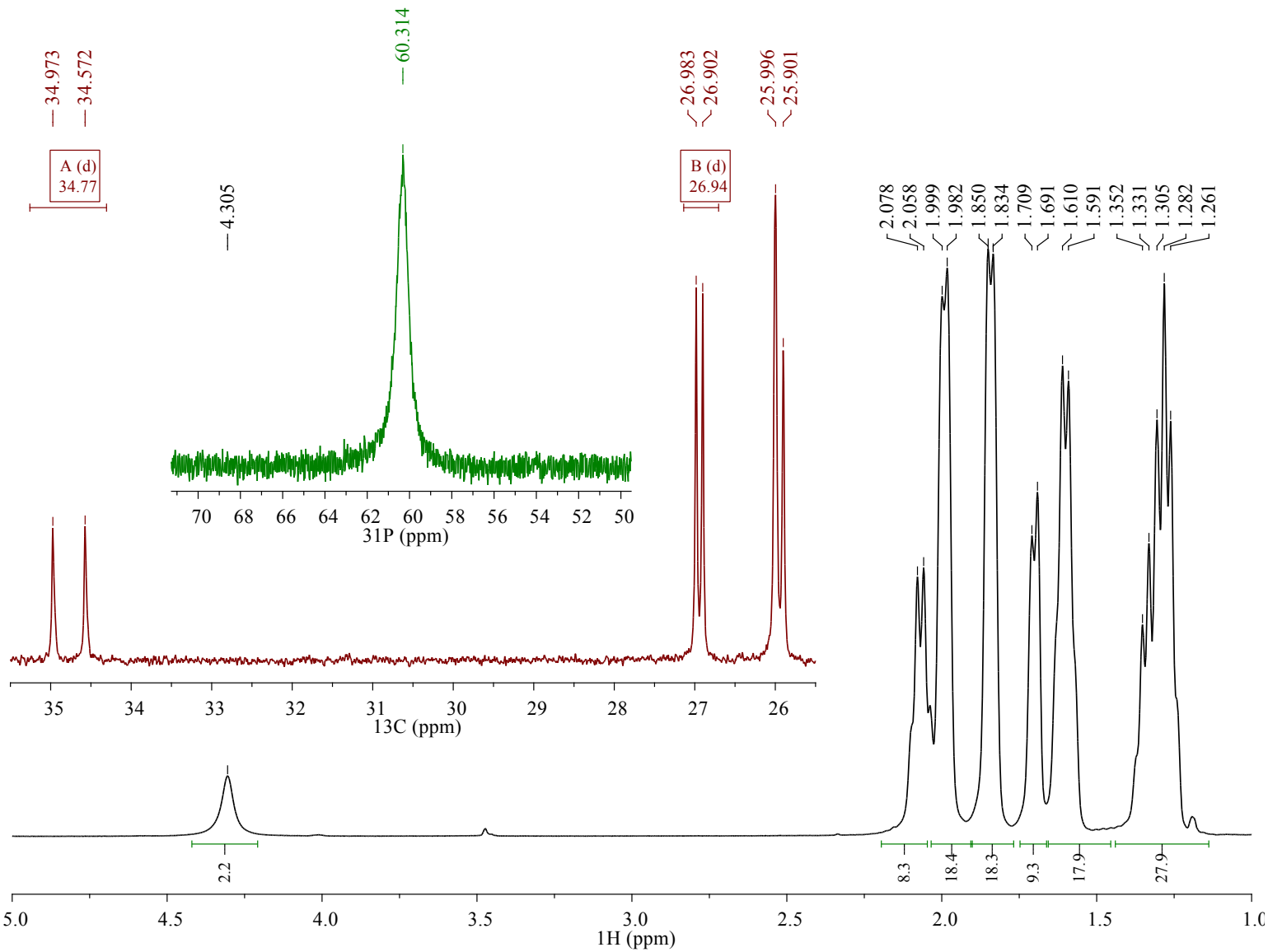

Figure S32. Multinuclear NMR spectra of **$LaBr_3(OPcy_3)_3$** at 298 K in $CDCl_3$, ^1H (black), $^{13}C\{^1H\}$ (red) and $^{31}P\{^1H\}$ (green).

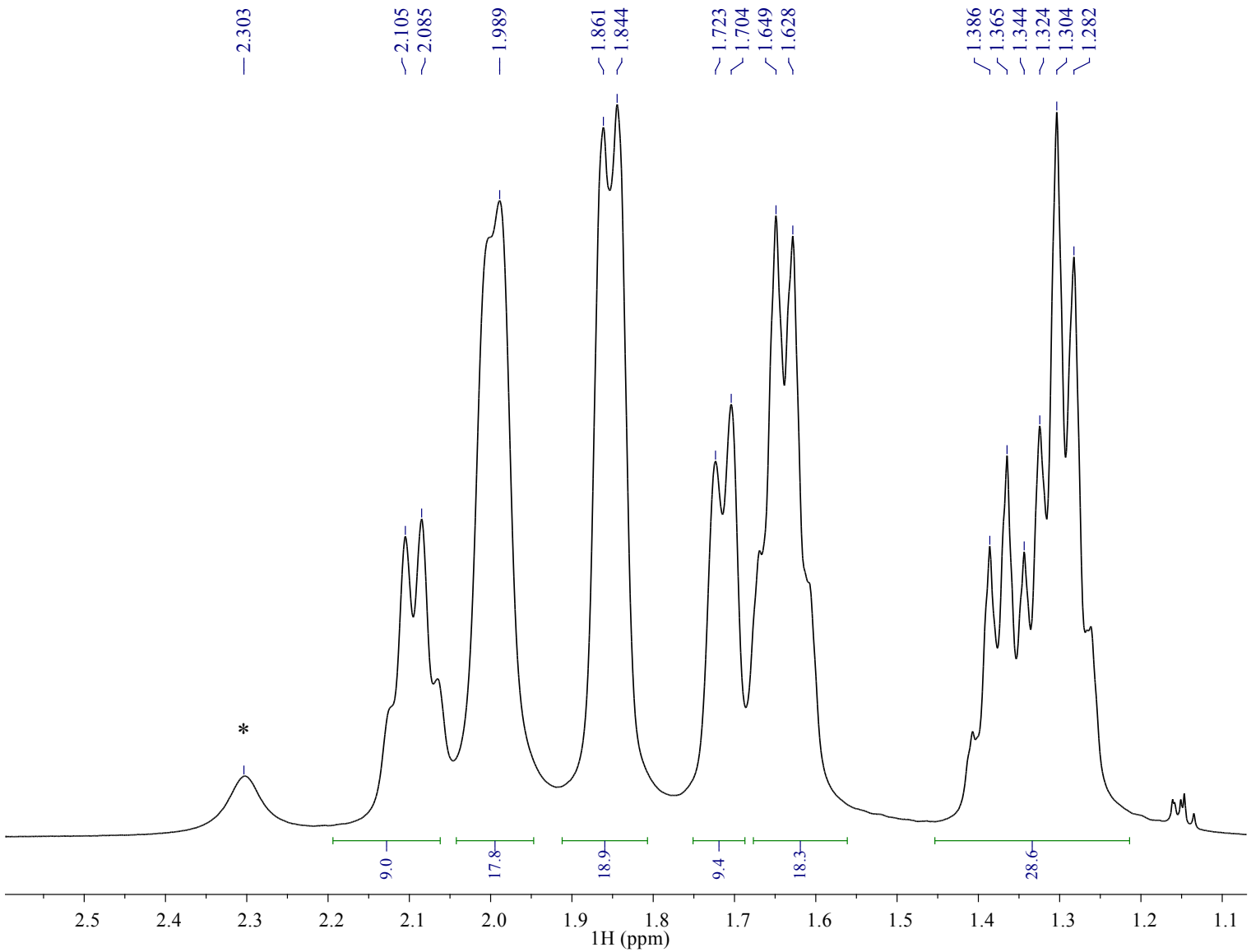

Figure S33. ^{1}H NMR spectrum of **$LaBr_3(OPcy_3)_3$** at 298 K in CD_2Cl_2, *unidentified impurity.

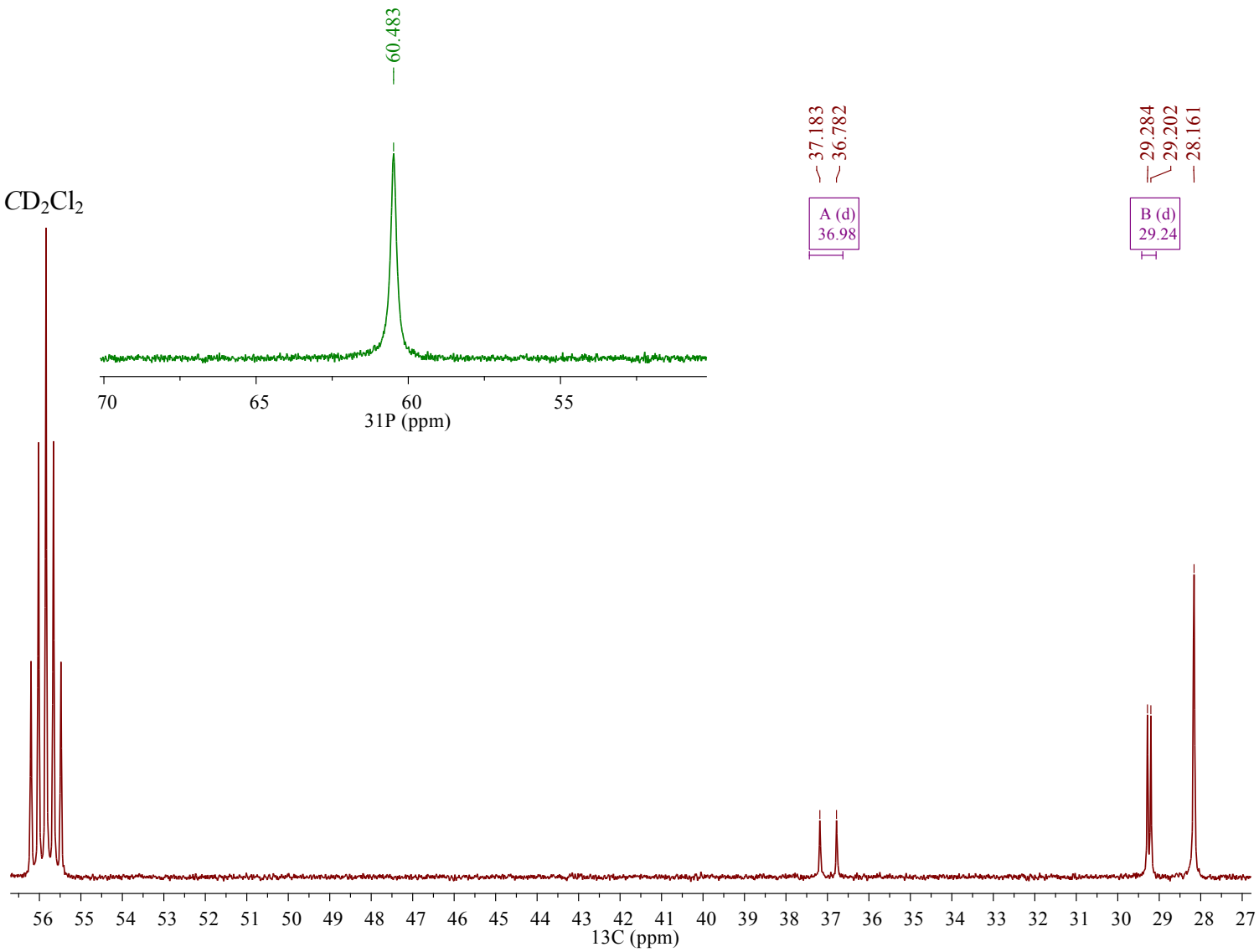

Figure S34. Multinuclear NMR spectra of **$LaBr_3(OPcy_3)_3$** at 298 K in CD_2Cl_2, $^{13}C\{^1H\}$ (red) and $^{31}P\{^1H\}$ (green).

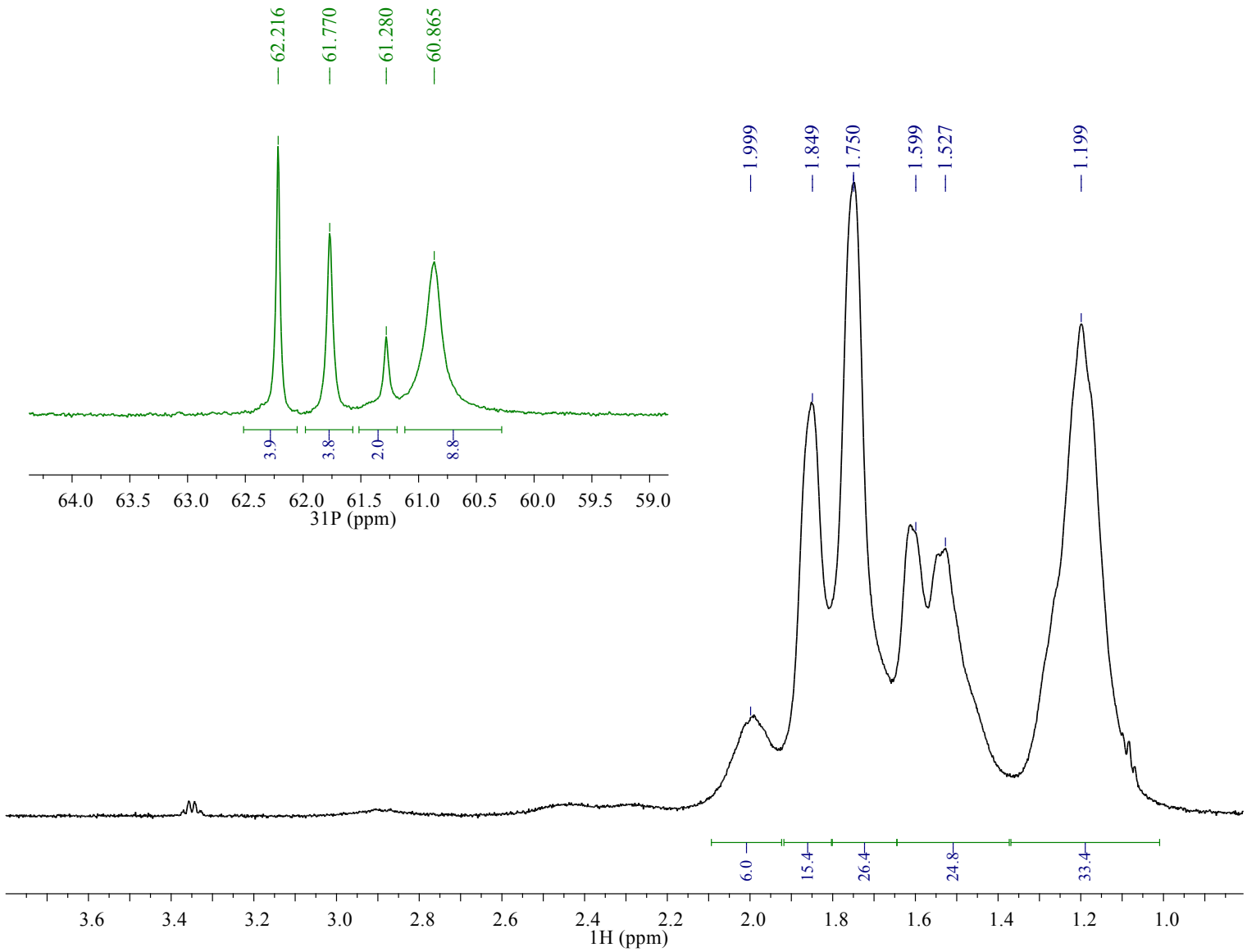

Figure S35. Multinuclear NMR spectra of **$LaBr_3(OPcy_3)_3$** at 187 K in CD_2Cl_2, ^1H (black), and $^{31}P\{^1H\}$ (green).

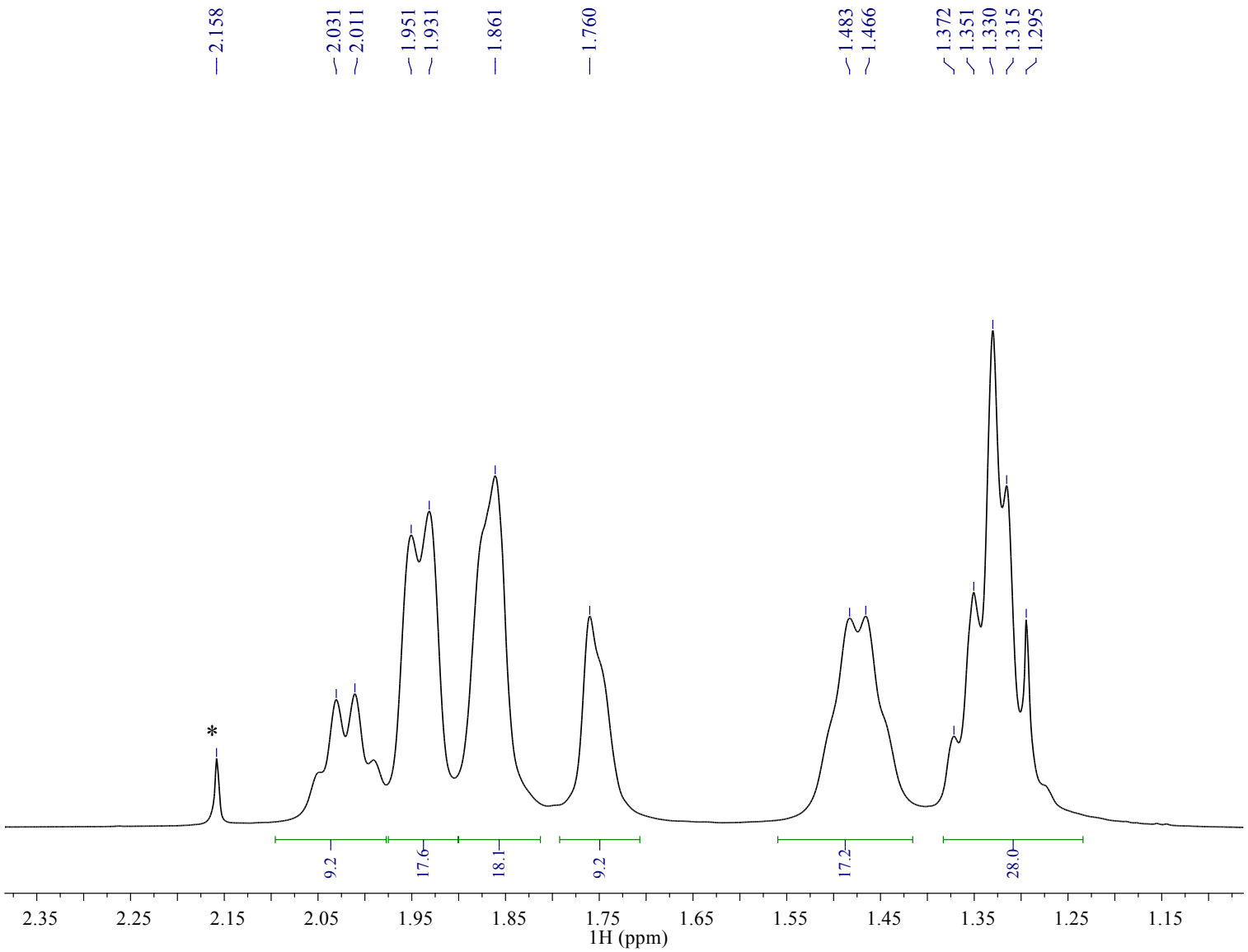

Figure S36. ^{1}H NMR spectrum of **$LaBr_3(OPcy_3)_3$** at 298 K in MeOD-d_4, *unidentified impurity.

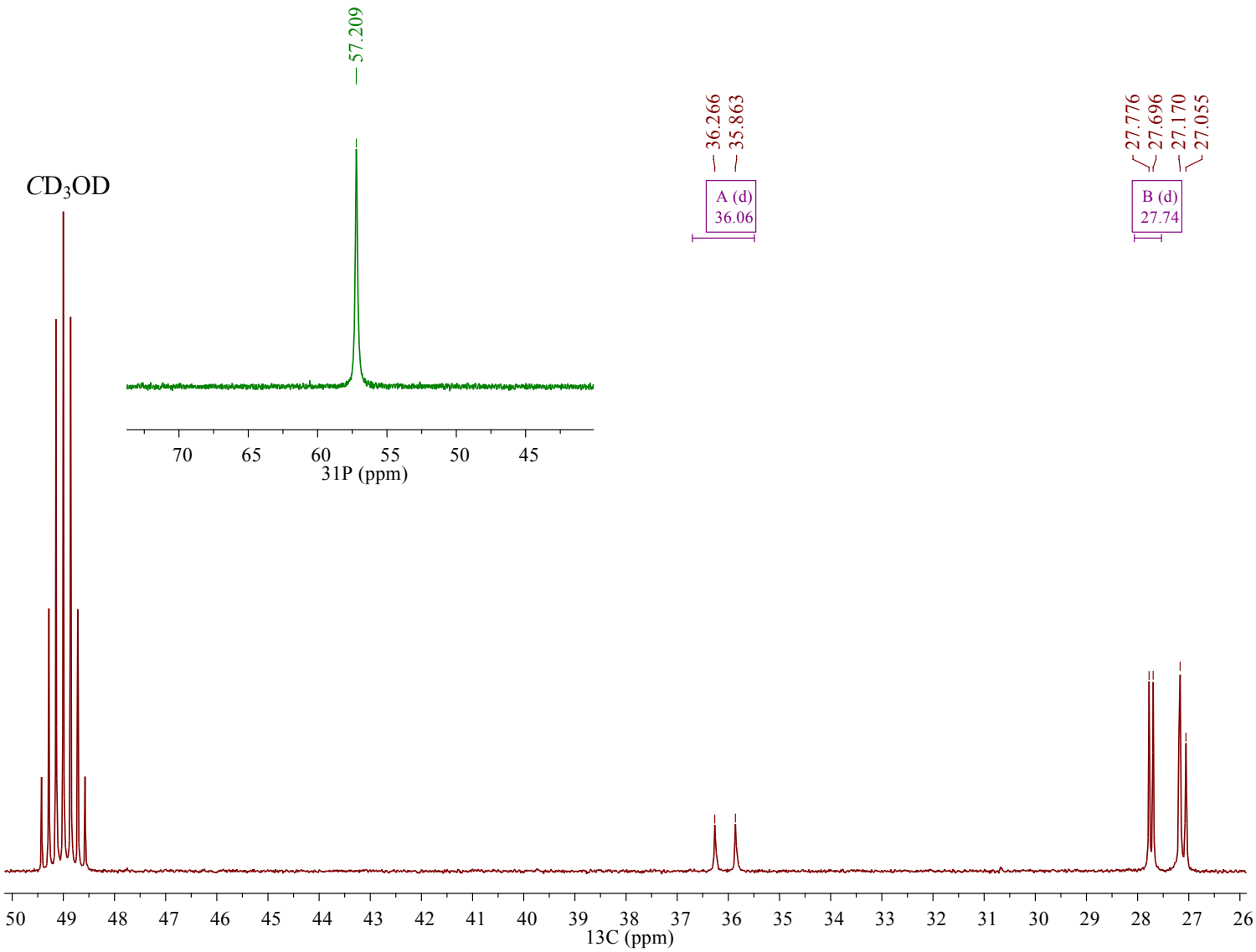

Figure S37. Multinuclear NMR spectra of **$LaBr_3(OPcy_3)_3$** at 298 K in MeOD-d_4, $^{13}C\{^1H\}$ (red) and $^{31}P\{^1H\}$ (green).

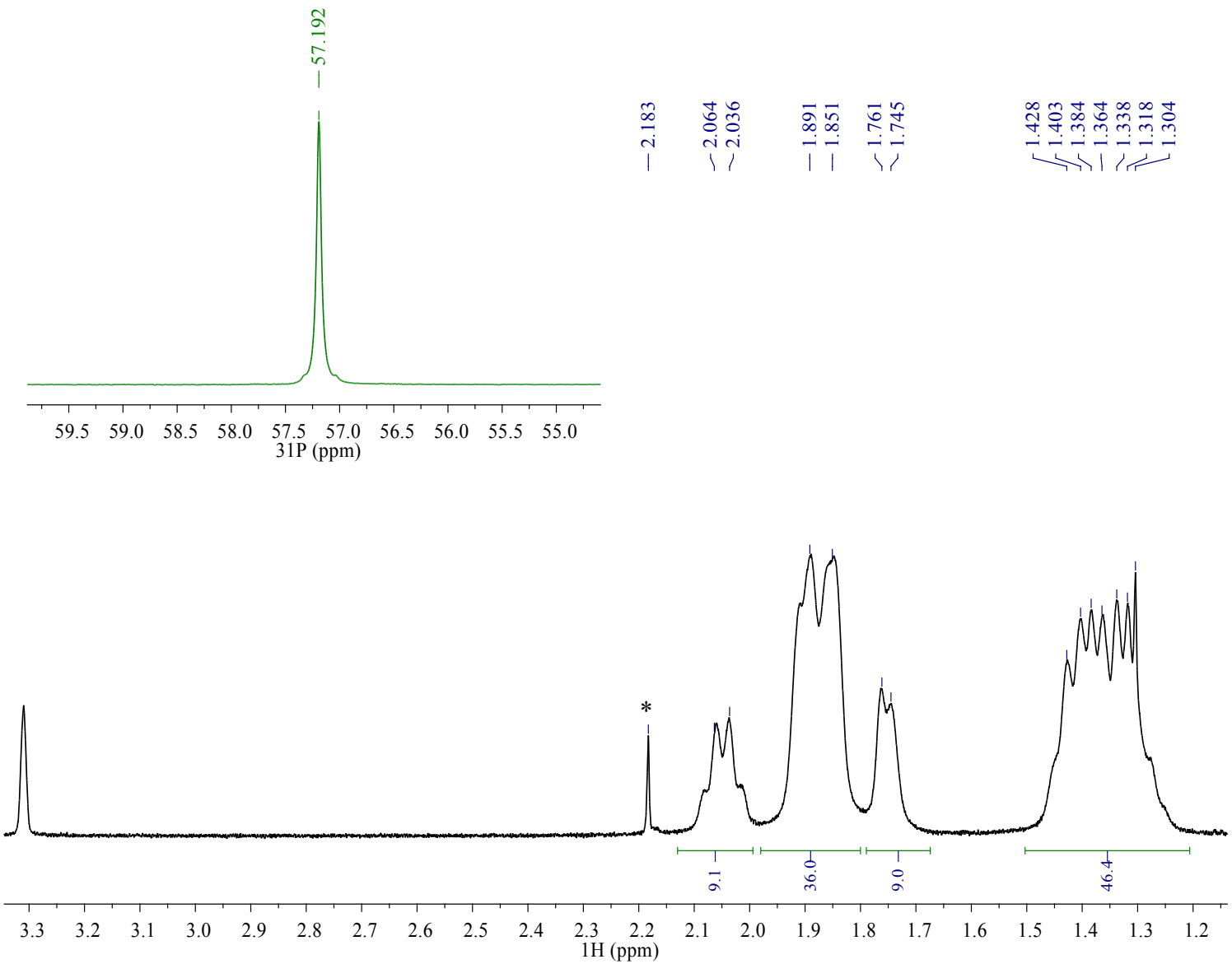

Figure S38. Multinuclear NMR spectra of **$LaBr_3(OPcy_3)_3$** at 187 K in MeOD-d_4, ^{1}H (black), and ^{31}P{^{1}H} (green), *unidentified impurity.

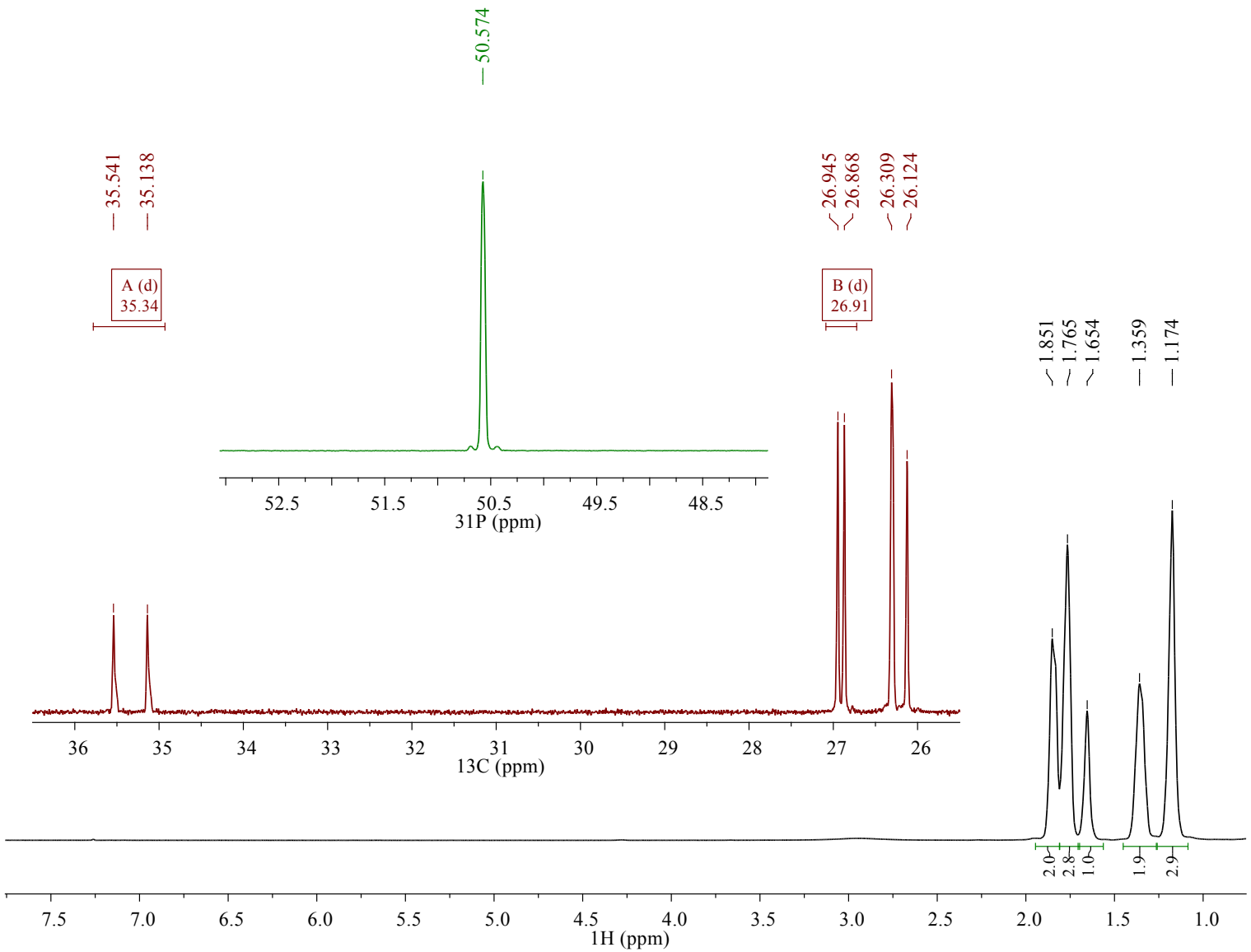

Figure S39. Multinuclear NMR spectra of **OPcy$_3$** at 298 K in $CDCl_3$, ^1H (black), $^{13}C\{^1H\}$ (red) and $^{31}P\{^1H\}$ (green).

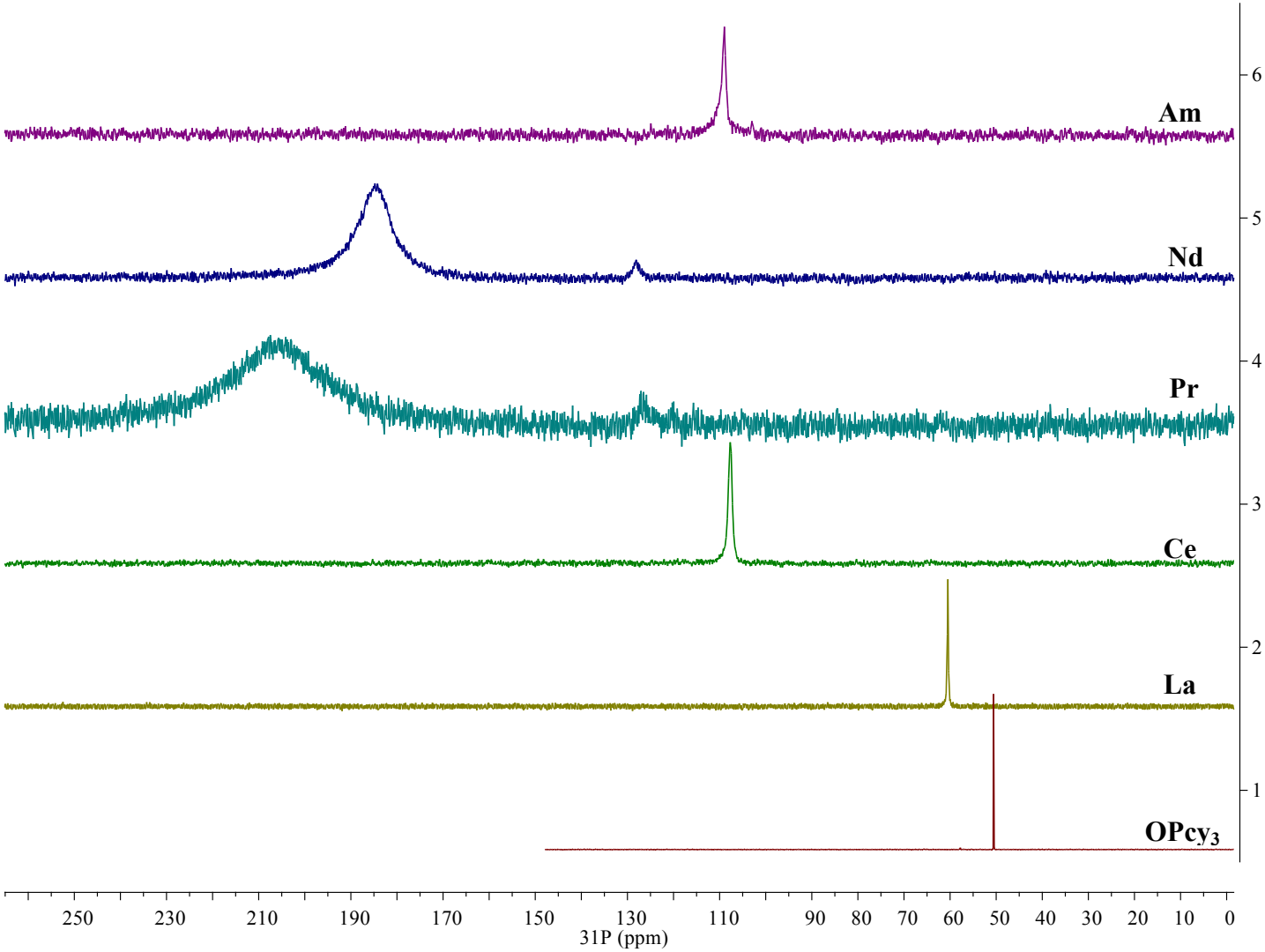

Figure S40. Stacked $^{31}P\{^{1}H\}$ NMR spectra of **$MBr_3(OPcy_3)_3$** (M = Am, Nd, Pr, Ce, La) including **$OPcy_3$** in $CDCl_3$ or CD_2Cl_2 at 298 K.

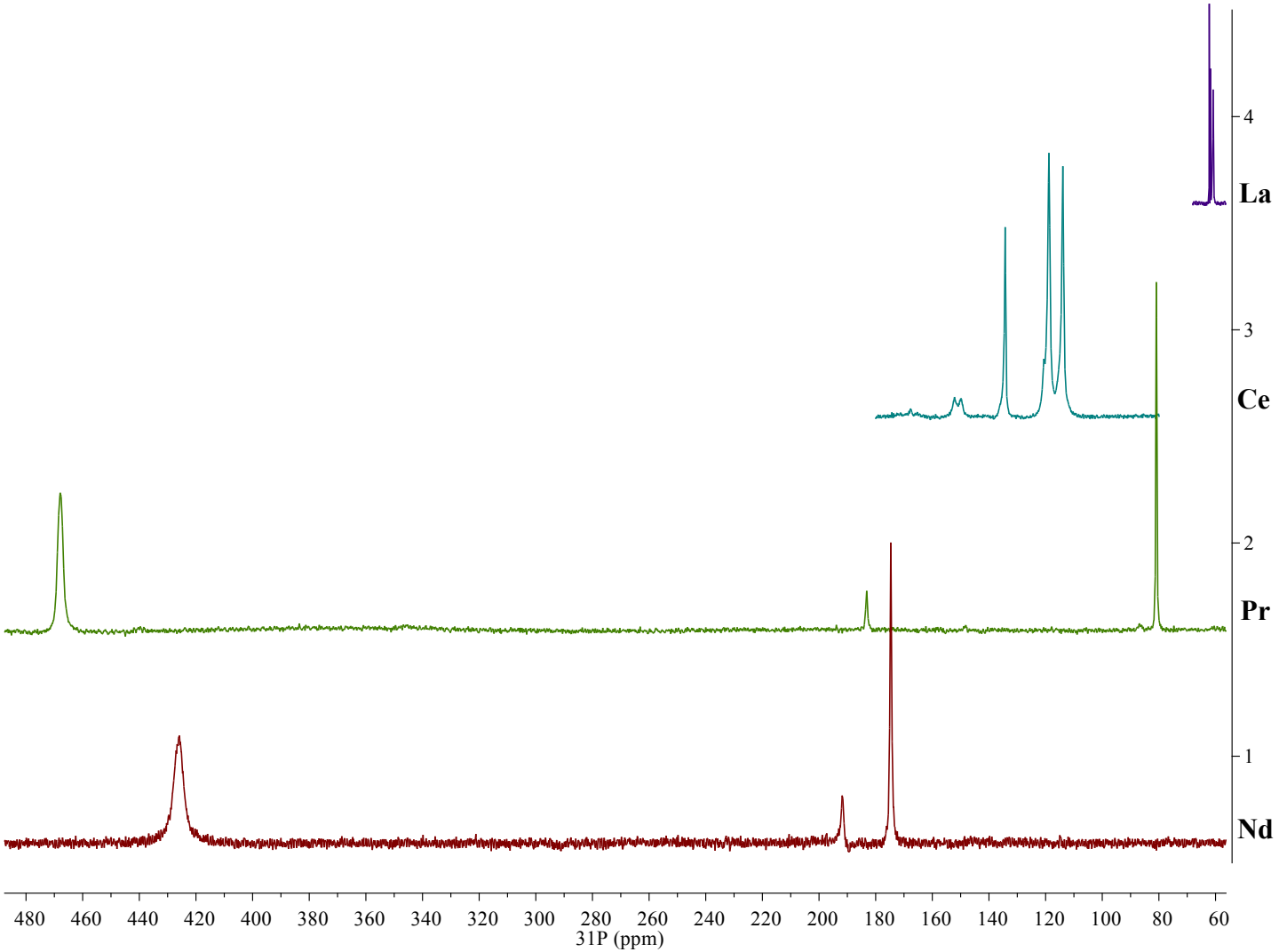

Figure S41. Stacked $^{31}P\{^{1}H\}$ NMR spectra of **$MBr_3(OPcy_3)_3$** (M = Nd, Pr, Ce, La) in CD_2Cl_2 at 187 K.

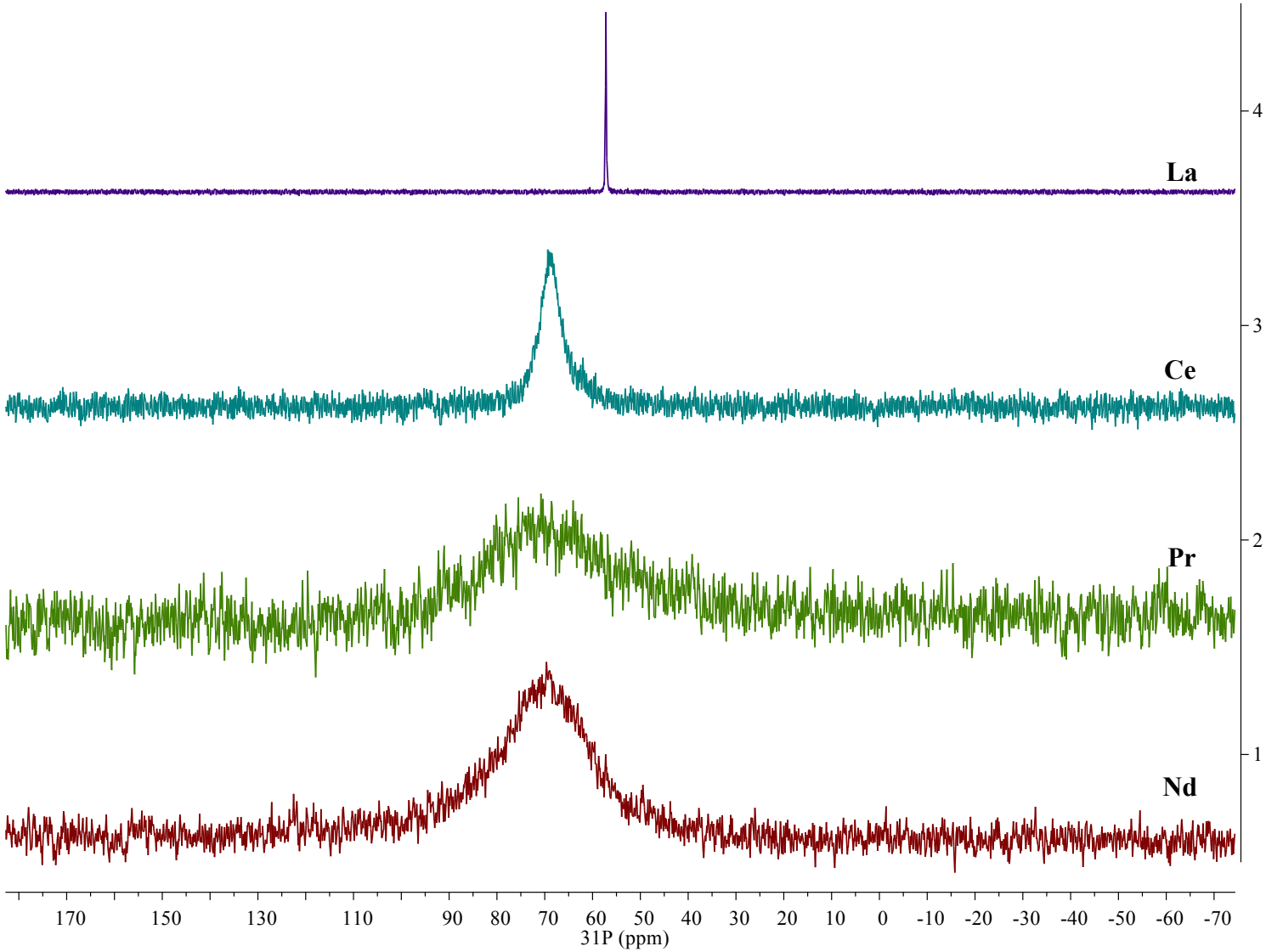

Figure S42. Stacked $^{31}P\{^{1}H\}$ NMR spectra of **$MBr_3(OPcy_3)_3$** (M = Nd, Pr, Ce, La) in MeOD-d_4 at 298 K.

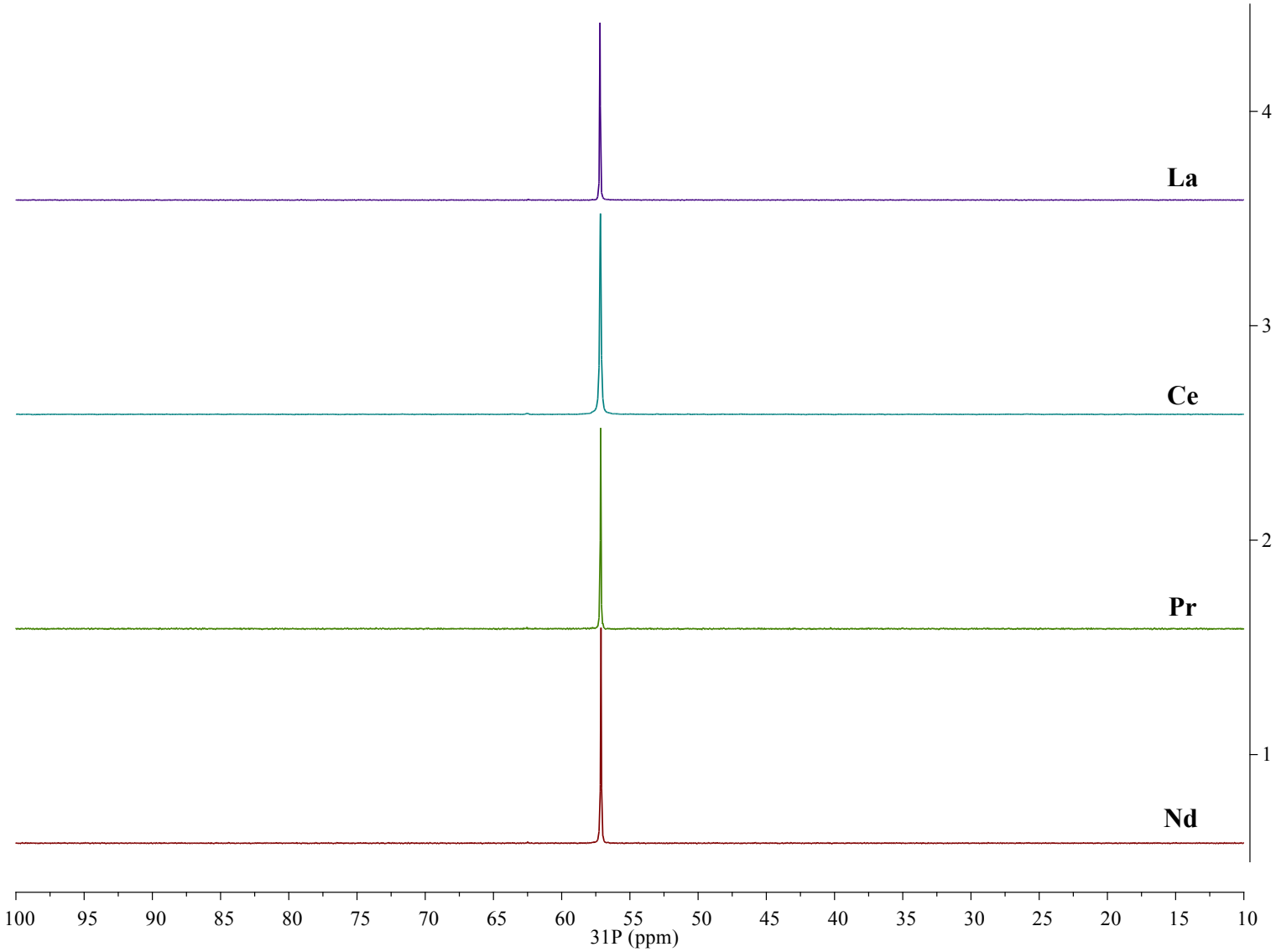

Figure S43. Stacked $^{31}P\{^{1}H\}$ NMR spectra of **$MBr_3(OPcy_3)_3$** (M = Nd, Pr, Ce, La) in MeOD-d_4 at 187 K.

THEORETICAL CALCULATIONS

Table S1. Bond distances (Å) of all-electron geometry optimizations of **$MBr_3(OPMe_3)_3$** (M = Ce, Nd, Am) in gas phase at PBE/TZP level of theory.

Bond	Ce	Nd	Am
M – O1	2.406	2.376	2.366
M – O2	2.406	2.389	2.364
M – O3	2.431	2.391	2.411
M – Br1	2.881	2.839	2.866
M – Br2	2.917	2.886	2.856
M – Br3	2.994	2.903	2.857

Table S2. QTAIM metrics derived from SR-CAS wave functions for **$MBr_3(OPcy)_3$** (M = Ce, Nd, Am) complexes. With the following definitions: ρ(r) – electron density, (eÅ^{-3}), δ(r) – delocalization indices, V(r) – potential energy density (kJmol^{-1}Å^{-3}), G(r) – kinetic energy density (kJmol^{-1}Å^{-3}), and H(r) – total energy density (kJmol^{-1}Å^{-3}). H(r)/ ρ(r) represents a "normalized" energy density per electron (kJmol^{-1}).

	ρ(r)			δ(r)			V(r)			G(r)		
	Ce	**Nd**	**Am**	**Ce**	**Nd**	**Am**	**Ce**	**Nd**	**Am**	**Ce**	**Nd**	**Am**
M(1)-Br(1)	0.257	0.269	0.283	0.232	0.217	0.151	−556.2	−600.1	−666.8	5.30	7.45	9.63
M(1)-Br(2)	0.261	0.264	0.285	0.209	0.173	0.119	−570.3	−586.0	−686.1	5.19	5.52	3.96
M(1)-Br(3)	0.246	0.251	0.268	0.241	0.308	0.239	−522.9	−547.4	−619.4	9.00	3.61	1.0
M(1)-O(1)	0.409	0.402	0.438	0.229	0.229	0.230	−136.9	−148.4	−159.0	5.54	6.15	1.84
M(1)-O(2)	0.407	0.401	0.486	0.262	0.268	0.207	−134.6	−144.1	−232.4	1.49	9.73	3.9
M(1	0.	0.	0.	0.	0.	0.	−1	−1	−1	1	1	1

)-O(3)	3.7329	3.7792	3.9822	2.6682	2.5972	2.8334	207.2	259.8	391.4	175.6	240.5	359.8

Table S2 Continued.

	|V(r)|/G(r)			H(r)			H(r)/ρ(r)		
	Ce	**Nd**	**Am**	**Ce**	**Nd**	**Am**	**Ce**	**Nd**	**Am**
M(1)-Br(1)	11.1001	11.1001	11.1031	−50.9	−52.6	−77.2	−1197.9	−1195.5	−2172.4
M(1)-Br(2)	11.1101	11.1001	11.1041	−54.4	−50.9	−82.5	−2107.7	−1192.3	−2184.8
M(1)-Br(3)	11.0109	11.0109	11.0112	−43.9	−43.9	−68.4	−1178.1	−1174.3	−2154.8
M(1)-O(1)	11.0054	11.0044	11.0044	−61.4	−57.9	−63.2	−1150.2	−1136.2	−1144.0
M(1)-O(2)	11.0054	11.0044	11.0044	−63.2	−54.4	−68.4	−1155.0	−1130.0	−1153.2
M(1)-O(3)	11.0100	11.0100	11.0100	−31.6	−19.3	−31.6	−84.6	−51.1	−79.3

	3 2 2		

Table S3. Molecular orbital (MO) composition of **$AmBr_3(OPMe_3)_3$** for the following orbital populations: Am – 6*p*, 5*f*, 6*d*; O – 2*s*, 2*p*; Br – 4*s*, 4*p*; P – 3*s*, 3*p*. Percentages in bold represent the main contribution to the MO. Energies given are relative to the first O 2*s* MO.

E(eV)	Molecular orbital composition								
	Am 6*p*	Am 5*f*	Am 6*d*	O 2*s*	O 2*p*	Br 4*s*	Br 4*p*	P 3*s*	P 3*p*
0.0	14%			**66%**				8%	4%
0.1	6%			**69%**	3%			11%	5%
0.4				**73%**	3%			11%	5%
2.6	**96%**					1%			
2.7	**89%**			1%	3%			2%	
2.8	**78%**			5%	7%			5%	
8.1						**100%**			
8.3						**100%**			
8.4	2%					**97%**			
14.7					**31%**				
14.8					**42%**				10%
15.4				5%	**40%**				5%
17.4			3%		**64%**				
17.5			2%		**68%**				
17.7			3%		**61%**				
17.7					**68%**				
17.8					**66%**				
17.9					**66%**				
18.9			4%				**84%**		
19.5		3%	3%				**87%**		
19.7		2%	3%				**91%**		
19.8		6%	3%				**88%**		
19.9		3%					**93%**		
20.0			2%				**92%**		
20.0		4%					**91%**		
20.0		2%					**92%**		
20.3		2%					**97%**		
22.2		**100%**							
22.3		**95%**					1%		
22.3		**100%**							
22.3		**95%**					1%		
22.5		**89%**					4%		
22.5		**89%**					6%		
22.5		**91%**							

Table S4. Molecular orbital (MO) composition of **$CeBr_3(OPMe_3)_3$** for the following orbital populations: Ce – 5*p*, 4*f*, 5*d*; O – 2*s*, 2*p*; Br – 4*s*, 4*p*; P – 3*s*, 3*p*. Percentages in bold represent the main contribution to the MO. Energies given are relative to the first O 2*s* MO.

E(eV)	Molecular orbital composition								
	Ce 5*p*	Ce 4*f*	Ce 5*d*	O 2*s*	O 2*p*	Br 4*s*	Br 4*p*	P 3*s*	P 3*p*
0.0	2%			**71%**	4%			11%	6%
0.1	4%			**72%**	2%			10%	6%
0.3				**72%**	1%			12%	6%
4.6	**68%**				7%			9%	
4.7	**70%**				4%	1%			7%
4.8	**93%**					5%			
8.2						**100%**			
8.4	2%					**96%**			
8.5	5%					**94%**			
14.7					**37%**				
14.8				4%	**44%**				4%
15.5					**23%**				
17.3			3%		**64%**				1%
17.4			2%		**68%**				1%
17.5			3%		**67%**				
17.6					**69%**				
17.7					**69%**				
17.7					**70%**				
19.1			2%				**85%**		
19.6		1%	4%				**89%**		
19.8			6%				**90%**		
19.9		2%					**93%**		
19.9	2%						**94%**		
20.0			3%		1%		**93%**		
20.0							**100%**		
20.1			1%				**95%**		
20.4							**100%**		
23.5		**100%**							
23.6		**100%**							
23.6		**100%**							
23.6		**100%**							
23.7		**89%**					2%		
23.7		**94%**					3%		
23.7		**94%**							

Table S5. Molecular orbital (MO) composition of **$NdBr_3(OPMe_3)_3$** for the following orbital populations: Nd – 5*p*, 4*f*, 5*d*; O – 2*s*, 2*p*; Br – 4*s*, 4*p*; P – 3*s*, 3*p*. Percentages in bold represent the main contribution to the MO. Energies given are relative to the first O 2*s* MO.

E (eV)	Molecular orbital composition								
	Nd 5*p*	Nd 4*f*	Nd 5*d*	O 2*s*	O 2*p*	Br 4*s*	Br 4*p*	P 3*s*	P 3*p*
0.0	4%			**71%**	3%			10%	5%
0.0	6%			**70%**	1%			10%	4%
0.3				**72%**	4%			12%	8%
3.6	**82%**				6%			5%	
3.6	**89%**				3%	1%		3%	
3.7	**95%**					3%			
8.2			1%			**99%**			
8.4						**97%**			
8.4	3%					**97%**			
14.8			4%		**36%**				
14.8				4%	**42%**				4%
15.5	3%			6%	**46%**				6%
17.3			3%		**64%**				1%
17.5			2%		**69%**				1%
17.6			3%		**65%**				
17.7					**69%**				
17.7					**68%**				
17.8					**70%**				
19.1			6%				**85%**		
19.6		2%	4%				**88%**		
19.8			5%				**92%**		
19.9		4%	2%				**92%**		
19.9	2%						**94%**		
20.0			4%		2%		**93%**		
20.0		2%					**94%**		
20.0							**95%**		
20.4							**98%**		
22.3		**100%**							
22.3		**100%**							
22.4		**100%**							
22.4		**100%**							
22.5		**93%**					2%		
22.5		**93%**							
22.5		**93%**					4%		

Table S6. Slater-Condon parameters of the 5/6*p* semi-core electrons derived from LF-DFT for the free-ions, $[M(H_2O)_9]^{3+}$, and **$MBr_3(OPcy)_3$** complexes (M = Ce, Nd, Am).

	$F^2(p,p)$ (eV)			$\zeta_{5/6p}$ (eV)		
	Free-ion	$[M(H_2O)_9]^{3+}$	$MBr_3(OPcy)_3$	Free-ion	$[M(H_2O)_9]^{3+}$	$MBr_3(OPcy)_3$
Ce^{III}	7.715	5.557	2.320	1.774	1.454	0.938
Nd^{III}	7.970	6.259	4.520	2.063	1.754	1.492
Am^{III}	7.583	6.112	4.207	5.818	4.985	4.259

Table S7. Natural localized molecular orbitals (NLMOs) involving pseudo-core 5*s* (6*s*), 5*p* (6*p*), and 4*f* (5*f*) electrons in $MBr_3(OPMe_3)_3$ (M = Ce, Nd, Am). Uranyl has been also included as a reference structure with strong ITI.

$[UO_2]^{2+}$	**NLMO composition**	**Natural hybrid orbital composition**
NLMO (1)	100% U	99% 6*p* + 1% 5*f*
NLMO (2)	100% U	99% 6*p* + 1% 5*f*
NLMO (3)	100% U	98% 6*s* + 2% 6*d*
NLMO (4)	99.8% U	76% 6*p* + 24% 5*f*
	0.2% O	2% 2*s* + 98% 2*p*
$CeBr_3(OPMe_3)_3$	**NLMO composition**	**Natural hybrid orbital composition**
NLMO (1)	100% Ce	98% 5*p* + 2% 4*f*
NLMO (2)	100% Ce	2% 5*p* + 98% 4*f*
NLMO (3)	99.8% Ce	59% 5*s* + 41% 5*p*
	*0.2% O, P	
NLMO (4)	99.5% Ce	41% 5*s* + 59% 5*p*
	*0.5% O, P	
NLMO (5)	99.3% Ce	100% 5*p*
	*0.7% O, P	

$NdBr_3(OPMe_3)_3$	NLMO composition	Natural hybrid orbital composition
NLMO (1)	99.9% Nd	100% 5*p*
NLMO (2)	99.8% Nd	55% 5*s* + 43% 5*p* + 2% 4*f*
	*0.2% O, P	
NLMO (3)	99.8% Nd	100% 4*f*
	*0.2% O, P	
NLMO (4)	99.7% Nd	4% 5*s* + 96% 4*f*
	*0.3% O, P	
NLMO (5)	99.6% Nd	2% 5*s* + 2% 5*p* + 96% 4*f*
	*0.4% O, P	
NLMO (6)	99.6% Nd	40% 5*s* + 54% 5*p* + 6% 4*f*
	*0.4% O, P	
NLMO (7)	99.5% Nd	100% 5*p*
	*0.5% O, P	
$AmBr_3(OPMe_3)_3$	**NLMO composition**	**Natural hybrid orbital composition**
NLMO (1)	100% Am	98% 6*p* + 2% 5*f*
NLMO (2)	100% Am	2% 6*s* + 5% 6*p* + 93% 5*f*
NLMO (3)	99.9% Am	44% 6*s* + 42% 6*p* + 14% 5*f*
	*0.1% O, P	
NLMO (4)	99.9% Am	31% 6*s* + 21% 6*p* + 48% 5*f*
	*0.1% O, P	
NLMO (5)	99.8% Am	11% 6*s* + 26% 6*p* + 63% 5*f*
	0.2% O, P	
NLMO (6)	99.8% Am	32% 6*p* + 68% 5*f*
	*0.2% O, P	
NLMO (7)	99.7% Am	9% 6*s* + 29% 6*p* + 62% 5*f*
	*0.3% O, P	
NLMO (8)	99.7% Am	2% 6*s* + 10% 6*p* + 88% 5*f*
	*0.3% O, P	
NLMO (9)	99.6% Am	1% 6*s* + 10% 6*p* + 89% 5*f*
	*0.4% O, P	
NLMO (10)	99.3% Am	28% 6*p* + 72% 5*f*
	*0.7% O, P	

*O, P contributions are *sp* hybrid orbitals in different ratios, so they were not explicitly written for the sake of simplicity.

**All structures differ in number of NLMOs due to occupancy of *f*–electrons, i.e. in addition to the 4 orbitals (3*p* + 1*s*) U^{6+} corresponds to an f^0 configuration, Ce^{3+} to an f^1, Nd^{3+} to an f^3, and Am^{3+} to an f^6, giving rise to 4, 5, 7, and 10 NLMOs, respectively.

Table S8. NLMOs involving main Am–Ligand interactions in **$CeBr_3(OPMe_3)_3$**.

$CeBr_3(OPMe_3)_3$	**NLMO composition**	**Natural hybrid orbital composition**
NLMO (6)	2% Ce	1% 6*s* + 72% 5*d* + 27% 4*f*
	92% O1	100% 2*p*
	4% P1	76% 3*p* + 24% 3*d*
NLMO (7)	2% Ce	72% 5*d* + 28% 4*f*
	92% O2	100% 2*p*
	4% P2	76% 3*p* + 24% 3*d*
NLMO (8)	2% Ce	71% 5*d* + 29% 4*f*
	92% O3	100% 2*p*
	4% P3	76% 3*p* + 24% 3*d*
NLMO (9)	8% Ce	26% 6*s* + 57% 5*d* + 17% 4*f*
	92% Br1	31% 4*s* + 69% 4*p*
NLMO (10)	8% Ce	26% 6*s* + 57% 5*d* + 17% 4*f*
	87% Br2	31% 4*s* + 69% 4*p*
NLMO (11)	8% Ce	26% 6*s* + 57% 5*d* + 17% 4*f*
	89% Br3	31% 4*s* + 69% 4*p*

Table S9. NLMOs involving main Am–Ligand interactions in **$NdBr_3(OPMe_3)_3$**.

$NdBr_3(OPMe_3)_3$	**NLMO composition**	**Natural hybrid orbital composition**
NLMO (8)	1% Nd	1% 6*s* + 81% 5*d* + 18% 4*f*
	92% O1	100% 2*p*
	4% P1	76% 3*p* + 24% 3*d*
NLMO (9)	2% Nd	4% 6*s* + 71% 5*d* + 25% 4*f*
	92% O2	100% 2*p*
	4% P2	76% 3*p* + 24% 3*d*
NLMO (10)	1% Nd	81% 5*d* + 19% 4*f*
	92% O3	100% 2*p*
	4% P3	77% 3*p* + 23% 3*d*
NLMO (11)	10% Nd	24% 6*s* + 49% 5*d* + 27% 4*f*
	92% Br1	24% 4*s* + 76% 4*p*
NLMO (12)	10% Nd	24% 6*s* + 50% 5*d* + 26% 4*f*
	87% Br2	24% 4*s* + 76% 4*p*
NLMO (13)	9% Nd	24% 6*s* + 51% 5*d* + 25% 4*f*
	89% Br3	25% 4*s* + 75% 4*p*

Table S10. NLMOs involving main Am–Ligand interactions in **$AmBr_3(OPMe_3)_3$**.

$AmBr_3(OPMe_3)_3$	**NLMO composition**	**Natural hybrid orbital composition**
NLMO (11)	3% Am	10% 7*s* + 51% 6*d* + 39% 5*f*
	91% O1	3% 2*s* + 97% 2*p*
	4% P1	79% 3*p* + 21% 3*d*
NLMO (12)	3% Am	9% 7*s* + 56% 6*d* + 35% 5*f*
	91% O2	3% 2*s* + 97% 2*p*
	4% P2	79% 3*p* + 21% 3*d*
NLMO (13)	3% Am	10% 7*s* + 48% 6*d* + 42% 5*f*
	91% O3	3% 2*s* + 97% 2*p*
	4% P3	79% 3*p* + 21% 3*d*
NLMO (14)	13% Am	22% 7*s* + 39% 6*d* + 39% 5*f*
	87% Br1	17% 4*s* + 83% 4*p*
NLMO (15)	13% Am	22% 7*s* + 40% 6*d* + 38% 5*f*
	87% Br2	18% 4*s* + 82% 4*p*
NLMO (16)	11% Am	24% 7*s* + 47% 6*d* + 29% 5*f*
	89% Br3	21% 4*s* + 79% 4*p*

Further Electronic Structure Discussion.

The ground and low-lying excited states in **$AmBr_3(OPcy_3)_3$** were calculated to gain a better understanding what role the ligands play in bonding to americium. For comparison, the same calculations were performed on the cerium and neodymium complexes to determine the ground state multiplet splitting. The ground multiplet splitting in **$CeBr_3(OPcy_3)_3$** corresponds to the usual $J = {}^5/_2$ for a Ce(III) complex, and is reflected in the spitting of the low-lying Kramer's doublets (KDs) at 831.5 cm^{-1}. The closest reported value is 1036.6 cm^{-1} for **$\{(C_8H_6(SiMe_3)_2]_2Ce\}^-$**.[1] A simple calculation of the free-Ce(III) ion shows a splitting of 2 cm^{-1}, which highlights the role of the phosphine oxide ligand. When the same analysis is performed on **$NdBr_3(OPcy_3)_3$** a ground state $J = {}^9/_2$ multiplet that spans an energy window of 413.8 cm^{-1} is calculated and is comparable to the ~495 cm^{-1} experimentally determined value for Nd_2O_3 crystals.[2] Unfortunately, this analysis cannot be performed for **$AmBr_3(OPcy_3)_3$** because there is no splitting due to the $J = 0$ ground state. However, it is clear that the *quasi*-octahedral environment provides a strong ligand field environment capable of modifying the electronic properties of these complexes.

ITI COMPARISONS AND CALCULATIONS OF LITERATURE COMPOUNDS

Table S11. ITI Calculations of Newly Reported and Previously Reported **$LnBr_3(OPcy_3)_3$** Compounds.[a,b]

	La[c]	**La**[3]	**Ce**[c]	**Pr**[c]	**Pr**[3]	**Nd**[c]	**Nd**[3]	**Gd**[3]	**Ho**[3]
Radius (Å)	1.032	1.032	1.01	0.99	0.99	0.983	0.983	0.938	0.901
$ITI_{M–Br}$	99.1(1)	99.7(1)	99.0(2)	98.9(2)	98.7(5)	98.9(2)	98.7(3)	98.7(3)	98.7(3)
$ITI_{M–O}$	99.0(3)	99.0(3)	98.56(8)	98.4(2)	98.3(2)	98.6(3)	98.7(2)	99.0(1)	98.5(3)

[a]Given with calculated standard error in parentheses [b]6-Coordinate Shannon Ionic Radius.[4] [c]This work

Table S12. ITI Calculations of **$LnI_3(Et_2O)_3$** Compounds.[5,a,b]

	Ce	**Pr**	**Nd**	**Sm**	**Gd**	**Tb**
Radius (Å)	1.01	0.99	0.983	0.958	0.938	0.923
$ITI_{M–I}$	101.21(2)	101.22(2)	99.87[7]	101.16(2)	100.96(2)	101.00(2)
$ITI_{M–O}$	95.8(1)	95.4(2)	97.6[7]	95.1(2)	96.1(1)	95.9(2)

[a]Given with calculated standard errors in parentheses and propagated error in square brackets. [b]6-Coordinate Shannon Ionic Radius.[4]

Table S13. ITI Calculations of **$LnCl_3(HMPA)_3$** Compounds.[a,b]

	Pr[6]	**Dy**[7]	**Yb**[8]
Radius (Å)	0.99	0.912	0.868
$ITI_{M–Cl}$	100.8(1)	100.4(1)	100.3(1)
$ITI_{M–O}$	100.1(1)	98.92(2)	100.3(1)

[a]Given with calculated standard errors in parentheses. [b]6-Coordinate Shannon Ionic Radius.[4]

Table S14. ITI Calculations of **$YbX_3(THF)_3$** Compounds.[a]

	Cl[9]	**Br**[10]	**I**[11]
$ITI_{M–X}$	100.7(1)	101.6[1]	101.34[2]
$ITI_{M–O}$	96.9(5)	96.8[5]	97.3[3]

[a]Given with calculated standard errors in parentheses and propagated error in square brackets.

CRYSTALLOGRAPHY

Table S15. Summary of Crystallographic Collections for **$MBr_3(OPcy_3)_3$**.

Compound	**Am**	**La**	**Ce**	**Pr**	**Nd**
Empirical Formula	$C_{54}H_{99}O_3P_3Br_3Am$	$C_{54}H_{99}O_3P_3Br_3La$	$C_{54}H_{99}O_3P_3Br_3Ce$	$C_{54}H_{99}O_{3.5}P_3Br_3Pr$	$C_{54}H_{99}O_3P_3Br_3Nd$
Temperature (K)	120(2)	130(2)	120(2)	120(2)	120(2)
Crystal System	Orthorhombic	Orthorhombic	Orthorhombic	Orthorhombic	Orthorhombic
Space Group	$Pca2_1$	$Pca2_1$	$Pca2_1$	$Pca2_1$	$Pca2_1$
***a* (Å)**	28.768(9)	28.879(2)	28.920(5)	28.716(1)	28.706(1)
***b* (Å)**	11.456(4)	11.4223(7)	11.434(2)	11.4126(4)	11.4228(4)
***c* (Å)**	18.185(6)	18.208(1)	18.209(3)	18.1299(8)	18.1359(7)
α (°)	90	90	90	90	90
β (°)	90	90	90	90	90
γ (°)	90	90	90	90	90
Volume (Å^3)	5993(3)	6006.3(6)	6021(2)	5941.5(4)	5946.8(4)
Z	4	4	4	4	4
ρ_{calcd} (Mg/m^3)	1.521	1.402	1.400	1.420	1.422
μ (mm^{-1})	3.398	2.824	2.864	2.956	3.007
R1^a ($I > 2.0\sigma$(I))	0.0399	0.0348	0.0353	0.0317	0.0405
wR2 (all data)	0.0858	0.0620	0.0726	0.0617	0.0777
BASF	0.02978	0.01767	0.03608	0.00891	-0.00554

[a]Definitions: $wR2 = \{\Sigma[w(F_o^2-F_c^2)^2] / \Sigma[w(F_o^2)^2]\}^{1/2}$ $R1 = \Sigma||F_o|-|F_c|| / \Sigma|F_o|$

Goof = $S = \{\Sigma[w(F_o^2-F_c^2)^2] / (n-p)\}^{1/2}$ where n is the number of reflections and p is the total number of parameters refined.

Table S16. Relevant bond lengths [Å] and angles [°] for **$AmBr_3(OPcy_3)_3$**.

Am(1)-Br(1)	2.882(1)	O(1)-Am(1)-Br(2)	89.73(19)
Am(1)-Br(2)	2.870(1)	O(1)-Am(1)-Br(3)	89.44(18)
Am(1)-Br(3)	2.912(1)	O(1)-Am(1)-O(3)	90.2(3)
Am(1)-O(1)	2.312(7)	O(2)-Am(1)-Br(1)	90.44(18)
Am(1)-O(2)	2.302(7)	O(2)-Am(1)-Br(2)	91.00(18)
Am(1)-O(3)	2.349(6)	O(2)-Am(1)-Br(3)	88.81(18)
P(1)-O(1)	1.520(8)	O(2)-Am(1)-O(1)	178.1(2)
P(2)-O(2)	1.523(7)	O(2)-Am(1)-O(3)	91.6(3)
P(3)-O(3)	1.518(6)	O(3)-Am(1)-Br(1)	87.6(2)
		O(3)-Am(1)-Br(2)	85.2(2)
Br(1)-Am(1)-Br(3)	95.60(5)	O(3)-Am(1)-Br(3)	176.7(2)
Br(2)-Am(1)-Br(1)	172.74(3)	P(1)-O(1)-Am(1)	159.4(5)
Br(2)-Am(1)-Br(3)	91.54(5)	P(2)-O(2)-Am(1)	164.8(5)
O(1)-Am(1)-Br(1)	89.05(18)	P(3)-O(3)-Am(1)	170.8(5)

Table S17. Relevant bond lengths [Å] and angles [°] for **$LaBr_3(OPcy_3)_3$**.

La(1)-Br(1)	2.9365(7)	O(1)-La(1)-Br(2)	90.73(10)
La(1)-Br(2)	2.9425(7)	O(1)-La(1)-Br(3)	88.27(9)
La(1)-Br(3)	2.9649(5)	O(1)-La(1)-O(2)	178.16(13)
La(1)-O(1)	2.351(4)	O(1)-La(1)-O(3)	91.97(14)
La(1)-O(2)	2.363(4)	O(2)-La(1)-Br(1)	89.62(10)
La(1)-O(3)	2.382(3)	O(2)-La(1)-Br(2)	88.79(10)
P(1)-O(1)	1.511(4)	O(2)-La(1)-Br(3)	90.01(10)
P(2)-O(2)	1.513(4)	O(2)-La(1)-O(3)	89.78(15)
P(3)-O(3)	1.513(3)	O(3)-La(1)-Br(1)	85.23(12)
		O(3)-La(1)-Br(2)	87.53(12)
Br(1)-La(1)-Br(2)	172.59(2)	O(3)-La(1)-Br(3)	176.61(12)
Br(1)-La(1)-Br(3)	91.39(3)	P(1)-O(1)-La(1)	166.3(2)
Br(2)-La(1)-Br(3)	95.84(3)	P(2)-O(2)-La(1)	160.7(2)
O(1)-La(1)-Br(1)	91.08(10)	P(3)-O(3)-La(1)	170.9(3)

Table S18. Relevant bond lengths [Å] and angles [°] for **$CeBr_3(OPcy_3)_3$**.

Ce(1)-Br(1)	2.9268(8)	O(1)-Ce(1)-Br(2)	91.16(10)
Ce(1)-Br(2)	2.9166(8)	O(1)-Ce(1)-Br(3)	88.33(11)
Ce(1)-Br(3)	2.9504(8)	O(1)-Ce(1)-O(2)	177.66(14)
Ce(1)-O(1)	2.332(4)	O(1)-Ce(1)-O(3)	92.37(16)
Ce(1)-O(2)	2.336(4)	O(2)-Ce(1)-Br(1)	89.08(11)
Ce(1)-O(3)	2.368(4)	O(2)-Ce(1)-Br(2)	89.55(11)
P(1)-O(1)	1.516(4)	O(2)-Ce(1)-Br(3)	89.42(11)
P(2)-O(2)	1.515(4)	O(2)-Ce(1)-O(3)	89.91(16)
P(3)-O(3)	1.523(4)	O(3)-Ce(1)-Br(1)	87.42(13)
		O(3)-Ce(1)-Br(2)	85.48(13)
Br(1)-Ce(1)-Br(3)	95.47(3)	O(3)-Ce(1)-Br(3)	177.02(12)
Br(2)-Ce(1)-Br(1)	172.78(2)	P(1)-O(1)-Ce(1)	166.2(3)
Br(2)-Ce(1)-Br(3)	91.61(3)	P(2)-O(2)-Ce(1)	171.2(3)
O(1)-Ce(1)-Br(1)	90.50(10)	P(3)-O(3)-Ce(1)	160.7(3)

Table S19. Relevant bond lengths [Å] and angles [°] for **$PrBr_3(OPcy_3)_3$**.

Pr(1)-Br(1)	2.8781(7)	O(1)-Pr(1)-Br(2)	90.53(10)
Pr(1)-Br(2)	2.8894(7)	O(1)-Pr(1)-Br(3)	88.55(10)
Pr(1)-Br(3)	2.9145(5)	O(1)-Pr(1)-O(2)	177.63(13)
Pr(1)-O(1)	2.294(4)	O(1)-Pr(1)-O(3)	92.17(15)
Pr(1)-O(2)	2.302(4)	O(2)-Pr(1)-Br(1)	89.61(10)
Pr(1)-O(3)	2.336(3)	O(2)-Pr(1)-Br(2)	89.18(10)
P(1)-O(1)	1.514(4)	O(2)-Pr(1)-Br(3)	89.13(10)
P(2)-O(2)	1.515(4)	O(2)-Pr(1)-O(3)	90.17(15)
P(3)-O(3)	1.510(3)	O(3)-Pr(1)-Br(1)	85.72(12)
		O(3)-Pr(1)-Br(2)	87.57(12)
Br(1)-Pr(1)-Br(2)	173.18(2)	O(3)-Pr(1)-Br(3)	177.02(11)
Br(1)-Pr(1)-Br(3)	91.37(3)	P(1)-O(1)-Pr(1)	165.4(3)
Br(2)-Pr(1)-Br(3)	95.32(2)	P(2)-O(2)-Pr(1)	159.6(3)
O(1)-Pr(1)-Br(1)	90.95(10)	P(3)-O(3)-Pr(1)	171.0(3)

Table S20. Relevant bond lengths [Å] and angles [°] for **$NdBr_3(OPcy_3)_3$**.

Nd(1)-Br(1)	2.8796(8)	O(1)-Nd(1)-Br(2)	90.45(13)
Nd(1)-Br(2)	2.8908(9)	O(1)-Nd(1)-Br(3)	88.59(12)
Nd(1)-Br(3)	2.9168(6)	O(1)-Nd(1)-O(2)	177.70(16)
Nd(1)-O(1)	2.297(5)	O(1)-Nd(1)-O(3)	92.20(19)
Nd(1)-O(2)	2.309(5)	O(2)-Nd(1)-Br(1)	89.81(14)
Nd(1)-O(3)	2.336(4)	O(2)-Nd(1)-Br(2)	88.95(13)
P(1)-O(1)	1.513(5)	O(2)-Nd(1)-Br(3)	89.26(13)
P(2)-O(2)	1.511(5)	O(2)-Nd(1)-O(3)	89.99(19)
P(3)-O(3)	1.513(4)	O(3)-Nd(1)-Br(1)	85.78(15)
		O(3)-Nd(1)-Br(2)	87.49(15)
Br(1)-Nd(1)-Br(2)	173.15(3)	O(3)-Nd(1)-Br(3)	177.06(14)
Br(1)-Nd(1)-Br(3)	91.38(3)	P(1)-O(1)-Nd(1)	165.2(3)
Br(2)-Nd(1)-Br(3)	95.34(3)	P(2)-O(2)-Nd(1)	159.2(3)
O(1)-Nd(1)-Br(1)	91.04(13)	P(3)-O(3)-Nd(1)	171.2(3)

X-ray Data Collection, Structure Solution and Refinement for $AmBr_3(OPcy_3)_3$.

An amber crystal of approximate dimensions 0.06 x 0.12 x 0.196 mm was mounted on a nylon loop and transferred to a Bruker D8 Quest diffractometer. The APEX3[12] program package was used to determine the unit-cell parameters and for data collection (17 sec/frame scan time for a calculated scan of diffraction data and a detector distance of 41 mm). The raw frame data was processed using SAINT[13] and SADABS[14] to yield the reflection data file. Subsequent calculations were carried out using the SHELXTL[15] or OLEX2[16] program. The diffraction symmetry was *mmm* and the systematic absences were consistent with the orthorhombic space groups *Pbcm* and $Pca2_1$. It was later determined that space group $Pca2_1$ was correct.

The initial structure was solved by direct methods using Pu in place of Am, since Am is not recognized by APEX3. The structure was refined on F^2 by full-matrix least-squares techniques using Am, the scattering factors for which were taken from the International Tables for Crystallography Volume C.[17] The analytical scattering factors for neutral atoms were used throughout the analysis.[17] Hydrogen atoms were included using a riding model.

The absolute structure was assigned by refinement of the Flack parameter.[18] Based on the Flack parameter, the data was refined as a 2-component twin with BASF = 0.02978. The compound was found to isomorphous with its lanthanide analogs: Pr (BUGRIG),[3] Nd (BUGROM),[3] Gd (BUGRUS),[3] Ho (ROVNUN),[3] which are all reported as a hemi-hydrate, which was not located in the Fourier map for Am.

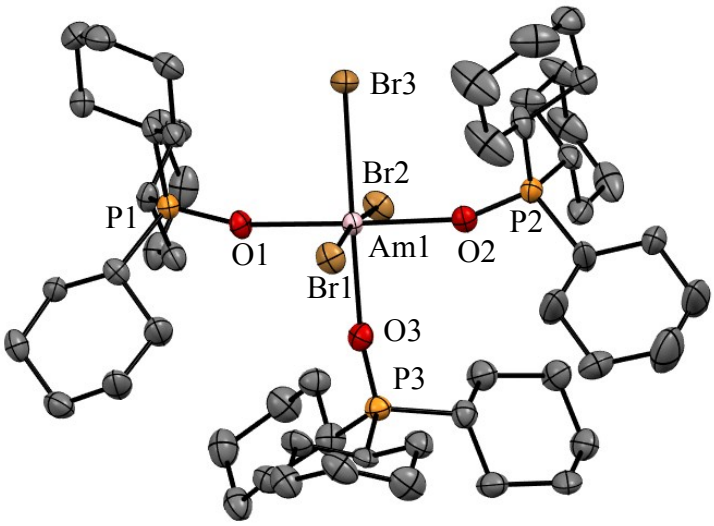

Figure S44. Thermal ellipsoid plot of **$AmBr_3(OPcy_3)_3$** drawn at the 50% probability level with hydrogen atoms omitted for clarity.

Table S21. Crystal data and structure refinement for **$AmBr_3(OPcy_3)_3$**.

Identification code	cjw84 (Cory Windorff)	
Empirical formula	$C_{54}H_{99}O_3P_3Br_3Am$	
Formula weight	1371.97	
Temperature	120(2) K	
Wavelength	0.71073 Å	
Crystal system	Orthorhombic	
Space group	*Pca*2_1	
Unit cell dimensions	a = 28.768(9) Å	α = 90°.
	b = 11.456(4) Å	β = 90°.
	c = 18.185(6) Å	γ = 90°.
Volume	5993(3) $Å^3$	
Z	4	
Density (calculated)	1.521 Mg/m^3	
Absorption coefficient	3.398 mm^{-1}	
F(000)	2768	
Crystal color	clear yellow	
Crystal size	0.196 x 0.12 x 0.06 mm^3	
Theta range for data collection	2.217 to 27.521°	
Index ranges	$-35 \leq h \leq 37$, $-14 \leq k \leq 14$, $-23 \leq l \leq 20$	
Reflections collected	70455	
Independent reflections	12088 [R(int) = 0.0751]	
Completeness to theta = 25.242°	99.9 %	
Absorption correction	Semi–empirical from equivalents	
Max. and min. transmission	0.0949 and 0.0640	
Refinement method	Full–matrix least–squares on F^2	
Data / restraints / parameters	12088 / 1 / 578	
Goodness-of-fit on F^2	1.081	
Final R indices [I>2sigma(I) = 9606 data]	R1 = 0.0399, wR2 = 0.0787	
R indices (all data, 0.77 Å)	R1 = 0.0606, wR2 = 0.0858	
Absolute structure parameter	0.004(7)	
Largest diff. peak and hole	2.033 and −2.008 $e.Å^{-3}$	
BASF	0.02978	

X-ray Data Collection, Structure Solution and Refinement for $LaBr_3(OPcy_3)_3$.

A colorless crystal of approximate dimensions 0.153 x 0.157 x 0.267mm was mounted on a nylon loop and transferred to a Bruker D8 Quest diffractometer. The APEX3[12] program package was used to determine the unit-cell parameters and for data collection (15 sec/frame scan time for a calculated scan of diffraction data and a detector distance of 33 mm). The raw frame data was processed using SAINT[13] and SADABS[14] to yield the reflection data file. Subsequent calculations were carried out using the SHELXTL[15] or OLEX2[16] program. The diffraction symmetry was *mmm* and the systematic absences were consistent with the orthorhombic space groups *Pbcm* and $Pca2_1$. It was later determined that space group $Pca2_1$ was correct.

The structure was solved by direct methods and refined on F^2 by full-matrix least-squares techniques. The analytical scattering factors for neutral atoms were used throughout the analysis.[17] Hydrogen atoms were included using a riding model.

The absolute structure was assigned by refinement of the Flack parameter.[18] Based on the Flack parameter, the data was refined as a 2-component twin with BASF = 0.01767. The compound was not isomorphous with its previous report (BUGREC),[3] and was found to isomorphous with its other lanthanide analogs: Pr (BUGRIG),[3] Nd (BUGROM),[3] Gd (BUGRUS),[3] and Ho (ROVNUN),[3] which are all reported as a hemi-hydrate, which was not located in the Fourier map for La.

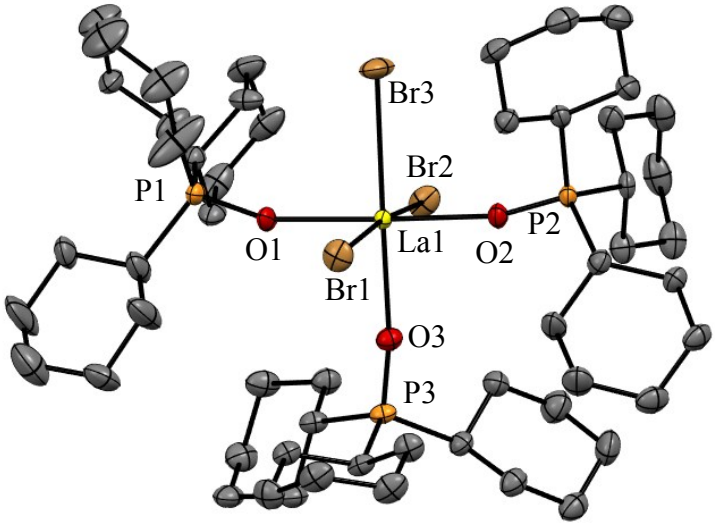

Figure S45. Thermal ellipsoid plot of **$LaBr_3(OPcy_3)_3$** drawn at the 50% probability level with hydrogen atoms omitted for clarity.

Table S22. Crystal data and structure refinement for **$LaBr_3(OPcy_3)_3$**.

Identification code	cjw86 (Cory Windorff)	
Empirical formula	$C_{54}H_{99}O_3P_3Br_3La$	
Formula weight	1267.88	
Temperature	130(2) K	
Wavelength	0.71073 Å	
Crystal system	Orthorhombic	
Space group	*Pca*2_1	
Unit cell dimensions	a = 28.8790(16) Å	α = 90°.
	b = 11.4223(7) Å	β = 90°.
	c = 18.2083(10) Å	γ = 90°.
Volume	6006.3(6) $Å^3$	
Z	4	
Density (calculated)	1.402 Mg/m^3	
Absorption coefficient	2.824 mm^{-1}	
F(000)	2616	
Crystal color	clear colorless	
Crystal size	0.267 x 0.157 x 0.153 mm^3	
Theta range for data collection	2.220 to 27.545°	
Index ranges	$-37 \leq h \leq 37$, $-14 \leq k \leq 14$, $-22 \leq l \leq 23$	
Reflections collected	109745	
Independent reflections	13561 [R(int) = 0.0669]	
Completeness to theta = 25.500°	99.9 %	
Absorption correction	Semi–empirical from equivalents	
Max. and min. transmission	0.7456 and 0.6638	
Refinement method	Full–matrix least–squares on F^2	
Data / restraints / parameters	13561 / 1 / 578	
Goodness-of-fit on F^2	1.092	
Final R indices [I>2sigma(I) = 11489 data]	R1 = 0.0348, wR2 = 0.0566	
R indices (all data, 0.77 Å)	R1 = 0.0510, wR2 = 0.0620	
Absolute structure parameter	0.018(9)	
Largest diff. peak and hole	0.757 and −0.569 e.$Å^{-3}$	
BASF	0.01767	

X-ray Data Collection, Structure Solution and Refinement for $CeBr_3(OPcy_3)_3$.

An orange crystal of approximate dimensions 0.123 x 0.156 x 0.268 mm was mounted on a nylon loop and transferred to a Bruker D8 Quest diffractometer. The APEX3[12] program package was used to determine the unit-cell parameters and for data collection (60 sec/frame scan time for a calculated scan of diffraction data and a detector distance of 42 mm). The raw frame data was processed using SAINT[13] and SADABS[14] to yield the reflection data file. Subsequent calculations were carried out using the SHELXTL[15] or OLEX2[16] program. The diffraction symmetry was *mmm* and the systematic absences were consistent with the orthorhombic space groups *Pbcm* and $Pca2_1$. It was later determined that space group $Pca2_1$ was correct.

The structure was solved by direct methods and refined on F^2 by full-matrix least-squares techniques. The analytical scattering factors for neutral atoms were used throughout the analysis.[17] Hydrogen atoms were included using a riding model.

The absolute structure was assigned by refinement of the Flack parameter.[18] Based on the Flack parameter, the data was refined as a 2-component twin with BASF = 0.03608. The compound is isomorphous with its other lanthanide analogs: Pr (BUGRIG),[3] Nd (BUGROM),[3] Gd (BUGRUS),[3] and Ho (ROVNUN),[3] which are all reported as a hemi-hydrate, which was not located in the Fourier map for Ce.

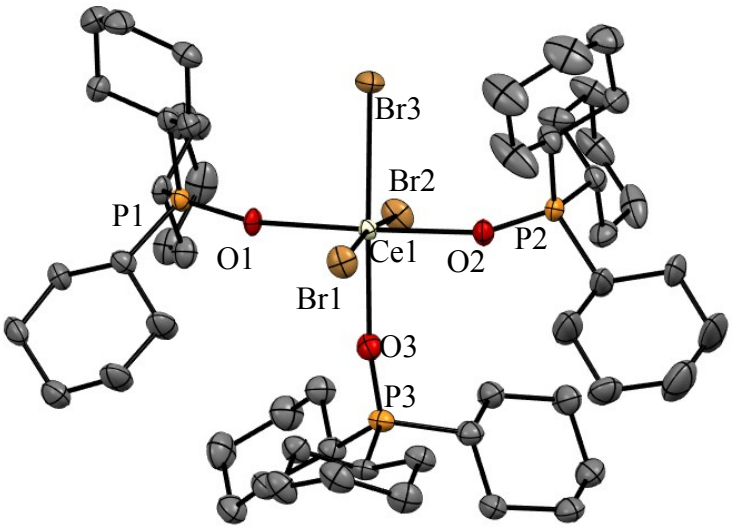

Figure S46. Thermal ellipsoid plot of **$CeBr_3(OPcy_3)_3$** drawn at the 50% probability level with hydrogen atoms omitted for clarity.

Table S23. Crystal data and structure refinement for **$CeBr_3(OPcy_3)_3$**.

Identification code	cjw61 (Cory Windorff)	
Empirical formula	$C_{54}H_{99}O_3P_3Br_3Ce$	
Formula weight	1269.09	
Temperature	120(2) K	
Wavelength	0.71073 Å	
Crystal system	Orthorhombic	
Space group	*Pca*2_1	
Unit cell dimensions	a = 28.920(5) Å	α = 90°.
	b = 11.434(2) Å	β = 90°.
	c = 18.209(3) Å	γ = 90°.
Volume	6021.2(18) $Å^3$	
Z	4	
Density (calculated)	1.400 Mg/m^3	
Absorption coefficient	2.864 mm^{-1}	
F(000)	2620	
Crystal color	clear orange	
Crystal size	0.268 x 0.156 x 0.123 mm^3	
Theta range for data collection	2.218 to 27.511°	
Index ranges	$-37 \leq h \leq 37$, $-14 \leq k \leq 14$, $-23 \leq l \leq 23$	
Reflections collected	122286	
Independent reflections	13805 [R(int) = 0.0685]	
Completeness to theta = 25.242°	99.9 %	
Absorption correction	Semi–empirical from equivalents	
Max. and min. transmission	0.7456 and 0.6448	
Refinement method	Full–matrix least–squares on F^2	
Data / restraints / parameters	13805 / 1 / 578	
Goodness-of-fit on F^2	1.057	
Final R indices [I>2sigma(I) = 11775 data]	R1 = 0.0353, wR2 = 0.0664	
R indices (all data, 0.77 Å)	R1 = 0.0499, wR2 = 0.0726	
Absolute structure parameter	−0.001(4)	
Largest diff. peak and hole	0.956 and −0.784 e.$Å^{-3}$	
BASF	0.03608	

X-ray Data Collection, Structure Solution and Refinement for $PrBr_3(OPcy_3)_3$.

A colorless crystal of approximate dimensions 0.315 x 0.205 x 0.188 mm was mounted on a nylon loop and transferred to a Bruker D8 Quest diffractometer. The APEX3[12] program package was used to determine the unit-cell parameters and for data collection (15 sec/frame scan time for a calculated scan of diffraction data at a detector distance of 35 mm). The raw frame data was processed using SAINT[13] and SADABS[14] to yield the reflection data file. Subsequent calculations were carried out using the SHELXTL[15] or OLEX2[16] program. The diffraction symmetry was *mmm* and the systematic absences were consistent with the orthorhombic space groups *Pbcm* and $Pca2_1$. It was later determined that space group $Pca2_1$ was correct.

The structure was solved by direct methods and refined on F^2 by full-matrix least-squares techniques. The analytical scattering factors for neutral atoms were used throughout the analysis.[17] Hydrogen atoms were included using a riding model.

The absolute structure was assigned by refinement of the Flack parameter.[18] Based on the Flack parameter, the data was refined as a 2-component twin with BASF = 0.00891. The compound is a redetermination of the previously data (BUGRIG),[3] and is isomorphous with its other lanthanide analogs: Nd (BUGROM),[3] Gd (BUGRUS),[3] and Ho (ROVNUN).[3]

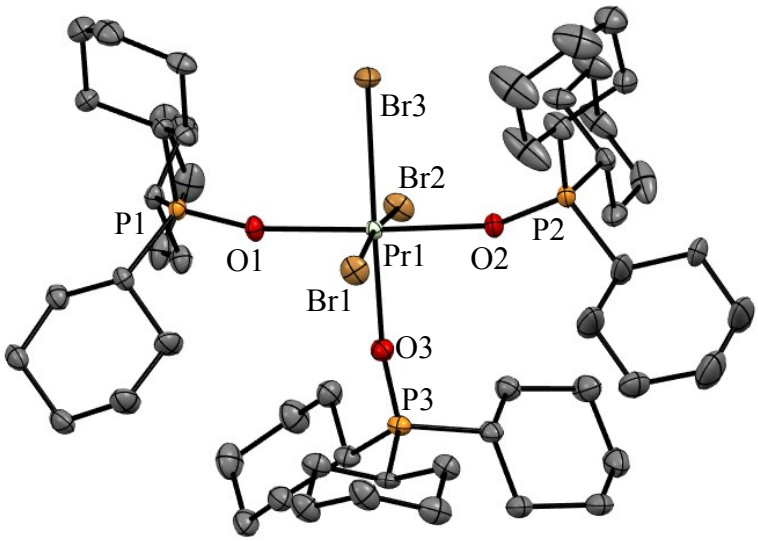

Figure S47. Thermal ellipsoid plot of $PrBr_3(OPcy_3)_3$ drawn at the 50% probability level with hydrogen atoms (and lattice solvent) omitted for clarity.

Table S24. Crystal data and structure refinement for **$PrBr_3(OPcy_3)_3$**.

Identification code	cjw94 (Cory Windorff)	
Empirical formula	$C_{54}H_{99}O_3P_3Br_3Pr$	
Formula weight	1269.88	
Temperature	120(2) K	
Wavelength	0.71073 Å	
Crystal system	Orthorhombic	
Space group	*Pca*2_1	
Unit cell dimensions	a = 28.716(1) Å	α = 90°.
	b = 11.4126(4) Å	β = 90°.
	c = 18.1299(8) Å	γ = 90°.
Volume	5941.5(4) $Å^3$	
Z	4	
Density (calculated)	1.420 Mg/m^3	
Absorption coefficient	2.956 mm^{-1}	
F(000)	2624	
Crystal color	clear colorless	
Crystal size	0.315 x 0.205 x 0.188 mm^3	
Theta range for data collection	2.225 to 27.551°	
Index ranges	$-37 \leq h \leq 37$, $-14 \leq k \leq 14$, $-23 \leq l \leq 23$	
Reflections collected	106432	
Independent reflections	13677 [R(int) = 0.0613]	
Completeness to theta = 25.500°	99.9 %	
Absorption correction	Semi-empirical from equivalents	
Max. and min. transmission	0.7456 and 0.6775	
Refinement method	Full-matrix least-squares on F^2	
Data / restraints / parameters	13677 / 1 / 578	
Goodness-of-fit on F^2	1.055	
Final R indices [I>2sigma(I) = 11537 data]	R1 = 0.0317, wR2 = 0.0556	
R indices (all data, 0.77 Å)	R1 = 0.0481, wR2 = 0.0617	
Absolute structure parameter	0.009(9)	
Largest diff. peak and hole	0.990 and −0.720 e.$Å^{-3}$	
BASF	0.00891	

X-ray Data Collection, Structure Solution and Refinement for $NdBr_3(OPcy_3)_3$.

A colorless crystal of approximate dimensions 0.224 x 0.202 x 0.170 mm was mounted on a nylon loop and transferred to a Bruker D8 Quest diffractometer. The APEX3[12] program package was used to determine the unit-cell parameters and for data collection (10 sec/frame scan time for a hemisphere of diffraction data with a scan width of 0.5° and a detector distance of 35 mm). The raw frame data was processed using SAINT[13] and SADABS[14] to yield the reflection data file. Subsequent calculations were carried out using the SHELXTL[15] or OLEX2[16] program. The diffraction symmetry was *mmm* and the systematic absences were consistent with the orthorhombic space groups *Pbcm* and $Pca2_1$. It was later determined that space group $Pca2_1$ was correct.

The structure was solved by direct methods and refined on F^2 by full-matrix least-squares techniques. The analytical scattering factors for neutral atoms were used throughout the analysis.[17] Hydrogen atoms were included using a riding model.

The absolute structure was assigned by refinement of the Flack parameter.[18] Based on the Flack parameter, the data was refined as a 2-component twin with BASF = -0.00554. The structure is known (BUGROM)[3] and was re-determined. The compound is isomorphous with its other lanthanide analogs: Pr (BUGRIG),[3] Gd (BUGRUS),[3] and Ho (ROVNUN),[3] which are all reported as a hemi-hydrate, which was not located in the Fourier map for Nd.

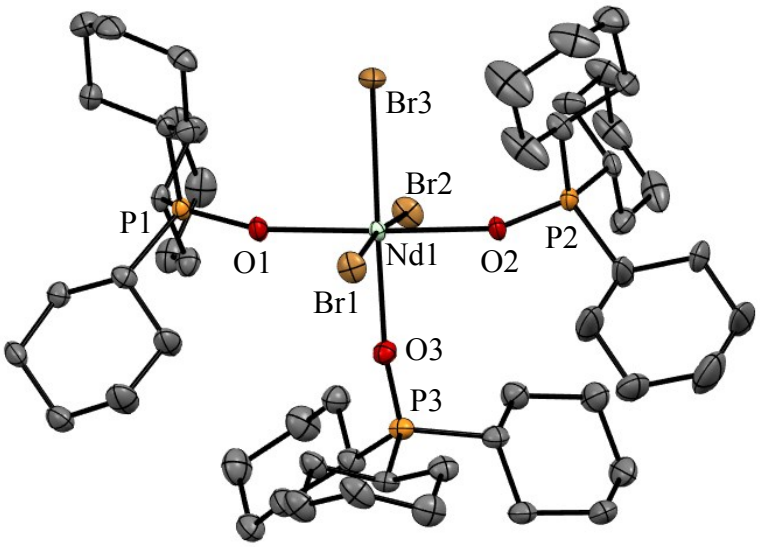

Figure S48. Thermal ellipsoid plot of **$NdBr_3(OPcy_3)_3$** drawn at the 50% probability level with hydrogen atoms omitted for clarity.

Table S25. Crystal data and structure refinement for **$NdBr_3(OPcy_3)_3$**.

Identification code	cjw93 (Cory Windorff)	
Empirical formula	$C_{54}H_{99}O_3P_3Br_3Nd$	
Formula weight	1273.21	
Temperature	120(2) K	
Wavelength	0.71073 Å	
Crystal system	Orthorhombic	
Space group	*Pca*2_1	
Unit cell dimensions	a = 28.7074(14) Å	α = 90°.
	b = 11.4137(6) Å	β = 90°.
	c = 18.1291(10) Å	γ = 90°.
Volume	5946.8(4) $Å^3$	
Z	4	
Density (calculated)	1.422 Mg/m^3	
Absorption coefficient	3.007 mm^{-1}	
F(000)	2628	
Crystal color	clear colorless	
Crystal size	0.224 x 0.202 x 0.170 mm^3	
Theta range for data collection	2.223 to 27.557°	
Index ranges	$-37 \leq h \leq 37$, $-14 \leq k \leq 14$, $-22 \leq l \leq 23$	
Reflections collected	106339	
Independent reflections	13649 [R(int) = 0.0874]	
Completeness to theta = 25.500°	99.9 %	
Absorption correction	Semi-empirical from equivalents	
Max. and min. transmission	0.7456 and 0.6784	
Refinement method	Full-matrix least-squares on F^2	
Data / restraints / parameters	13649 / 1 / 578	
Goodness-of-fit on F^2	1.037	
Final R indices [I>2sigma(I) = 11307 data]	R1 = 0.0405, wR2 = 0.0680	
R indices (all data, 0.77 Å)	R1 = 0.0608, wR2 = 0.0777	
Absolute structure parameter	-0.006(12)	
Largest diff. peak and hole	1.021 and −1.569 $e.Å^{-3}$	
BASF	-0.00554	

REFERENCES

1. Singh, S. K.; Gupta, T.; Ungur, L.; Rajaraman, G., *Chem. Eur. J.* **2015,** *21*, 13812-13819.
2. Mann, M. M.; DeShazer, L. G., *J. Appl. Phys.* **1970,** *41*, 2951-2957.
3. Bowden, A.; Lees, A. M. J.; Platt, A. W. G., *Polyhedron* **2015,** *91*, 110-119.
4. Shannon, R., *Acta Cryst.* **1976,** *A32*, 751-767.
5. Gompa, T. P.; Rice, N. T.; Russo, D. R.; Aguirre Quintana, L. M.; Yik, B. J.; Bacsa, J.; La Pierre, H. S., *Dalton Trans.* **2019,** *48*, 8030-8033.
6. Radonovich, L. J.; Glick, M. D., *J. Inorg. Nucl. Chem.* **1973,** *35*, 2745-2752.
7. Zhang, X.-W.; Li, X.-F.; Benetollo, F.; Bombieri, G., *Inorg. Chim. Acta* **1987,** *139*, 103-104.
8. Hou, Z.; Kobayashi, K.; Yamazaki, H., *Chem. Lett.* **1991,** *20*, 265-268.
9. Deacon, G. B.; Feng, T.; Junk, P. C.; Skelton, B. W.; Sobolev, A. N.; White, A. H., *Aust. J. Chem.* **1998,** *51*, 75-89.
10. Deacon, G. B.; Feng, T.; Junk, P. C.; Meyer, G.; Scott, N. M.; Skelton, B. W.; White, A. H., *Aust. J. Chem.* **2000,** *53*, 853 - 865.
11. Emge, T. J.; Kornienko, A.; Brennan, J. G., *Acta Cryst.* **2009,** *C65*, m422-m425.
12. *APEX3*, 2017.3-0; Bruker AXS, Inc.: Madison, WI, 2017.
13. *SAINT*, 8.34a; Bruker AXS, Inc: Madison, WI, 2013.
14. Sheldrick, G. M. *SADABS*, 2012/1; Bruker AXS, Inc: Madison, WI, 2012.
15. Sheldrick, G. M. *SHELXTL*, Bruker AXS, Inc: Madison, WI, 2012.
16. *Olex2*, 1.2.10; OlexSys Ltd: 2004-2018.
17. Prince, E., 1st online ed.; International Union of Crystallography: 2006; Vol. C: Mathematical, Physical and Chemical Tables.
18. Flack, H., *Acta Cryst.* **1983,** *A39*, 876-881.